Bulletin of Mathematical Biology (2023) 85:48
https://doi.org/10.1007/s11538-023-01150-7

Society for Mathematical Biology

ORIGINAL ARTICLE

Natural Parameter Conditions for Singular Perturbations of Chemical and Biochemical Reaction Networks

Justin Eilertsen[1] · **Santiago Schnell**[2,3] · **Sebastian Walcher**[4]

Received: 19 November 2022 / Accepted: 23 March 2023 / Published online: 26 April 2023
© The Author(s), under exclusive licence to Society for Mathematical Biology 2023

Abstract

We consider reaction networks that admit a singular perturbation reduction in a certain parameter range. The focus of this paper is on deriving "small parameters" (briefly for small perturbation parameters), to gauge the accuracy of the reduction, in a manner that is consistent, amenable to computation and permits an interpretation in chemical or biochemical terms. Our work is based on local timescale estimates via ratios of the real parts of eigenvalues of the Jacobian near critical manifolds. This approach modifies the one introduced by Segel and Slemrod and is familiar from computational singular perturbation theory. While parameters derived by this method cannot provide universal quantitative estimates for the accuracy of a reduction, they represent a critical first step toward this end. Working directly with eigenvalues is generally unfeasible, and at best cumbersome. Therefore we focus on the coefficients of the characteristic polynomial to derive parameters, and relate them to timescales. Thus, we obtain distinguished parameters for systems of arbitrary dimension, with particular emphasis on reduction to dimension one. As a first application, we discuss the Michaelis–Menten reaction mechanism system in various settings, with new and perhaps surprising results. We proceed to investigate more complex enzyme catalyzed reaction mechanisms (uncompetitive, competitive inhibition and cooperativity) of dimension three, with reductions

✉ Santiago Schnell
santiago.schnell@nd.edu

Justin Eilertsen
jse@ams.org

Sebastian Walcher
walcher@matha.rwth-aachen.de

1 Mathematical Reviews, American Mathematical Society, 416 4th Street, Ann Arbor, MI 48103, USA

2 Department of Biological Sciences, University of Notre Dame, Notre Dame, IN 46556, USA

3 Department of Applied and Computational Mathematics and Statistics, University of Notre Dame, Notre Dame, IN 46556, USA

4 Mathematik A, RWTH Aachen, 52056 Aachen, Germany

to dimension one and two. The distinguished parameters we derive for these three-dimensional systems are new. In fact, no rigorous derivation of small parameters seems to exist in the literature so far. Numerical simulations are included to illustrate the efficacy of the parameters obtained, but also to show that certain limitations must be observed.

Keywords Reaction network · Dimension reduction · Perturbation parameter · Timescale · Eigenvalue · Symmetric polynomial · Quasi-steady-state approximation · Lyapunov function · Singular perturbation

Mathematics Subject Classification 92C45 · 34D15 · 80A30 · 13P10

1 Introduction

Reducing the dimension of chemical and biochemical reaction networks or mechanisms is of great relevance both for theoretical considerations and for laboratory practice. For instance, the fundamental structure of a reaction mechanism is frequently known, or assumed from educated guesswork, but reaction rate constants are a priori unknown. Moreover, due to possible wide discrepancies in timescales, as well as limitations on experimentally obtainable data, it is important to identify scenarios and parameter regions that guarantee accuracy of a suitably chosen reduction. Singular perturbations frequently appear here,[1] and the fundamental theorems by Tikhonov (1952) and Fenichel (1979) provide a procedure to determine a reduced equation, and reliable convergence results. These theorems require an a priori identification of a perturbation parameter (also called "small parameter"). From a qualitative perspective, one actually considers a critical manifold together with an associated small parameter, and a corresponding slow invariant manifold. Given a well-defined limiting process for the small parameter, theory guarantees convergence of solutions of the full system to corresponding solutions of the reduced system. From a practical ("laboratory") perspective, however, convergence theorems are not sufficient, and quantitative results are needed to gauge the accuracy of fitting procedures. This implies the need for an appropriate small parameter, which we denote by ε_S for the moment, that also reflects quantitative features. In contrast to the critical manifold, from a qualitative perspective the perturbation parameter is far from unique.[2] From a quantitative perspective, ideally ε_S should provide an upper estimate for the discrepancy between the exact and approximate solutions over the whole course of the slow dynamics. From a biochemical perspective it should elucidate the influence of reaction parameters. In many application-oriented publications, the authors assume (explicitly or implicitly) that certain perturbation parameters provide a quantitative estimate for the approximation; see, e.g., Heineken et al. (1967), Segel (1988), Tzafriri (2003), Schnell (2014), Choi

[1] Other types of reduction scenarios do occur, but we will not discuss these in the present work.

[2] Even for the familiar Michaelis–Menten system there are several parameters in use.

et al. (2017).[3] However, while heuristical arguments may support such assumptions, no mathematical proof is given [see the discussion of the Michaelis–Menten system in Eilertsen et al. (2022)]. From the applied perspective, in absence of rigorous results on quantitative error estimates for reductions of biochemical reaction networks or mechanisms, there is no alternative to employing heuristics. Thus, there exists a sizable gap between available theoretical results and applications, and closing this gap requires further theoretical results. The present paper is intended as a contribution toward narrowing the gap, invoking mathematical theory.

From an overall perspective (based on a derivation of singular perturbation theorems), one could say that finding ideal small parameters for a given singular perturbation scenario requires a three-step procedure:

1. In a first step, estimate the approach of a particular solution to the slow manifold: A common method employs Lyapunov functions. Thus, one obtains a parameter that measures the discrepancy between the right-hand sides of the full system and the reduced equation, following a short initial transient.
2. In a second step, estimate a suitable critical time at which the slow dynamics sets in, and estimate the solution at this critical time. This is needed to guarantee that the transient phase is indeed short, and to obtain a suitable initial value for the reduced equation.
3. In a third step, estimate the approximation of the exact solution by the corresponding solution of the reduced equation.[4]

At first glance, this procedure seems to pose no problems. The feasibility of the steps outlined above is guaranteed by standard results about ordinary differential equations. But, the hard part lies in their practical implementation for a given parameter-dependent system. Generally, it is not easy to obtain meaningful and reasonably sharp estimates. A case-by-case discussion seems unavoidable [see, Schnell and Maini (2000), Eilertsen et al. (2018, 2021a), Eilertsen and Schnell (2018, 2020) for examples employing various alternative approaches], for each given system.

With the three steps as a background, our goal is to make a significant contribution toward the first step, via linear timescale arguments. We will both expand and improve existing results, and moreover obtain perturbation parameters for higher-dimensional systems for which no rigorous results have previously been reported. In a biochemical context, it seems that timescale arguments were first introduced by Segel (1988), and Segel and Slemrod (1989). Conceptually, we build upon this approach, but we take a consistent local perspective. Thus, we consider (real parts of) eigenvalue ratios, based on the idea that underlies computational singular perturbation theory, going back to Lam and Goussis (1994). Our emphasis is on obtaining parameters that are workable for application-oriented readers in mathematical enzymology, and admit an interpretation in biochemical terms.

[3] In several instances this assumption seems to be coupled with a too literal interpretation of the expression $\varepsilon \ll 1$.

[4] The proximity of the phase–space trajectory to the slow manifold does not ensure that the time evolutions of the approximate solution and the true solution are close; see, e.g., Eilertsen et al. (2022, Fig. 4).

1.1 Background

A solid mathematical foundation for qualitative viability of most reduction procedures in chemistry and biochemistry is provided by singular perturbation theory (Tikhonov 1952; Fenichel 1979). This was first clearly stated and utilized in Heineken et al. (1967).

For illustrative purposes, and as further motivation, we consider a familiar system from biochemistry, viz. the (irreversible) Michaelis–Menten reaction mechanism or network (Michaelis and Menten 1913), which is modeled by the two-dimensional differential equation

$$\begin{aligned} \dot{s} &= -k_1 e_0 s + (k_1 s + k_{-1})c, \\ \dot{c} &= k_1 e_0 s - (k_1 s + k_{-1} + k_2)c. \end{aligned} \tag{1}$$

For small initial enzyme concentration with respect to the initial substrate concentration, Briggs and Haldane (1925) assumed quasi-steady state (QSS) for complex concentration, thus obtaining the QSS manifold given by

$$c = \frac{k_1 e_0 s}{k_{-1} + k_2 + k_1 s}; \tag{2}$$

and reduction to the Michaelis–Menten equation

$$\dot{s} = -\frac{k_1 k_2 e_0 s}{k_{-1} + k_2 + k_1 s}. \tag{3}$$

To quantify the notion of smallness for enzyme concentration, they introduced the dimensionless parameter

$$\varepsilon_{BH} := \frac{e_0}{s_0} \tag{4}$$

[later utilized by Heineken et al. (1967) in the first application of singular perturbation theory to this reaction], and required $\varepsilon_{BH} \ll 1$ as a necessary condition for accuracy of the reduction. Further parameters to ensure accuracy of approximation by the Michaelis–Menten equation were introduced later on. Reich and Selkov (1974) introduced

$$\varepsilon_{RS} := k_1 e_0/(k_{-1} + k_2), \tag{5}$$

for which Palsson and Lightfoot (1984) later gave a justification based on linearization at the stationary point 0.[5] Moreover, Segel and Slemrod (1989) derived

$$\varepsilon_{SSl} := \frac{k_1 e_0}{k_{-1} + k_2 + k_1 s_0}. \tag{6}$$

[5] In a recent paper, Patsatzis and Goussis (2019) suggested a parameter involving s and c along a trajectory; taking the maximum over s and c yields ε_{RS}.

The fundamental approach by Segel and Slemrod (1989), obtaining perturbation parameters by comparing suitable timescales, has been used widely in the literature ever since.[6]

For Michaelis–Menten reaction mechanism, singular perturbation theory shows convergence of solutions of (1) to corresponding solutions of the reduced equation as $e_0 \to 0$, in which case all of the parameters ε_{BH}, ε_{RS}, ε_{SSl} approach zero. But on the other hand, it is *not* generally true that $\varepsilon_{BH} \to 0$, or $\varepsilon_{RS} \to 0$, or $\varepsilon_{SSl} \to 0$, implies convergence to the solution of the reduced system. This, as well as related matters, was discussed in detail in Eilertsen et al. (2022), with a presentation of counterexamples. We also invite the readers to see other examples in Sect. 4.

These facts illustrate that considering a single parameter—without context and without a clearly defined notion of the limiting process—will generally not be sufficient to ensure the validity of some particular reduction. In a singular perturbation setting the critical manifold is the basic object, and one generally needs to specify the way in which corresponding small parameters approach zero.

With regard to the procedure outlined in Steps 1 to 3 above, a wish list for small parameters includes the following physically motivated conditions:

- ε_S is dimensionless;
- ε_S is composed of reaction rates and initial values (admitting an interpretation in physical terms);
- ε_S is controllable in experiments.

These requirements will be taken into account as well.

Our vantage point is work by Goeke et al. (2015, 2017), which provides an algorithmic approach to determine critical parameter values (Tikhonov–Fenichel parameter values, TFPV), and their critical manifolds: Choosing a curve in parameter space (with curve parameter ε) that starts at a TFPV gives rise to a singularly perturbed system, based on a clearly defined approach of the small parameter to zero.

Pursuing a less ambitious goal than the one outlined in Steps 1 to 3 above, we will utilize the separation of timescales on the slow manifold, adapting work by Lam and Goussis (1994) on computational singular perturbation theory. We focus attention on local considerations. Timescales are identified as inverse absolute real parts of eigenvalues of the linearization of a vector field, near stationary points. Restriction to the vicinity of stationary points is an essential condition here. Given a singular perturbation setting, Zagaris et al. (2004) proved that the approach via "small eigenvalue ratios" is consistent. Unless some eigenvalues of large modulus are purely imaginary, the eigenvalue approach provides a small parameter that satisfies the requirement in Step 1 above, up to a multiplicative constant that remains to be determined.[7] But dealing directly with eigenvalues (even in the rare case when they are explicitly known) is generally too cumbersome to allow productive work and concrete conclusions.

The emphasis of the present paper lies on local (linear) timescale estimates and comparisons, using a mix of algebraic and analytic tools. We will obtain parameters

[6] The particular argument in Segel and Slemrod (1989) is somewhat problematic since the notion of timescale is ambiguous for nonlinear systems.

[7] A proof of this fact is sketched in Appendix 9.1, which also indicates that eigenvalue ratios are relevant for Step 3. The multiplicative constant reflects the effect of a coordinate transformation.

that are palatable to application-oriented readers and allow for interpretation in a biochemical context. Most of the parameters obtained have not appeared in the literature before, and some perhaps are unexpected.

1.2 Overview of Results

Given a chemical or biochemical reaction network or mechanism, we will present a method to obtain distinguished dimensionless parameters. These parameters are directly related to the local fast-slow dynamics of the singularly perturbed system. In contrast to many existing timescale estimates in the literature, the one employed here is conceptually consistent. Timescale considerations mutate from artwork to a relatively routine procedure, and we establish necessary conditions for timescale separation and singular perturbation reductions.

In the preparatory Sect. 2, we collect some notions and results related to singular perturbation theory. In particular, we recall Tikhonov–Fenichel parameter values (TFPV). We also note properties of the Jacobian and its characteristic polynomial on the critical manifold. It should be emphasized that our search always begins with identifying a TFPV and its associated critical manifold; all our small parameter estimates are rooted in this scenario. We establish a repository of dimensionless parameters from coefficients of the characteristic polynomial, and we recall the relation between these coefficients and the eigenvalues of the Jacobian. Finally, we fix some notation and establish some blanket nondegeneracy conditions that are assumed throughout the paper.

Section 3 is devoted to one-dimensional critical manifolds, which are of considerable relevance to experimentalists. Generally, the timecourse of a single product or substrate is measured in an experiment. Specific kinetic parameters (such as the Michaelis constant) are estimated via nonlinear regression, in which the recorded timecourse data is fitted to a one-dimensional and autonomous QSS model that approximates substrate depletion (or product formation) of the reaction on the slow timescale; see, for example, Stroberg and Schnell (2016) and Choi et al. (2017). In the one-dimensional setting, near the critical manifold there is one and only one eigenvalue of the Jacobian with small absolute real part. From the characteristic polynomial, we obtain distinguished small parameters, and we establish their correspondence to timescales. The parameters thus obtained admit an interpretation in terms of reaction parameters, so they satisfy a crucial practical requirement. They measure the ratio of the slow to the fastest timescale, and thus provide a necessary condition for timescale separation. But, in dimension greater than two, this condition is not strong enough when there are large discrepancies within the fast timescales. According to Appendix, Sect. 9.1, the ratio of the slow to the "slowest of the fast" timescales is the relevant quantity. To estimate this ratio, we introduce another type of parameter that yields sharp estimates whenever all eigenvalues are "essentially real" [borrowing terminology of Lam and Goussis (1994)]. We then specialize our results to systems of dimensions two and three.

In Sect. 4, we apply the results from Sect. 3 to the (reversible and irreversible) Michaelis–Menten system in various circumstances. We obtain a distinguished parameter for the reversible system with small enzyme concentration; this seems to be new. Specializing to the irreversible case, we obtain a parameter ε_{MM} and conclude, via an argument different from Palsson and Lightfoot (1984), that the Reich-Selkov parameter ε_{RS} is the most suitable among the standard parameters in the irreversible system. Moreover, we obtain a rather surprising distinguished parameter for the partial equilibrium approximation with slow product formation. To support the claim that this is indeed an appropriate parameter for Step 1, as stated above, we determine relevant Lyapunov estimates, and we add some observations with regard to Step 3. To illustrate the necessity of some technical restrictions in our results, we close this section by discussing a degenerate scenario with a singular critical variety.

In Sect. 5, we turn to critical manifolds of dimension greater than one. Imitating the approach for one-dimensional critical manifolds and invoking results from local analytic geometry, we obtain distinguished parameters that measure the ratio of the fastest timescale to the "fastest of the slow" timescales. We provide a detailed analysis for three-dimensional systems with two-dimensional critical manifold.

In Sect. 6, we apply our theory to some familiar three-dimensional systems from biochemistry, viz. cooperative systems with two complexes, and competitive as well as uncompetitive inhibition, for low enzyme concentration. For these systems the only available perturbation parameters in common use seem to be $\varepsilon_{BH} = e_0/s_0$, ε_{SSl} and ad hoc variants of these. There seems to exist no derivation of small parameters via timescale arguments (in the spirit of Segel and Slemrod) in the literature. We thus break new ground, and we obtain meaningful and useful distinguished parameters. We illustrate our results with several numerical examples, to verify the efficacy of the parameters. But, we also include simulations to show their limited applicability in certain regions of parameter space. Such limitations were to be expected, since Steps 2 and 3 are needed for a complete analysis. These examples also illustrate the necessity of additional hypotheses imposed in the derivation of the distinguished parameters.

In Sect. 7, we consider some reductions of three-dimensional systems obtained via projection onto two-dimensional critical manifolds. Specifically, we compute some two-dimensional reductions of the competitive and uncompetitive inhibitory reaction mechanisms, and we derive distinguished parameters that are relevant for the accuracy of these reductions. Again, we illustrate our results by numerical simulations. To finish, we discuss a three timescale scenario that leads to a hierarchical structure in which the two-dimensional slow manifold contains an embedded one-dimensional "very slow" manifold.

Section 9, an Appendix, is a recapitulation of the Lyapunov function method for singularly perturbed systems, also outlining the relevance of the eigenvalue ratios for Step 1, and some observations on Steps 2 and 3. Moreover, Appendix contains a summary of some facts from the literature, and proofs for some technical results. Sections 2, 3 and 5 as well as Appendix (Sect. 9) are mostly technical. Readers primarily interested in applications may want to skim these only, and focus on the applications in Sects. 4, 6 and 7.

2 Preliminaries

We will discuss parameter-dependent ordinary differential equations

$$\dot{x} = h(x, \pi), \quad x \in \mathbb{R}^n, \quad \pi \in \Pi, \quad \Pi \subseteq \mathbb{R}^m \text{ closed}, \tag{7}$$

with the right-hand side a polynomial in x and π. Our main motivation is the study of chemical mass action reaction mechanisms and their singular perturbation reductions.

2.1 Tikhonov–Fenichel Parameter Values (a Review)

We consider singular perturbation reductions that are based on the classical work by Tikhonov (1952) and Fenichel (1979). Frequently the pertinent theorems are stated for systems in slow-fast standard form

$$\begin{aligned} \dot{u}_1 &= \varepsilon\, f_1(u_1, u_2, \varepsilon), \\ \dot{u}_2 &= f_2(u_1, u_2, \varepsilon), \end{aligned} \tag{8}$$

with a small parameter ε, subject to certain additional conditions. In slow time, $\tau = \varepsilon t$, the reduced system takes the form

$$\begin{aligned} \frac{\mathrm{d}u_1}{\mathrm{d}\tau} &= f_1(u_1, u_2, \varepsilon), \\ 0 &= f_2(u_1, u_2, \varepsilon), \end{aligned}$$

and the above mentioned conditions ensure that the second equation admits a local resolution for u_2 as a function of u_1 and ε. For general parameter-dependent systems (7) one first needs to identify the parameter values from which such reductions emanate. We recall some notions and results (slightly modified from Goeke et al. 2015):

1. A parameter $\widehat{\pi} \in \Pi$ is called a *Tikhonov–Fenichel parameter value (TFPV) for dimension s* ($1 \le s \le n-1$) of system (7) whenever the following hold:
   (i) An irreducible component of the critical variety, i.e., of the zero set $\mathcal{V}(h(\cdot, \widehat{\pi}))$ of $x \mapsto h(x, \widehat{\pi})$, contains a (Zariski dense) local submanifold $\widetilde{Y}$ of dimension s, which is called the critical manifold.
   (ii) For all $x \in \widetilde{Y}$ one has rank $D_1 h(x, \widehat{\pi}) = n - s$ and
   $$\mathbb{R}^n = \mathrm{Ker}\ D_1 h(x, \widehat{\pi}) \oplus \mathrm{Im}\ D_1 h(x, \widehat{\pi}).$$
   Here D_1 denotes the partial derivative with respect to x.
   (iii) For all $x \in \widetilde{Y}$ the nonzero eigenvalues of $D_1 h(x, \widehat{\pi})$ have real parts < 0.
2. Given a TFPV, for any smooth curve $\varepsilon \mapsto \widehat{\pi} + \varepsilon\rho + \cdots$ in parameter space Π, the system
   $$\dot{x} = h(x, \widehat{\pi} + \varepsilon\rho + \cdots) = h(x, \widehat{\pi}) + \varepsilon D_2 h(x, \widehat{\pi})\, \rho + \cdots =: h^{(0)}(x) + \varepsilon h^{(1)}(x) + \cdots,$$

with D_2 denoting the partial derivative with respect to π, admits a singular perturbation (Tikhonov–Fenichel) reduction.
A standard method is to fix a parameter direction and a "ray" $\varepsilon \mapsto \widehat{\pi} + \varepsilon\rho$ in parameter space. In a chemical interpretation this may correspond to a gradual increase of some parameters, such as initial concentrations. Our work will always be based on this procedure; by this specification we avoid ambiguities about the range of parameters.

3. The computation of a reduction in the coordinate-free setting is described in Goeke and Walcher (2014): Assuming the TFPV conditions in item 1, there exist rational functions P, with values in $\mathbb{R}^{n\times(n-s)}$, and μ, with values in $\mathbb{R}^{n-s}$, such that

$$h^{(0)}(x) = P(x)\mu(x) \text{ on } \widetilde{Y},$$

and $P(x)$ as well as $D\mu(x)$ have full rank on $\widetilde{Y}$. The reduced equation on $\widetilde{Y}$ then has the representation

$$\dot{x} = \varepsilon \left(I - P(x) \left(D\mu(x) P(x) \right)^{-1} D\mu(x) \right) h^{(1)}(x), \tag{9}$$

which is correct up to $O(\varepsilon^2)$. By Tikhonov and Fenichel, solutions of (7) that start near $\widetilde{Y}$ will converge to solutions of the reduced system as $\varepsilon \to 0$. But some caveats are in order:

- The reduction is guaranteed only locally, for neighborhoods of compact subsets of the critical manifold and for sufficiently small ε. Determining a neighborhood explicitly for which the reduction is valid poses an individual problem for each system.[8]
- In particular, the distance of the initial value of (7) from the slow manifold (not only from the critical manifold) is relevant for the reduction. In general, an approximate initial value for the reduced equation on the slow manifold must be determined.
- If the transversality condition in (ii) above breaks down, standard singular perturbation theory is no longer applicable. But, even when it is satisfied, the range of validity for the reduction may be quite small. This reflects the effect of a local transformation to Tikhonov standard form.
- Finally, the reduced equation may be trivial, in which case higher-order terms in ε are dominant and no conclusion can be drawn from the first order reduction. By the same token, if the term following ε in (9) is small, then the quality of the reduction may be poor.

4. Turning to computational matters, consider the characteristic polynomial

$$\chi(\tau, x, \pi) = \tau^n + \sigma_1(x,\pi)\tau^{n-1} + \cdots + \sigma_{n-1}(x,\pi)\tau + \sigma_n(x,\pi) \tag{10}$$

[8] A similar problem is familiar from linearly stable stationary points.

of the Jacobian $D_1 h(x, \pi)$. Then, given $0 < s < n$, a parameter value $\widehat{\pi}$ is a TFPV with locally exponentially attracting critical manifold $\widetilde{Y}$ of dimension s, and $x_0 \in \widetilde{Y}$, only if the following hold:

- $h(x_0, \widehat{\pi}) = 0$.
- The characteristic polynomial $\chi(\tau, x, \pi)$ satisfies
  (i) $\sigma_n(x_0, \widehat{\pi}) = \cdots = \sigma_{n-s+1}(x_0, \widehat{\pi}) = 0$;
  (ii) all roots of $\chi(\tau, x_0, \widehat{\pi})/\tau^s$ have negative real parts.

This characterization shows that x_0 satisfies an overdetermined system of equations (more than n equations in n variables), which in turn allows to algorithmically determine conditions on $\widehat{\pi}$ by way of elimination theory; see Goeke et al. (2015). Due to the Hurwitz-Routh theorem (see, e.g., Gantmacher 2005),

$$\sigma_k(x_0, \widehat{\pi}) > 0 \text{ for } x_0 \in \widetilde{Y},\ 1 \leq k \leq n - s$$

is a necessary consequence of condition (ii). Necessary and sufficient conditions for TFPV are stated in Goeke et al. (2015), but we will not need them here.

2.2 Dimensionless Parameters

From Goeke et al. (2015), one finds critical parameter values and corresponding critical manifolds, but there remains to specify the notion of "small perturbation," and to relate it to reaction parameters. Singular perturbation theory guarantees convergence in the limit $\varepsilon \to 0$, but for a given system estimates for the rate of convergence are desirable.

To be physically meaningful, relevant small parameters should be dimensionless. The only dimensions appearing in reaction parameters are time and concentration, thus by dimensional analysis (Buckingham Pi Theorem; see, e.g., Wan 2018), there exist $\geq m-2$ independent dimensionless Laurent monomials in the parameters, such that every dimensionless analytic function of the reaction parameters can locally be expressed as a function of these.[9] This collection may be quite large; we impose the additional requirement that parameters should correspond to timescales. In a preliminary step, we therefore list an inventory of rational dimensionless quantities for the network or mechanism.

Lemma 1 *Let* (7) *correspond to a CRN with mass action kinetics, and* χ *as in* (10). *Then:*

(a) *The coefficient* σ_k *of* χ *has dimension* $(\text{Time})^{-k}$.
(b) *Whenever* $i_1, \ldots, i_p \geq 1$ *and* $j_1, \ldots, j_q \geq 1$ *are integers such that* $i_1 + \cdots + i_p = j_1 + \cdots + j_q$, *the expression*

$$\frac{\sigma_{i_1} \cdots \sigma_{i_p}}{\sigma_{j_1} \cdots \sigma_{j_q}}$$

(when defined) is dimensionless.

[9] Generically, there are exactly $m - 2$.

Proof Every monomial on the right-hand side of (7) has dimension Concentration/Time, since this holds for the left-hand side. The entries of the Jacobian $D_1 h$ are obtained via differentiation with respect to some x_i, hence have dimension $(\text{Time})^{-1}$. Since σ_i is a polynomial in the matrix enries of degree i, part (a) follows. Part (b) is an immediate consequence.

2.3 Timescales

There exist various notions of timescale in the literature, and in some cases this ambiguity influences the derivation of small parameters. For a case in point, we invite the reader to see Segel and Slemrod (1989), who use different notions of timescale for the fast and slow dynamics. But, for systems that decay or grow exponentially, and by extension for linear and approximately linear systems, there exists a well-defined notion:

Definition 1 Let $A : \mathbb{R}^n \to \mathbb{R}^n$ be a linear map, and consider the linear differential equation $\dot{x} = A\,x$. For λ an eigenvalue of A, with nonzero real part, we call $|\text{Re}\,\lambda|^{-1}$ the *timescale* corresponding to λ.

The timescale of an invariant subspace $V \subseteq \mathbb{R}^n$ (which is a subspace of a sum of generalized eigenspaces) is defined as the slowest timescale of the eigenvalues involved.

For a single eigenvalue, the timescale characterizes the speed of growth or decay of solutions along the generalized eigenspace of λ. For an invariant subspace, it characterizes the speed for generic initial values.

We will work with this consistent notion of linear timescale, and its extension to linearizations of nonlinear systems near stationary points, throughout the paper. Thus, we adopt the perspective taken in Lam and Goussis (1994), which is justified by Fenichel's local characterization of the dynamics near the critical manifold $\widetilde{Y}$ (Fenichel 1979, Section V), as proven by Zagaris et al. (2004). Indeed, the time evolution near $\widetilde{Y}$ is governed by the linearization $D_1 h(x, \widehat{\pi} + \varepsilon\rho)$, with $\pi = \widehat{\pi} + \varepsilon\rho$ close to a TFPV $\widehat{\pi}$, and $x \in \widetilde{Y}$. For $\pi = \widehat{\pi}$ the Jacobian has vanishing eigenvalues, hence for π near $\widehat{\pi}$ one will have eigenvalues of small modulus, while all nonzero eigenvalues of $D_1 h(x, \widehat{\pi})$ have negative real parts.

From a practical perspective, eigenvalues are at best inconvenient to work with. Moreover, in our context, resorting to numerical approximations is not a viable option. To obtain more palatable parameters, we recall the correspondence between the eigenvalues $\lambda_1, \ldots, \lambda_n$ of $D_1 h(x, \widehat{\pi} + \varepsilon\rho)$ and the coefficients σ_k of the characteristic polynomial. One has

$$\sigma_k = (-1)^k \sum \lambda_{i_1} \cdots \lambda_{i_k}$$

with the summation extending over all tuples $i_1, \ldots, i_k$ such that $1 \leq i_1 < \cdots < i_k \leq n$. In particular

$$\begin{aligned} -\sigma_1 &= \lambda_1 + \cdots + \lambda_n; \\ (-1)^{n-1}\sigma_{n-1} &= \sum_{i=1}^{n} \prod_{j\neq i} \lambda_j; \\ (-1)^n \sigma_n &= \lambda_1 \cdots \lambda_n; \\ \frac{\sigma_{n-1}}{\sigma_n} &= -\sum \frac{1}{\lambda_j}. \end{aligned} \tag{11}$$

2.4 Blanket Assumptions

The principal goal of the present paper is to provide consistent and workable local timescale estimates in terms of the reaction parameters. Throughout the remainder of the paper, the following notions will be used and the following assumptions will be understood:

1. We consider a polynomial parameter-dependent system (7), and a TFPV $\widehat{\pi}$ for dimension $s \geq 1$, with critical manifold $\widetilde{Y}$. The entries of $\widehat{\pi}$ are not uniquely determined by the critical manifold. We allow these entries to range in a suitable compact subset of parameter space (to be restricted by requirements in the following items).
2. We fix ρ in the parameter space, and consider the singularly perturbed system for the ray in parameter space $\widehat{\pi} + \varepsilon\rho$, with $0 \leq \varepsilon \leq \varepsilon_{\max}$, and restrictions on $\varepsilon_{\max} > 0$ to be specified.
3. Moreover, we let $K \subset \mathbb{R}^n$ be a compact set with nonempty interior, such that $\widetilde{Y} \cap K$ is also compact. K should contain the initial values for all relevant solutions of (7).[10]
4. Since $\widehat{\pi}$ is a TFPV, we have $\sigma_k(x, \widehat{\pi}) > 0$ for all $x \in \widetilde{Y} \cap K$, $1 \leq k \leq n - s$. We choose $\varepsilon_{\max}$ so that $\sigma_k(x, \widehat{\pi} + \varepsilon\rho)$ is defined and bounded above and below by positive constants on

$$K^* = K^*(\varepsilon_{\max}) = \left(\widetilde{Y} \cap K\right) \times [0, \varepsilon_{\max}], \tag{12}$$

   for $1 \leq k \leq n - s$. Such a choice is possible by compactness and continuity, given a suitable compact set in parameter space.
5. As a crucial basic condition, we require that Tikhonov–Fenichel reduction is accurate up to order ε^2 in a compact neighborhood $\widetilde{K}$ of $\widetilde{Y} \cap K$, with $\varepsilon \leq \varepsilon_{\max}$. Consult Sect. 9.1 to verify that this requirement can be satisfied.

We emphasize that the present paper focuses on *asymptotic timescale estimates* near the critical manifold, which are based on Fenichel's local theory. The determination of $\varepsilon_{\max}$ (and by extension, the range of applicability) will not be addressed in general. Moreover, in applications we may replace sharp estimates by weaker ones that permit an interpretation in biochemical terms.

[10] In many applications, it will be possible to choose a positively invariant compact neighborhood, but this will not be required a priori.

3 Critical Manifolds of Dimension One

In this technical section, we consider system (7) in $\mathbb{R}^n$, $n \geq 2$ with a critical manifold of dimension $s = 1$. We will derive two types of distinguished parameters that characterize timescale discrepancies, and discuss systems of dimensions two and three in some detail.

We have $\sigma_n(x, \widehat{\pi}) = 0$ on $\widetilde{Y}$, and $\sigma_k(x, \widehat{\pi} + \varepsilon\rho) > 0$ for $1 \leq k \leq n-1$, $x \in \widetilde{Y} \cap K$ and $0 \leq \varepsilon \leq \varepsilon_{\max}$. Moreover

$$\sigma_n(x, \widehat{\pi} + \varepsilon\rho) = \varepsilon\widehat{\sigma}_n(x, \widehat{\pi}, \rho, \varepsilon) \tag{13}$$

with a polynomial $\widehat{\sigma}_n$. We require the *nondegeneracy condition*

$$\widehat{\sigma}_n(x, \widehat{\pi}, \rho, 0) \neq 0 \text{ for all } x \in \widetilde{Y} \cap K. \tag{14}$$

Denote by $\lambda_1, \ldots, \lambda_n$ the eigenvalues of $D_1 h(x, \pi)$, choosing the labels so that $\lambda_n(x, \widehat{\pi}) = 0$ for all $x \in \widetilde{Y} \cap K$.

The following facts are known. We recall some proofs in Appendix, for the reader's convenience.

Lemma 2 (a) *One has*

$$\lambda_n(x, \widehat{\pi} + \varepsilon\rho) = \varepsilon\widehat{\lambda}_n(x, \widehat{\pi}, \rho, \varepsilon),$$

with $\widehat{\lambda}_n$ analytic, and $\widehat{\lambda}_n(x, \widehat{\pi}, \rho, 0) \neq 0$ on K.

(b) *Given $\beta > 1$, there exist $\Theta > 0$, $\theta > 0$ such that $-\Theta/\beta \leq \operatorname{Re}\lambda_i(x, \widehat{\pi}) \leq -\beta\theta$ for all $x \in \widetilde{Y} \cap K$, $1 \leq i \leq n-1$.*

(c) *For suitably small $\varepsilon_{\max}$, one has*

$$-\Theta \leq \operatorname{Re}\lambda_i(x, \widehat{\pi} + \varepsilon\rho) \leq -\theta$$

for all $(x, \varepsilon) \in K^*$, $1 \leq i \leq n-1$.

3.1 Distinguished Small Parameters

We turn to the construction of small parameters from the repository in Lemma 1. Consider the rational function

$$(x, \varepsilon) \mapsto \frac{\sigma_n(x, \widehat{\pi} + \varepsilon\rho)}{\sigma_1(x, \widehat{\pi} + \varepsilon\rho) \cdot \sigma_{n-1}(x, \widehat{\pi} + \varepsilon\rho)}, \quad x \in \widetilde{Y} \cap K,\ \varepsilon \in [0, \varepsilon_{\max}]. \tag{15}$$

Definition 2 (i) Let

$$\begin{aligned} L(\widehat{\pi}, \rho) &:= \inf_{x \in \widetilde{Y} \cap K} \left| \frac{\widehat{\sigma}_n(x, \widehat{\pi}, \rho, 0)}{\sigma_1(x, \widehat{\pi}) \cdot \sigma_{n-1}(x, \widehat{\pi})} \right|, \\ U(\widehat{\pi}, \rho) &:= \sup_{x \in \widetilde{Y} \cap K} \left| \frac{\widehat{\sigma}_n(x, \widehat{\pi}, \rho, 0)}{\sigma_1(x, \widehat{\pi}) \cdot \sigma_{n-1}(x, \widehat{\pi})} \right|. \end{aligned} \tag{16}$$

(ii) We call,

$$\varepsilon^*(\widehat{\pi}, \rho, \varepsilon) := \varepsilon \cdot U(\widehat{\pi}, \rho), \tag{17}$$

the *distinguished upper bound for the TFPV* $\widehat{\pi}$ *with parameter direction* ρ of system (7), and we call,

$$\varepsilon_*(\widehat{\pi}, \rho, \varepsilon) := \varepsilon \cdot L(\widehat{\pi}, \rho), \tag{18}$$

the *distinguished lower bound for the TFPV* $\widehat{\pi}$ *with parameter direction* ρ.

By the nondegeneracy condition, one has $U(\widehat{\pi}, \rho) \geq L(\widehat{\pi}, \rho) > 0$. We obtain the following asymptotic inequalities:

Proposition 1 *Given* $\alpha > 0$*, for sufficiently small* $\varepsilon_{\max}$*, the inequalities*

$$\frac{1}{(1+\alpha)} L(\widehat{\pi}, \rho) \leq \left| \frac{\widehat{\sigma}_n(x, \widehat{\pi}, \rho, \varepsilon)}{\sigma_1(x, \widehat{\pi} + \varepsilon\rho) \cdot \sigma_{n-1}(x, \widehat{\pi} + \varepsilon\rho)} \right| \leq (1+\alpha) U(\widehat{\pi}, \rho) \tag{19}$$

hold on K^*.

Proof By analyticity in ε one has, for $\varepsilon_{\max}$ sufficiently small,

$$\left| \frac{\widehat{\sigma}_n(x, \widehat{\pi}, \rho, \varepsilon)}{\sigma_1(x, \widehat{\pi} + \varepsilon\rho) \cdot \sigma_{n-1}(x, \widehat{\pi} + \varepsilon\rho)} - \frac{\widehat{\sigma}_n(x, \widehat{\pi}, \rho, 0)}{\sigma_1(x, \widehat{\pi}) \cdot \sigma_{n-1}(x, \widehat{\pi})} \right| \leq \text{const.} \cdot \varepsilon$$

for all $(x, \varepsilon) \in K^*$. The assertion follows.

Remark 1 There are two points to make:

- By definition, determining the distinguished upper and lower bounds amounts to determining the maximum and minimum of a rational function on a compact set. It may not be possible (or not advisable) to determine ε^* or ε_* exactly, and one may have be content with sufficiently tight upper resp. lower estimates.
- The derivation of the small parameters involves the critical manifold and the TFPV $\widehat{\pi}$, hence they depend on these choices. Moreover, there is some freedom of choice for the parameter direction ρ, which also influences the bounds. For these reasons one should not assume universal efficacy of any small parameter without further context.

3.2 The Correspondence to Timescales

We now discuss the correspondence between timescales and the parameters determined from (15). By direct verification, via (11) one finds for the eigenvalues $\lambda_1, \ldots, \lambda_n$ of $D_1 h(x, \pi)$:

Lemma 3 (a) *The identity*

$$\sum_{i\neq j}\frac{\lambda_i}{\lambda_j}=\frac{\sigma_1\sigma_{n-1}}{\sigma_n}-n \tag{20}$$

holds whenever all $\lambda_i\neq 0$.

(b) *With* $(x,\varepsilon)\in K^*$, *for* $\varepsilon\neq 0$ *one has*

$$\frac{1}{\varepsilon}\sum_{i<n}\lambda_i/\widehat{\lambda}_n+\sum_{i\neq j;\,i,j<n}\lambda_i/\lambda_j+\varepsilon\sum_{i<n}\widehat{\lambda}_n/\lambda_i=\frac{1}{\varepsilon}\frac{\sigma_1\sigma_{n-1}}{\widehat{\sigma}_n}-n.$$

This gives rise to further asymptotic inequalities:

Proposition 2 *Let* β, θ *and* Θ *be as in Lemma 2, and* $\alpha>0$. *Then, for sufficiently small* $\varepsilon_{\max}>0$, *the following hold:*

(a) *For all* $(x,\varepsilon)\in K^*$,

$$\frac{1}{(1+\alpha)}\varepsilon_*(\widehat{\pi},\rho,\varepsilon)\leq\left|\frac{\lambda_n(x,\widehat{\pi}+\varepsilon\rho)}{\sum_{i<n}\lambda_i(x,\widehat{\pi}+\varepsilon\rho)}\right|\leq(1+\alpha)\varepsilon^*(\widehat{\pi},\rho,\varepsilon). \tag{21}$$

In particular, there exist constants C_1, C_2, *such that*

$$C_1\varepsilon\leq\left|\frac{\lambda_n(x,\widehat{\pi}+\varepsilon\rho)}{\sum_{i<n}\lambda_i(x,\widehat{\pi}+\varepsilon\rho)}\right|\leq C_2\varepsilon.$$

(b) *The global estimates*

$$\frac{1}{(1+\alpha)}\varepsilon_*\leq\frac{\inf|\lambda_n|}{(n-1)\Theta}\leq\frac{\sup|\lambda_n|}{(n-1)\theta}\leq(1+\alpha)\varepsilon^* \tag{22}$$

hold, with infimum and supremum being taken over all $(x,\varepsilon)\in K^*$.

Proof From Lemma 3 one obtains that

$$\frac{|\widehat{\lambda}_n(x,\widehat{\pi},\rho,\varepsilon)|}{|\sum_{i=1}^{n-1}\lambda_i(x,\widehat{\pi}+\varepsilon\rho)|}=\left|\frac{\widehat{\sigma}_n(x,\widehat{\pi},\rho,\varepsilon)}{\sigma_1(x,\widehat{\pi}+\varepsilon\rho)\sigma_{n-1}(x,\widehat{\pi}+\varepsilon\rho)}\right|+\varepsilon\eta(x,\widehat{\pi},\rho,\varepsilon)$$

for all $(x,\varepsilon)\in K^*$, with bounded η. Combining this with Proposition 1 yields the assertions of part (a), and also

$$\frac{1}{(1+\alpha)}L(\widehat{\pi},\rho)\leq\left|\frac{\widehat{\lambda}_n(x,\widehat{\pi},\rho,\varepsilon)}{\sum_{i<n}\lambda_i(x,\widehat{\pi}+\varepsilon\rho)}\right|\leq(1+\alpha)U(\widehat{\pi},\rho)$$

for all $(x,\varepsilon)\in K^*$, provided $\varepsilon_{\max}$ is sufficiently small. Noting

$$|\sum_{i=1}^{n-1}\lambda_i(x,\pi)|=|\sum_{i=1}^{n-1}\mathrm{Re}\,\lambda_i(x,\pi)|=\sum_{i=1}^{n-1}|\mathrm{Re}\,\lambda_i(x,\pi)|,$$

the second statement follows by standard estimates.

Informally speaking, Proposition 2 provides estimates for the ratio of the slowest to the fastest timescale, with $\sum_{i<n}\lambda_i$ being dominated by the real part with largest modulus. Thus, for dimension $n > 2$, the estimates may be unsatisfactory whenever $\Theta \gg \theta$. For applications the second estimate in (22) is more relevant, since the fast dynamics will be governed by the smallest absolute real part of $\lambda_1, \dots, \lambda_{n-1}$ (see, Sect. 9.1). The parameter ε^* by itself does not completely characterize the timescale discrepancies, as should be expected. If there is more than one eigenvalue ratio to consider then a single quantity cannot measure all of them.

However, in the following—specialized but relevant—setting a general estimate can be obtained from the coefficients of the characteristic polynomial.

Proposition 3 *Let β, θ and Θ be as in Lemma 2, and $\alpha > 0$. Moreover assume that the eigenvalues $\lambda_1, \dots, \lambda_{n-1}$ satisfy $|\mathrm{Re}\,\lambda_j| > |\mathrm{Im}\,\lambda_j|$, and let $|\mathrm{Re}\,\lambda_1| \geq \cdots \geq |\mathrm{Re}\,\lambda_{n-1}|$. Define*

$$\mu^* := \varepsilon \cdot \sup_{x \in \widetilde{Y} \cap K} \left| \frac{\widehat{\sigma}_n(x, \widehat{\pi}, \rho, 0) \cdot \sigma_{n-2}(x, \widehat{\pi})}{\sigma_{n-1}(x, \widehat{\pi})^2} \right|. \tag{23}$$

Then, for sufficiently small $\varepsilon_{\max} > 0$, one has

$$\sup_{(x,\varepsilon) \in K^*} \left| \frac{\lambda_n}{\mathrm{Re}\,\lambda_{n-1}} \right| \leq \sqrt{2}(1+\alpha)\,\mu^*. \tag{24}$$

Whenever $\lambda_{n-1} \in \mathbb{R}$, then the estimate can be sharpened to

$$\sup_{(x,\varepsilon) \in K^*} \left| \frac{\lambda_n}{\mathrm{Re}\,\lambda_{n-1}} \right| \leq (1+\alpha)\,\mu^*. \tag{25}$$

Proof (i) Preliminary observation: Let $k \geq 2$ and $\beta_1, \dots, \beta_k \in \mathbb{C}$ with negative real parts, and $|\mathrm{Re}\,\beta_1| \geq \cdots \geq |\mathrm{Re}\,\beta_k|$. Moreover denote by $(-1)^\ell \tau_\ell$ the ℓ^{th} elementary symmetric polynomial in the β_j. If $|\mathrm{Re}\,\beta_j| > |\mathrm{Im}\,\beta_j|$ for $j = 1, \dots, k$, then

$$|\mathrm{Re}\,\beta_k| \geq \frac{\tau_k}{\sqrt{2}\tau_{k-1}}, \text{ and } |\beta_k| \geq \frac{\tau_k}{\tau_{k-1}} \text{ when } \beta_k \in \mathbb{R}.$$

To verify this, recall

$$\sum_{i \neq j} \frac{\beta_i}{\beta_j} = \frac{\tau_1 \tau_{k-1}}{\tau_k} - k \leq \frac{\tau_1 \tau_{k-1}}{\tau_k} - 1.$$

Now, for complex numbers z, w with negative real parts and $|\mathrm{Re}\,z| > |\mathrm{Im}\,z|$, $|\mathrm{Re}\,w| > |\mathrm{Im}\,w|$, one has $\mathrm{Re}\,\frac{z}{w} > 0$. Therefore, all $\mathrm{Re}\,\beta_i/\beta_j > 0$, $1 \leq i, j \leq$

$k-1$, and since their sum is real we obtain the estimate

$$\frac{\tau_1}{|\beta_k|} = \sum_{i=1}^{k} \frac{\beta_i}{\beta_k} = 1 + \sum_{i=1}^{k-1} \frac{\beta_i}{\beta_k} \leq \frac{\tau_1 \tau_{k-1}}{\tau_k}.$$

With $|\mathrm{Re}\,\beta_k| \geq |\beta_k|/\sqrt{2}$ the assertion follows. For real β_k the factor $\sqrt{2}$ may be discarded.

(ii) We apply the above to the $\lambda_i(x,\widehat{\pi})$ and $\sigma_j(x,\widehat{\pi})$, $1 \leq i \leq n-1$, obtaining

$$\sigma_1 \leq \sqrt{2}|\mathrm{Re}\,\lambda_{n-1}|\,\frac{\sigma_1\sigma_{n-2}}{\sigma_{n-1}}.$$

By Lemma 3, we have (with arguments $x \in \widetilde{Y} \cap K$, $\widehat{\pi}$ and ρ suppressed)

$$\left|\frac{\sigma_1\sigma_{n-1}}{\widehat{\sigma}_n}\right| = \left|\frac{\lambda_1 + \cdots + \lambda_{n-1}}{\widehat{\lambda}_n}\right| = \left|\frac{\sigma_1}{\widehat{\lambda}_n}\right| \leq \sqrt{2}\left|\frac{\mathrm{Re}\,\lambda_{n-1}}{\widehat{\lambda}_n}\right| \cdot \left|\frac{\sigma_1\sigma_{n-2}}{\sigma_{n-1}}\right|,$$

and in turn

$$\left|\frac{\widehat{\lambda}_n(x,\widehat{\pi},\rho,0)}{\mathrm{Re}\,\lambda_{n-1}(x,\widehat{\pi})}\right| \leq \sqrt{2}\,\frac{\widehat{\sigma}_n(x,\widehat{\pi},\rho,0)\sigma_{n-2}(x,\widehat{\pi})}{\sigma_{n-1}(x,\widehat{\pi})^2}.$$

By continuity and compactness the assertion readily follows when $\varepsilon_{\max}$ is sufficiently small. As in (i) the factor $\sqrt{2}$ may be discarded for real λ_{n-1}.

Remark 2 There are four observations to make:

- As with the distinguished upper bound, determining μ^* amounts to finding the maximum of a rational function on a compact set.
- The proofs of Propositions 2 and 3 implicitly impose further restrictions on $\varepsilon_{\max}$.
- Proposition 3 holds in particular in settings when all eigenvalues are "essentially real," meaning small $|\mathrm{Im}\lambda|/|\mathrm{Re}\lambda|$. This is frequently the case for chemical networks and reaction mechanisms.
- One can obviously derive analogous, but weaker estimates, whenever the ratios $|\mathrm{Im}\lambda|/|\mathrm{Re}\lambda|$ are bounded above by some constant. Likewise, the estimates underlying part (i) of the proof could be sharpened.

3.3 Two-Dimensional Systems

We turn to systems of dimension two, where a TFPV necessarily refers to a critical manifold of dimension $s = 1$. We keep the notation and conventions from Sect. 2.4. Rather than specializing the asymptotic results from Propositions 2 and 3, we will retrace their derivation and obtain slightly sharper estimates.

First and foremost, the TFPV conditions imply that σ_1 must be bounded above and below by positive constants. The accuracy of the reduction is reflected in the ratio of

the eigenvalues $\lambda_1,\ \lambda_2$ of $D_1 h(x, \widehat{\pi} + \varepsilon\rho)$ with x in the critical manifold, and $\lambda_2 = 0$ at $\widehat{\pi}$. Then

$$\sigma_1 = -(\lambda_1 + \lambda_2), \quad \sigma_2 = \lambda_1\lambda_2$$

and moreover $\lambda_2 = \varepsilon\widehat{\lambda}_2$ and $\sigma_2 = \varepsilon\widehat{\sigma}_2$. For $n = 2$ the familiar identity

$$\frac{\lambda_2}{\lambda_1} + \frac{\lambda_1}{\lambda_2} = \frac{\lambda_1^2 + \lambda_2^2}{\lambda_1\lambda_2} = \frac{\sigma_1^2 - 2\sigma_2}{\sigma_2} = \frac{\sigma_1^2}{\sigma_2} - 2 \tag{26}$$

for $\lambda_1 \neq 0,\ \lambda_2 \neq 0$ yields sharper estimates than Proposition 2. Similar estimates were also used in Eilertsen et al. (2022).

Lemma 4 (a) *For all $M > 1,\ \widetilde{M} > 2,\ M^* > 3$ the implications*

$$\begin{aligned} &|\lambda_1/\lambda_2| > M \Rightarrow |\sigma_1^2/\sigma_2| > M + 2;\\ &|\sigma_1^2/\sigma_2| \leq \widetilde{M} \Rightarrow |\lambda_1/\lambda_2| \leq \widetilde{M} - 2;\\ &|\sigma_1^2/\sigma_2| > M^* \Rightarrow |\lambda_1/\lambda_2| > M^* - 3, \end{aligned}$$

hold whenever $|\lambda_2/\lambda_1| < 1$.

(b) *In the TFPV case,*

$$\frac{1}{\varepsilon} \cdot \frac{\sigma_1^2}{\widehat{\sigma}_2} = 2 + \varepsilon\frac{\widehat{\lambda}_2}{\lambda_1} + \frac{1}{\varepsilon}\frac{\lambda_1}{\widehat{\lambda}_2}$$

and with $\varepsilon \to 0$

$$\frac{\widehat{\sigma}_2(x, \widehat{\pi}, \rho, 0)}{\sigma_1^2(x, \widehat{\pi})} = \frac{\widehat{\lambda}_2(x, \widehat{\pi}, \rho, 0)}{\lambda_1(x, \widehat{\pi})}.$$

(c) *For given $\alpha > 0$, suitable choice of $\varepsilon_{\max}$ yields*

$$\frac{1}{(1+\alpha)}\varepsilon_* \leq \inf \frac{|\lambda_2|}{|\lambda_1|} \leq \sup \frac{|\lambda_2|}{|\lambda_1|} \leq (1+\alpha)\varepsilon^*, \tag{27}$$

with infimum and supremum taken over all $(x, \varepsilon) \in K^*$.

Lemma 4 shows that ε^* provides a tight global upper estimate for the eigenvalue ratio (and thus for the timescale ratio) as $\varepsilon \to 0$, with x running through $\widetilde{Y} \cap K$. Moreover, in the analysis of particular systems, one may retrace the arguments leading to the lemma, and determine estimates for $\varepsilon_{\max}$, e.g., from higher-order Taylor expansions.

3.4 Three-Dimensional Systems

We specialize the general results to dimension three. Given the blanket assumptions from Sect. 2.4, we denote by λ_1, λ_2, and $\lambda_3 = \varepsilon\widehat{\lambda_3}$ the eigenvalues of the linearization. We have

$$U(\widehat{\pi}, \rho) = \sup_{x \in \widetilde{Y} \cap K} \left| \frac{\widehat{\sigma_3}(x, \widehat{\pi}, \rho, 0)}{\sigma_1(x, \widehat{\pi}) \cdot \sigma_2(x, \widehat{\pi})} \right|, \quad \varepsilon^*(\widehat{\pi}, \rho, \varepsilon) = \varepsilon U(\widehat{\pi}, \rho), \tag{28}$$

and similar expressions for L and ε_*.

Proposition 4 *As for applicability of the parameter μ^*, one has:*

(a)
- *The eigenvalues λ_1 and λ_2 are real if and only if $\sigma_1^2 - 4\sigma_2 \geq 0$.*
- *Given that $\lambda_1 \notin \mathbb{R}$ and $\lambda_2 = \overline{\lambda}_1$, one has $|\mathrm{Re}\,\lambda_1| > |\mathrm{Im}\,\lambda_1|$ if and only if $\sigma_1^2 - 2\sigma_2 > 0$.*

(b) *Assume that one of the conditions in part (a) holds. Then, given $\alpha > 0$, for sufficiently small $\varepsilon_{\max}$ one has*

$$\sup_{(x,\varepsilon) \in K^*} \left| \frac{\lambda_3}{\mathrm{Re}\,\lambda_2} \right| \leq \sqrt{2}(1+\alpha)\,\mu^*,$$

resp.

$$\sup_{(x,\varepsilon) \in K^*} \left| \frac{\lambda_3}{\lambda_2} \right| \leq (1+\alpha)\,\mu^* \text{ whenever } \lambda_2 \in \mathbb{R};$$

with

$$\mu^* = \varepsilon \cdot \sup_{x \in \widetilde{Y} \cap K} \left| \frac{\widehat{\sigma_3}(x, \widehat{\pi}, \rho, 0) \cdot \sigma_1(x, \widehat{\pi})}{\sigma_2(x, \widehat{\pi})^2} \right|.$$

Proof To determine the nature of the eigenvalues on the critical manifold, we use the identity

$$\left(\frac{\lambda_1 - \lambda_2}{\lambda_1 + \lambda_2} \right)^2 = 1 - 4\frac{\sigma_2}{\sigma_1^2} \text{ on } \widetilde{Y}. \tag{29}$$

This implies the (of course well known) first statement of part (a). The second statement follows from

$$-\left(\frac{\mathrm{Im}\,\lambda_1}{\mathrm{Re}\,\lambda_1} \right)^2 = 1 - 4\frac{\sigma_2}{\sigma_1^2}.$$

The rest is straightforward with Proposition 3.

Remark 3 We make the following two points

- For λ_1 and λ_2 real and negative, one obtains a lower estimate from

$$\left|\frac{2\lambda_2}{\widehat{\lambda}_3}\right| \leq \left|\frac{\lambda_1+\lambda_2}{\widehat{\lambda}_3}\right| = \left|\frac{\sigma_1\sigma_2}{\widehat{\sigma}_3}\right| \Longrightarrow 2\left|\frac{\widehat{\sigma}_3}{\sigma_1\sigma_2}\right| \leq \left|\frac{\widehat{\lambda}_3}{\lambda_2}\right| \text{ on } \widetilde{Y}\cap K.$$

- If λ_1 is not real and $\lambda_2 = \overline{\lambda}_1$, with negative real parts, then the specialization of (20), viz.

$$\frac{\lambda_1+\lambda_2}{\lambda_3} + \left(\frac{\lambda_1}{\lambda_2}+\frac{\lambda_2}{\lambda_1}\right) + \left(\frac{\lambda_3}{\lambda_1}+\frac{\lambda_3}{\lambda_2}\right) = \frac{\sigma_1\sigma_2}{\sigma_3} - 3,$$

for real λ_3, $|\lambda_3| < |\mathrm{Re}\,\lambda_1|$, shows that both the second term and the third term on the left-hand side are bounded below by -2 and above by 2, and we obtain

$$\frac{\sigma_1\sigma_2}{\sigma_3} - 7 \leq \frac{2\mathrm{Re}\,\lambda_1}{\lambda_3} \leq \frac{\sigma_1\sigma_2}{\sigma_3} + 1.$$

In particular this yields an asymptotic timescale estimate

$$\left|\frac{\widehat{\lambda}_3}{\mathrm{Re}\,\lambda_1}\right| \to 2\left|\frac{\widehat{\sigma}_3}{\sigma_1\sigma_2}\right| \text{ as } \varepsilon \to 0.$$

Remark 4 When all eigenvalues are real then one obtains the ratio of λ_1 and λ_2, with $|\lambda_2| \leq |\lambda_1|$, from

$$\frac{\sigma_2}{\sigma_1^2} = \frac{\lambda_1\lambda_2 + \varepsilon(\cdots)}{(\lambda_1+\lambda_2+\varepsilon(\cdots))^2} = \frac{\lambda_2/\lambda_1}{(1+\lambda_2/\lambda_1)^2} + \varepsilon(\cdots)$$

and the arguments leading up to Lemma 4. With

$$\kappa_* := \inf_{x\in\widetilde{Y}\cap K}\left|\frac{\sigma_2(x,\widehat{\pi})}{\sigma_1(x,\widehat{\pi})^2}\right|, \quad \kappa^* := \sup_{x\in\widetilde{Y}\cap K}\left|\frac{\sigma_2(x,\widehat{\pi})}{\sigma_1(x,\widehat{\pi})^2}\right|, \tag{30}$$

the following hold for every $\alpha > 0$, with sufficiently small ε:

- On $\widetilde{Y}\cap K$ one has

$$\left|\frac{\lambda_2}{\lambda_1}\right| \geq \frac{\kappa_*}{1+\alpha}.$$

- If $|\lambda_2/\lambda_1| \leq \delta$ for all $x \in \widetilde{Y}\cap K$ then $\kappa^* \leq \dfrac{\delta}{2\delta+1}$.

Large discrepancy between λ_1 and λ_2 (in addition to $\mu^* \ll 1$) may indicate a scenario with three timescales (informally speaking): slow, fast and very fast. Cardin and Texeira (2017) provided a rigorous extension of Fenichel theory for such settings, providing solid ground for their analysis. Note that large discrepancy between ε^* and μ^* implies large discrepancy between λ_1 and λ_2, in view of the definitions.

4 Michaelis–Menten Reaction Mechanism Revisited

The reader may wonder why we include a rather long section on the most familiar reaction in biochemistry. The basic motivation is that some widely held beliefs on its QSS variants are problematic [see, Eilertsen et al. (2022), for a recent study]. Beyond this, the timescale ratio approach actually yields new results for the reversible Michaelis–Menten (MM) system, as well as for MM with slow product formation.

4.1 The Reversible Reaction with Low Enzyme Concentration

The reversible MM reaction mechanism with low enzyme concentration corresponds to the system

$$\begin{aligned} \dot{s} &= -k_1 e_0 s + (k_1 s + k_{-1})c \\ \dot{c} &= k_1 e_0 s \quad - (k_1 s + k_{-1} + k_2)c + k_{-2}(e_0 - c)(s_0 - s - c) \end{aligned} \tag{31}$$

with standard initial conditions $s(0) = s_0$, $c(0) = 0$. The earliest discussion of (31) dates back to Miller and Alberty (1958), but the reversible reaction has garnered relatively little attention compared to the irreversible one.

The parameter space $\Pi = \mathbb{R}^6_{\geq 0}$ has elements $(e_0, s_0, k_1, k_{-1}, k_2, k_{-2})^{\mathrm{tr}}$, and we set $x = (s,\ c)^{\mathrm{tr}}$. As is well known, setting $e_0 = 0$ and all other parameters > 0 defines a TFPV, with the critical manifold $\widetilde{Y}$ given by $c = 0$. For the reduced equation, one finds (see, e.g., Noethen and Walcher 2011)

$$\dot{s} = -e_0 \cdot \frac{s(k_1 k_2 + k_{-1}k_{-2}) - k_{-1}k_{-2}s_0}{k_1 s + k_{-1} + k_2 + k_{-2}(s_0 - s)}.$$

By the first blanket assumption in Sect. 2.4, we restrict $(s_0, k_1, k_{-1}, k_2, k_{-2})^{\mathrm{tr}}$ to a compact subset of the open positive orthant. With fixed $e_0^* > 0$ (with dimension concentration), we let $\rho = (e_0^*, 0, \ldots, 0)^{\mathrm{tr}}$. We will work with both e_0 and εe_0^*. Rather than obtaining ε_* and ε^* directly from Lemma 4, we retrace their derivation and get error estimates in the process. The coefficients of the characteristic polynomial with $x \in \widetilde{Y}$ are

$$\begin{aligned} \sigma_1(x, \widehat{\pi} + \varepsilon\rho) &= k_1 e_0 + k_1 s + k_{-1} + k_2 + k_{-2}(e_0 + s_0 - s); \\ \sigma_2(x, \widehat{\pi} + \varepsilon\rho) &= e_0\,(k_1 k_{-2}(e_0 + s_0) + k_1 k_2 + k_{-1}k_{-2})\,. \end{aligned}$$

The set K (compatible with the standard initial conditions), defined by $0 \leq s \leq s_0$ and $0 \leq c \leq e_0^*$, is compact and positively invariant.

We only discuss the case $k_1 \geq k_{-2}$. The other case amounts to reversing the roles of s and p. Note that σ_2 is independent of s. The minimum of $\sigma_1(x, \widehat{\pi} + \varepsilon\rho)$ on $\widetilde{Y} \cap K$ equals

$$k_1 e_0 + k_{-1} + k_2 + k_{-2}(e_0 + s_0),$$

and the maximum is

$$k_1(e_0 + s_0) + k_{-1} + k_2 + k_{-2}e_0.$$

In particular, the minimum of $\sigma_1(x, \widehat{\pi})$ on $\widetilde{Y} \cap K$ equals

$$k_{-1} + k_2 + k_{-2}s_0.$$

Moreover, we have

$$\widehat{\sigma}_2(x, \widehat{\pi}, 0) = k_1k_{-2}s_0 + k_1k_2 + k_{-1}k_{-2},$$

a positive constant.

By Lemma 4 and its derivation, we find

$$\frac{e_0\,(k_1k_{-2}(e_0 + s_0) + k_1k_2 + k_{-1}k_{-2})}{(k_1(e_0 + s_0) + k_{-1} + k_2 + k_{-2}e_0))^2} \leq \frac{\sigma_2}{\sigma_1^2} \leq \frac{e_0\,(k_1k_{-2}(e_0 + s_0) + k_1k_2 + k_{-1}k_{-2})}{(k_1e_0 + k_{-1} + k_2 + k_{-2}(e_0 + s_0))^2},$$

valid for all $\varepsilon > 0$. Neglecting higher-order terms in ε yields

$$\varepsilon_* = \frac{e_0\,(k_1k_{-2}s_0 + k_1k_2 + k_{-1}k_{-2})}{(k_{-1} + k_2 + k_1s_0)^2}; \quad \varepsilon^* = \frac{e_0\,(k_1k_{-2}s_0 + k_1k_2 + k_{-1}k_{-2})}{(k_{-1} + k_2 + k_{-2}s_0)^2}.$$

Therefore, it seems appropriate to define the distinguished local parameter for the reversible MM system as

$$\varepsilon_{MMR} := \varepsilon^* = \frac{e_0\,(k_1k_{-2}s_0 + k_1k_2 + k_{-1}k_{-2})}{(k_{-1} + k_2 + k_{-2}s_0)^2}. \tag{32}$$

It appears that this particular parameter has not been introduced so far, nor has any close relative. Indeed, there seem to exist no parameters in the literature that were specifically derived for the reversible reaction. In their discussion of the reversible system, Seshadri and Fritzsch (1980) worked with the parameter ε_{RS} that Reich and Selkov had designed for the irreversible system; see Eq. (5).

4.2 The Irreversible Reaction with Low Enzyme Concentration

We specialize to the irreversible case, and thus we have the differential equation (1) with $e_0 = \varepsilon e_0^*$. The QSS manifold of this system is defined by $c = g(s) := e_0 s/(K_M + s)$.

4.2.1 Distinguished Small Parameters

The parameters from the reversible scenario simplify to

$$\varepsilon_* = \frac{e_0k_1k_2}{(k_1s_0 + k_{-1} + k_2)^2}; \quad \varepsilon^* = \varepsilon_{MM} := \frac{e_0k_1k_2}{(k_{-1} + k_2)^2},$$

with

$$\min \sigma_1 = k_{-1} + k_2; \quad \widehat{\sigma_2} = k_1 k_2.$$

Note that the TFPV and nondegeneracy conditions, together with the compactness condition in parameter space, require that k_2 is bounded below by some positive constant.

As in the previous section, we find that ε_{MM} is a sharp upper estimate for the eigenvalue ratio. In fact,

$$\frac{\sigma_2}{\sigma_1^2} \leq \frac{k_2 k_1 e_0}{(k_1 e_0 + k_{-1} + k_2)^2} \leq \varepsilon_{MM}$$

throughout.

As noted in Introduction, various small parameters have been proposed for the irreversible MM system. Comparing these, we note

$$\varepsilon_{MM} = \frac{e_0 k_1}{k_{-1} + k_2} \cdot \frac{k_2}{k_{-1} + k_2} \leq \frac{e_0 k_1}{k_{-1} + k_2} = \varepsilon_{RS},$$

with the Reich-Selkov parameter. Whenever k_{-1} and k_2 have the same order of magnitude (in any case k_2 must be bounded away from 0 by nondegeneracy), the disparity between ε_{MM} and ε_{RS} may be seen as inessential.

The parameters ε_{MM} and ε_{RS} differ markedly from the most familiar small parameters, viz. ε_{BH} [see (4) as used by Heineken et al. (1967)], and ε_{SSl} [see (6) as introduced in Segel and Slemrod (1989)], which both involve the initial substrate concentration. As shown in Noethen and Walcher (2007), smallness of the Segel–Slemrod parameter is necessary and sufficient to ensure negligible loss of substrate in the initial phase. But, as noted in Patsatzis and Goussis (2019) and in Eilertsen et al. (2022), large initial substrate concentration—while ensuring a fast approach to the QSS manifold—is not sufficient to guarantee a good QSS approximation over the whole course of the reaction. A general argument in favor of ε_* and ε_{MM} is that they directly measure the local ratio of timescales.

4.2.2 Further Observations

We briefly discuss what can be inferred from

$$\varepsilon_{MM} = \frac{k_1 k_2 e_0}{(k_{-1} + k_2)^2} \to 0$$

alone, with no further restriction on the limiting process.

In the simplest imaginable scenario, letting a parameter tend to zero might automatically imply validity of some QSS approximation, but this is not the case here. The TFPV conditions on σ_1 imply that k_{-1} is bounded above and we obtain three cases: In addition to the case $e_0 \to 0$, we have the case $k_1 \to 0$, yielding a singular

perturbation reduction with the same critical manifold but a linear reduced equation. Furthermore we have the case $k_2 \to 0$, which leads to a singular perturbation scenario with a different critical manifold and different reduction (see, the next subsection).

This observation supports a statement from Introduction. A given small parameter by itself will in general not determine a unique singular perturbation scenario, and a transfer without reflection of the reduction procedure from one scenario to a different one may yield incorrect results. It is necessary to consider the complete setting, including TFPV, critical manifold and small parameter. Moreover, one needs to carefully stipulate how limits are taken. For instance, letting $s_0 \to \infty$, while ensuring $\varepsilon_{SSl} \to 0$, will fail to ensure convergence. Likewise, letting, e.g., $k_{-1} \to \infty$ in the Reich-Selkov parameter does not imply convergence.

For the irreversible reaction with substrate inflow at rate k_0, one obtains the same expressions for σ_2/σ_1^2 at the TFPV with $k_0 = 0$ and $e_0 = 0$ (all other parameters > 0), the critical manifold being given by $c = 0$. Before obtaining ε_*, ε^* one needs to choose appropriate initial conditions; we take $s(0) = c(0) = 0$ here. Solutions are not necessarily confined to compact sets, so one may not be able to choose the set K from Sect. 2.4 to be positively invariant. In the case $s(0) = c(0) = 0$ the computation of the distinguished upper bound ε^* works as in the case with no influx; the supremum exists and is equal to ε_{MM}. However, one gets $\varepsilon_* \to 0$ with increasing s when there exists no positive stationary point (all solutions are unbounded in positive time), hence the lower estimate provides no information. If there exists a finite positive stationary point $\widetilde{s}$ of the reduced equation, then one obtains $\varepsilon_* > 0$ by replacing s_0 by $\widetilde{s}$ in the lower estimate in 4.2.1. In this case, a compact positively invariant set exists with $s \leq \widetilde{s}$, as was shown in Eilertsen et al. (2021b).

4.3 The Irreversible Reaction with Slow Product Formation

We turn to the scenario with slow product formation, the other reactions being fast.[11] Here $k_2 = 0$, with all other parameters > 0, defines a TFPV with critical manifold $\widetilde{Y}$ given by

$$c = \frac{k_1 e_0 s}{k_1 s + k_{-1}}.$$

Although setting up $k_2 = 0$ appears counterintuitive for an enzyme catalayzed reaction, there is a family of enzymes, known as pseudoenzymes, that have either zero catalytic activity ($k_2 = 0$), or vestigial catalytic activity ($k_2 \approx 0$) due to the lack of catalytic amino acids or motifs (Eyers and Murphy 2016). These enzymes exist in all the kingdoms of life and are also named as "zombie" enzyme, dead enzyme, or prozymes. Pseudoenzymes play different functions in signaling network, such as serving as dynamic scaffolds, modulators of enzymes, or competitors in canonical signaling pathways (Murphy et al. 2017). Since one frequently finds incorrect reductions in the literature, it seems appropriate to recall correct ones. Heineken et al. (1967) provided a correct reduction (see, (34) below). In Goeke and Walcher (2013), a version

[11] Historically, this was the mechanism first discussed by Michaelis and Menten (1913).

for substrate concentration is given:

$$\dot{s} = -\frac{k_2 k_1 e_0 s(k_1 s + k_{-1})}{k_1 k_{-1} e_0 + (k_1 s + k_{-1})^2} = -\frac{k_2 e_0 s(s + K_S)}{K_S e_0 + (s + K_S)^2}; \qquad K_S := k_{-1}/k_1.$$

With known e_0, this equation[12] in principle allows to identify the limiting rate $k_2 e_0$ and the equilibrium constant K_S. It should be noted that one also needs an appropriate initial time and initial value for the reduction. Since one cannot assume negligible substrate loss in the transient phase, an appropriate fitting would require completion of Step 2 of the program outlined in Introduction.

4.3.1 Distinguished Small Parameters

Intersecting $\widetilde{Y}$ with the positively invariant compact set K defined by $0 \le s \le s_0$ and $0 \le c \le e_0$, amounts to restricting $0 \le s \le s_0$. The elements of the parameter space $\Pi = \mathbb{R}^5_{\ge 0}$ have the form $(e_0, s_0, k_1, k_{-1}, k_2)^{\mathrm{tr}}$, and a natural choice of ray direction is $\rho = (0, 0, 0, 0, k_2^*)^{\mathrm{tr}}$, with $k_2 = \varepsilon k_2^*$.

The coefficients of the characteristic polynomial on $\widetilde{Y}$ are

$$\sigma_1 = \frac{k_{-1} k_1 e_0}{k_1 s + k_{-1}} + k_1 s + k_{-1} + k_2,$$
$$\sigma_2 = e_0 k_1 k_2 \cdot \frac{k_{-1}}{k_1 s + k_{-1}}.$$

To distinguish small parameters, we need to consider the following steps:

- We first evaluate the nondegeneracy conditions for the coefficients of the characteristic polynomial, from TFPV requirements and compactness. The minimum of $\sigma_1(x, \widehat{\pi})$ on $\widetilde{Y} \cap K$ is equal to $k_{-1} + k_1 e_0$ when $k_1 e_0 \le k_{-1}$, and equal to $2\sqrt{k_{-1} k_1 e_0}$ otherwise. This minimum must be bounded below by some positive constant. Combining this observation with the boundedness of the maximum of

$$\widehat{\sigma}_2 = \frac{k_2^* k_{-1} k_1 e_0}{k_1 s + k_{-1}} \quad \text{on} \quad [0,\ s_0],$$

  which is equal to $k_2^* k_1 e_0$, one sees that $k_1 e_0$ and k_{-1} must be bounded above and below by positive constants.
- Turning to small parameters, in the asymptotic limit one obtains

$$\varepsilon^* = k_2 \sup \frac{a v}{(a + v^2)^2} \quad \text{with} \quad a = k_{-1} k_1 e_0,\ v = k_1 s + k_{-1},$$

  where the supremum is taken over $k_{-1} \le v \le k_{-1} + k_1 s_0$. By elementary calculus one finds the global maximum of this function on the unbounded interval $v \ge 0$,

[12] The commonly used quasi-steady state reduction (see, for instance, Keener and Sneyd 2009, Section 1.4.1) reads $\dot{s} = -\frac{k_2 e_0 s}{s + K_S}$ and thus neglects the term involving e_0 in the denominator, although e_0 is not negligible here.

thus for sufficiently large s_0 we obtain the maximum at $v = \sqrt{k_{-1}k_1e_0/3}$, and find the estimate

$$\varepsilon^* \leq \frac{3\sqrt{3}}{16}\frac{k_2}{\sqrt{k_{-1}\cdot k_1e_0}} =: \frac{3\sqrt{3}}{8}\cdot\varepsilon_{PE}, \quad \text{with } \varepsilon_{PE} := \frac{2k_2}{\sqrt{k_{-1}\cdot k_1e_0}}.$$

Note that ε_{PE} always yields an upper estimate for the eigenvalue ratio near the critical manifold. One could thus discard the factor $1+\alpha$ in Lemma 4.

- Depending on the given parameters, in some cases one may obtain sharper estimates for ε^* from the endpoints of the interval $[0, s_0]$. In any case, to determine ε_* one needs to consider the boundary points of this interval.
- The expression for ε_{PE} may look strange, but $\sqrt{k_2/k_{-1}}\cdot\sqrt{k_2/(k_1e_0)}$ is the geometric mean of two reaction rate ratios, thus admits a biochemical interpretation. There is little work in the literature on small parameters for the case of slow product formation. Heineken et al. (1967) suggested $k_2/(k_1s_0)$, while Patsatzis and Goussis introduced a parameter depending on s and c along a trajectory, taking the maximum over all s, c yields k_2/k_{-1}. The latter represents a commonly accepted "small parameter" for this scenario; see, Keener and Sneyd (2009, Section 1.4.1). In the limiting case $k_2 \to 0$, one also has $\varepsilon_{MM} \to 0$, but one should not conclude that the standard QSS approximation is valid here. Recall that, in the low enzyme setting, k_2 needs to be bounded away from zero due to nondegeneracy requirements.

4.3.2 Approach to the Slow Manifold

For MM reaction mechanism with slow product formation, we specialize the arguments in Appendix 9.1.1 to determine ε_L, and show that ε_{PE} appears naturally in this estimate.[13] We use the results (and refer to the notation) of Sect. 9.1.

We rewrite the system in Tikhonov standard form. Since $\frac{d}{dt}(s+c) = -k_2c$, $s+c$ is a first integral of the fast system in the limit $k_2 = 0$, with $x = s+c$, $y = s$ (so $c = x-y$, $x \geq y \geq 0$), and $k_2 = \varepsilon k_2^*$ we obtain

$$\begin{aligned}\dot{x} &= -k_2(x-y)\\ \dot{y} &= -k_1e_0y + (k_1y+k_{-1})(x-y)\\ &= -k_1(y-h_-(x))\cdot(y-h_+(x))\end{aligned} \tag{33}$$

with

$$h_\pm(x) := \frac{1}{2}\left(-(K_S+e_0-x) \pm q(x)\right); \quad q(x) := \sqrt{(K_S+e_0-x)^2+4K_Sx}.$$

We focus on the particular initial conditions with zero complex, thus

$$x(0) = y(0) = s_0.$$

[13] Step 1 for the case of low enzyme concentration is more involved. A complete discussion of Steps 1–3 will be given in a forthcoming paper.

The QSS variety $\widetilde{Y}$ is defined by $y = h_+(x)$, and the reduced equation reads

$$\dot{x} = -\frac{k_2}{2}\left((K_S + e_0 + x) - \sqrt{(K_S + e_0 - x)^2 + 4K_S x}\right). \tag{34}$$

We use the notation and apply the general procedure from the Sect. 9.1, with

$$A = -k_1(y - h_-(x)) = -k_1 q(x) \quad \text{on} \quad \widetilde{Y},$$

and $g(x) = h_+(x)$. We will use some properties of q in the following. The calculation of $q'(x)$ leads to

$$q'(x) = \frac{K_S + x - e_0}{\sqrt{(K_S + e_0 - x)^2 + 4K_S x}},$$

hence $|q'(x)| \leq 1$ for all $x \geq 0$. Moreover, the sign of q' changes from $-$ to $+$ at $x = e_0 - K_S$ when $e_0 - K_S \geq 0$, and is otherwise positive for all $x \geq 0$. Thus, the minimum of q is attained at 0, with value $K_S + e_0$, when $e_0 < K_S$, and is attained at $e_0 - K_S$, with value $2\sqrt{K_S e_0}$, when $e_0 \geq K_S$. By the arithmetic–geometric mean inequality, we thus have

$$q(x) \geq 2\sqrt{K_S e_0} \quad \text{for all } x \geq 0.$$

This shows

$$A \leq -2k_1\sqrt{K_S e_0} = -2\sqrt{k_1 e_0 k_{-1}},$$

and we arrive at

$$\gamma = \sqrt{k_1 e_0 k_{-1}}.$$

According to Sect. 9.1, γ^{-1} is an appropriate timescale for the approach to the slow manifold.

To determine κ, we have $g(x) = h_+(x) = \frac{1}{2}(x - K_S - e_0 + q(x))$, thus $|g'(x)| \leq 1$, and

$$|f_1(x, y)| = k_2(x - y) \leq k_2 e_0, \quad \text{since } x - y = c \leq e_0,$$

hence we may set $\kappa = k_2 e_0$.

Altogether, we obtain from the Lyapunov function the (dimensional) parameter

$$\varepsilon_L = \frac{2\kappa}{\gamma} = e_0 \cdot \varepsilon_{PE}. \tag{35}$$

To obtain a non-dimensional small parameter, normalization by e_0 seems to be the natural choice here, which yields

$$\widehat{\varepsilon}_L = \varepsilon_{PE}. \tag{36}$$

In this particular setting, the local timescale parameter completely characterizes the approach of the solution to the slow manifold.

4.3.3 Estimates for Long Times

We will not attempt to estimate a critical time for the onset of the slow dynamics, and without this we cannot determine approximation errors for solutions of the reduced equation (as outlined in Sect. 9.1.3). In this respect, the discussion of the MM reaction mechanism with slow product formation remains incomplete. But the following observation provides a relevant condition for the long-term behavior. Since $|y - g(x)| \to e_0 \cdot \varepsilon_{PE}$, the solution will enter the domain with $|y - g(x)| \leq 2e_0 \cdot \varepsilon_{PE}$ after some short transitory phase.[14] In this domain, we obtain the reduced equation with error term:

$$\begin{aligned} \dot{x} &= -k_2(x - g(x)) + k_2(y - g(x)) \\ &\leq -\frac{k_2}{2}\left((K_S + e_0 + x) - \sqrt{(K_S + e_0 - x)^2 + 4K_S x}\right) \\ &\quad + k_2 \cdot \frac{2k_2 e_0}{\sqrt{k_1 e_0 \cdot k_{-1}}} =: U(x). \end{aligned} \tag{37}$$

By a differential inequality argument, the solution of $\dot{x} = U(x)$, with positive initial value, is an upper bound for the first entry of the solution of (33), given appropriate initial values near the QSS variety. Moreover the solution of the reduced equation (34) with the same initial value remains positive. For $t \to \infty$, the absolute value of the difference of these solutions converges to the stationary point of $\dot{x} = U(x)$, which therefore indicates the discrepancy. We determine the stationary point, neglecting terms of order > 1 in k_2:

$$\begin{aligned} \left((K_S + e_0 + x) - 4\frac{k_2 e_0}{\sqrt{k_1 e_0 \cdot k_{-1}}}\right)^2 &= (K_S + e_0 - x)^2 + 4K_S x \\ \Rightarrow e_0 x &= \frac{2k_2 e_0}{\sqrt{k_1 e_0 \cdot k_{-1}}} \cdot (K_S + e_0 + x) + \cdots \\ \Rightarrow \frac{x}{e_0} &= 2\frac{k_2}{\sqrt{k_1 e_0 \cdot k_{-1}}} \cdot \frac{k_1 e_0 + k_{-1}}{k_1 e_0} + \cdots . \end{aligned}$$

Thus, we obtain the parameter

$$\varepsilon_\infty = \frac{k_1 e_0 + k_{-1}}{k_1 e_0} \cdot \frac{2k_2}{\sqrt{k_1 e_0 \cdot k_{-1}}} = \frac{k_1 e_0 + k_{-1}}{k_1 e_0} \cdot \varepsilon_{PE}, \tag{38}$$

[14] The factor 2 could be replaced by any constant > 1.

which provides an upper bound for the long-term discrepancy of the true solution and its approximation.

4.4 A Degenerate Scenario

To illustrate the limitations of the approach via Proposition 2, consider the irreversible system with TFPV $k_{-1} = k_2 = 0$, the other parameters positive, and $\rho = (0, 0, 0, k_{-1}^*, k_2^*)^{\mathrm{tr}}$. Here the critical variety is reducible, being the union of the lines Y_1, Y_2 defined by $e_0 - c = 0$ resp. $s = 0$, and the TFPV conditions fail at their intersection. We consider the case $e_0 < s_0$, and define $\widetilde{Y}_1$ by $c = e_0,\ s > 0$. The fast system admits the first integral $s + c$, so the initial value of the slow system on $\widetilde{Y}_1$ is close to $(s_0 - e_0, e_0)^{\mathrm{tr}}$. Proceeding, one may choose

$$K = \left\{(s, c)^{\mathrm{tr}};\ s + c \le s_0,\ s \ge \widetilde{s}\right\}, \quad 0 < \widetilde{s} < s_0 - e_0.$$

Then, $\widetilde{Y}_1 \cap K$ is compact, but not positively invariant, and on this set one has

$$\sigma_1 = k_1 s, \quad \sigma_2 = 0, \text{ and } \widehat{\sigma}_2 = 0.$$

Here, the nondegeneracy condition in (13) fails, and we obtain no timescale ratio by way of Lemma 4. A direct computation in a neigborhood of $\widetilde{Y}_1$ yields

$$\lambda_2/\lambda_1 = \varepsilon k_1 k_2^* (e_0 - c),$$

but this obscures the fact that both eigenvalues approach zero as $s \to 0$. Standard singular perturbation methods are not sufficient to analyze the dynamics of this system for small ε.

5 TFPV for Higher Dimensions

We keep the notation and conventions from Sects. 2.1 and 2.4, but now we will focus on a TFPV $\widehat{\pi}$ for dimension $s > 1$. The goal of this technical section is to identify distinguished parameters and discuss their relation to timescales. There is a rather obvious direct extension of results from the $s = 1$ case, but the timescale correspondence will be not as pronounced. Moreover, we will need to impose a stronger nondegeneracy condition. We abbreviate

$$\widetilde{\sigma}_i(x, \varepsilon) := \sigma_i(x, \widehat{\pi} + \varepsilon\rho), \quad 1 \le i \le n, \tag{39}$$

keeping in mind that $\widetilde{\sigma}_i(x, 0) > 0$ for all $x \in \widetilde{Y} \cap K$ and $1 \le i \le n - s$, due to $\widehat{\pi}$ being a TFPV. Additionally, we set $\widetilde{\sigma}_0 := 1$.

5.1 Distinguished Small Parameters

Some notions and results from Sect. 3 can easily be modified for the case $s > 1$. For suitable $\varepsilon_{\max} > 0$, we have

$$\sigma_i(x, \widehat{\pi} + \varepsilon\rho) > 0 \text{ for all } (x, \varepsilon) \in K^*, \quad 1 \le i \le n - s,$$

and due to $\sigma_{n-s+1}(x, \widehat{\pi}) = 0$ for $x \in \widetilde{Y} \cap K$, we obtain

$$\sigma_{n-s+1}(x, \widehat{\pi} + \varepsilon\rho) = \varepsilon\widehat{\sigma}_{n-s+1}(x, \widehat{\pi}, \rho, \varepsilon)$$

with a polynomial $\widehat{\sigma}_{n-s+1}$, for all $(x, \varepsilon) \in K^*$.

Definition 3 Let

$$\begin{aligned} L(\widehat{\pi}, \rho) &:= \inf_{x \in \widetilde{Y} \cap K} \left| \frac{\widehat{\sigma}_{n-s+1}(x, \widehat{\pi}, \rho, 0)}{\sigma_1(x, \widehat{\pi}) \cdot \sigma_{n-s}(x, \widehat{\pi})} \right|, \\ U(\widehat{\pi}, \rho) &:= \sup_{x \in \widetilde{Y} \cap K} \left| \frac{\widehat{\sigma}_{n-s+1}(x, \widehat{\pi}, \rho, 0)}{\sigma_1(x, \widehat{\pi}) \cdot \sigma_{n-s}(x, \widehat{\pi})} \right|. \end{aligned} \tag{40}$$

Now, we define

$$\varepsilon^*(\widehat{\pi}, \rho, \varepsilon) := \varepsilon U(\widehat{\pi}, \rho) \tag{41}$$

the *distinguished upper bound for the TFPV* $\widehat{\pi}$ *for dimension* s, *with parameter direction* ρ, of system (7). Moreover we call

$$\varepsilon_*(\widehat{\pi}, \rho, \varepsilon) := \varepsilon L(\widehat{\pi}, \rho) \tag{42}$$

the *distinguished lower bound for the TFPV* $\widehat{\pi}$ *for dimension* s *with parameter direction* ρ.

As in the case of reduction to dimension one, determining the distinguished parameters amounts to determining the extrema of a rational function on a compact set, or (when this is not possible, or not sensible) determining reasonably sharp estimates for these extrema. We note the following straightforward variant of Proposition 1.

Proposition 5 *Given* $\alpha > 0$, *for sufficiently small* $\varepsilon_{\max}$, *the estimates*

$$\frac{\varepsilon}{(1+\alpha)} L(\widehat{\pi}, \rho) \le \left| \frac{\sigma_{n-s+1}(x, \widehat{\pi} + \varepsilon\rho)}{\sigma_1(x, \widehat{\pi} + \varepsilon\rho) \cdot \sigma_{n-s}(x, \widehat{\pi} + \varepsilon\rho)} \right| \le \varepsilon(1+\alpha) U(\widehat{\pi}, \rho) \tag{43}$$

hold on K^*.

5.2 The Correspondence to Timescales

Proofs of the following statements are given in Appendix (Lemmas 6 and 7).

Let $\widehat{\pi}$ be a TFPV for dimension s, with critical manifold $\widetilde{Y}$. Then for all $x \in \widetilde{Y} \cap K$ one has

$$\widetilde{\sigma}_i(x,\varepsilon) = \varepsilon^{i-n+s}\widehat{\sigma}_i(x,\varepsilon) \text{ for all } x \in \widetilde{Y} \cap K, \quad n-s \le i \le n, \tag{44}$$

with polynomials $\widehat{\sigma}_i$.

Assume that (44) is given, and furthermore assume the nondegeneracy condition

$$\widehat{\sigma}_{n-s}(x,0) \neq 0 \text{ and } \widehat{\sigma}_n(x,0) \neq 0 \text{ on } \widetilde{Y} \cap K. \tag{45}$$

Then the zeros $\lambda_i(x, \widehat{\pi} + \varepsilon\rho)$ of the characteristic polynomial can be labeled such that

$$\lambda_1(x,\widehat{\pi}) \neq 0, \ldots, \lambda_{n-s}(x,\widehat{\pi}) \neq 0 \quad \text{on } \widetilde{Y} \cap K,$$

and

$$\lambda_i(x,\widehat{\pi}+\varepsilon\rho) = \varepsilon\widehat{\lambda}_i(x,\widehat{\pi},\rho,\varepsilon), \quad n-s+1 \le i \le n$$

with continuous functions in ε.

Given the nondegeneracy assumptions, we turn to discussing the correspondence of ε_* and ε^* to timescales. By (11), and by the definition of $\widetilde{\sigma}_i$ in (39), one has

$$\begin{aligned}
-\widetilde{\sigma}_1 &= \lambda_1 + \cdots + \lambda_{n-s} + \varepsilon(\cdots);\\
(-1)^{n-s}\widetilde{\sigma}_{n-s} &= \sum \lambda_{j_1}\cdots\lambda_{j_{n-s}} = \lambda_1\cdots\lambda_{n-s} + \varepsilon(\cdots);\\
(-1)^{n-s+1}\widetilde{\sigma}_{n-s+1} &= \sum \lambda_{i_1}\cdots\lambda_{i_{n-s+1}}\\
&= \lambda_1\cdots\lambda_{n-s}(\lambda_{n-s+1}+\cdots+\lambda_n) + \varepsilon^2(\cdots).
\end{aligned}$$

This directly provides a result on separation of timescales.

Proposition 6 *Assume that the nondegeneracy condition (45) holds.*

(a) *The identity*

$$\frac{\widetilde{\sigma}_{n-s+1}}{\widetilde{\sigma}_1\widetilde{\sigma}_{n-s}} = \frac{\lambda_{n-s+1}+\cdots+\lambda_n}{\lambda_1+\cdots+\lambda_{n-s}} + \varepsilon^2(\cdots) = \varepsilon\frac{\widehat{\lambda}_{n-s+1}+\cdots+\widehat{\lambda}_n}{\lambda_1+\cdots+\lambda_{n-s}} + \varepsilon^2(\cdots)$$

holds on K^*, with $(\cdots)$ representing a continuous function.

(b) *Given $\alpha > 0$, and $\varepsilon_{\max}$ sufficiently small, the estimates*

$$\frac{1}{(1+\alpha)}\varepsilon_*(\widehat{\pi},\rho,\varepsilon) \le \left|\frac{\sum_{i\le n-s}\lambda_i(x,\widehat{\pi}+\varepsilon\rho)}{\sum_{j>n-s}\lambda_j(x,\widehat{\pi}+\varepsilon\rho)}\right| \le (1+\alpha)\varepsilon^*(\widehat{\pi},\rho,\varepsilon) \tag{46}$$

hold for all $(x, \varepsilon) \in K^*$. *In particular, there exist constants* $C_1,\ C_2$ *such that*

$$C_1\varepsilon \leq \left| \frac{\sum_{i\leq n-s} \lambda_i(x, \widehat{\pi} + \varepsilon\rho)}{\sum_{j>n-s} \lambda_j(x, \widehat{\pi} + \varepsilon\rho)} \right| \leq C_2\varepsilon.$$

Thus, for higher dimensions of the critical manifold the coefficients of the characteristic polynomial still provide—albeit weaker—estimates for timescale ratios. Informally speaking, $\widetilde{\sigma}_{n-s+1}/(\widetilde{\sigma}_1\widetilde{\sigma}_{n-s})$ measures the ratio of the "fastest slow timescale" and the "fastest fast timescale." Similar to the situation for $s = 1$, a more relevant ratio is the one of the "fastest slow timescale" and the "slowest fast timescale." We invite readers to compare Sect. 9.1 in Appendix. We remark that for real or "essentially real" $\lambda_1, \ldots, \lambda_{n-s}$ one may obtain results similar to Proposition 3, but we will not pursue this further.

5.3 Further Dimensionless Parameters

Given the setting of (44), it is natural to ask about different types of dimensionless small parameters, in addition to the distinguished ones obtained from Proposition 5. We consider terms of the form

$$\frac{\widetilde{\sigma}_{n-s+k}}{\widetilde{\sigma}_{j_1} \cdots \widetilde{\sigma}_{j_\ell} \cdot \widetilde{\sigma}_{n-s+v_1} \cdots \widetilde{\sigma}_{n-s+v_m}}$$

with $k \geq 1$, $\ell \geq 0$, $m > 0$, and the indices $1 \leq j_1 \leq \cdots \leq j_\ell$, $1 \leq v_1 \leq \cdots \leq v_m$ subject to the following conditions:

(1) "Dimensionless": This mean by Lemma 1

$$j_1 + \cdots + j_\ell + (n-s) + v_1 + \cdots + (n-s) + v_m = (n-s) + k.$$

(2) "Order one in ε":

$$v_1 + \cdots + v_m = k - 1.$$

Proposition 7 *The only classes of dimensionless small parameters that satisfy (1) and (2) are the following:*

(a) $m = 1$ *with* $\ell = 1$ *and* $j_1 = 1$, *with parameters*

$$\frac{\widetilde{\sigma}_{n-s+k}}{\widetilde{\sigma}_1\, \widetilde{\sigma}_{n-s+k-1}}, \quad 2 \leq k \leq s. \tag{47}$$

(b) $m = 2$, $n \geq 4$, $s = n-1$ *and* $\ell = 0$, *with parameters*

$$\frac{\widetilde{\sigma}_{2+v_1+v_2}}{\widetilde{\sigma}_{1+v_1}\, \widetilde{\sigma}_{1+v_2}}, \quad 1 \leq v_1 \leq v_2, \quad v_1 + v_2 \leq n-2. \tag{48}$$

Proof Combining (1) and (2) one finds

$$j_1 + \cdots + j_\ell + (m-1)\,(n-s) = 1,$$

thus, necessarily $m \leq 2$ due to $s < n$. In case $m = 1$, one has $\ell = 1$ and $j_1 = 1$. In case $m = 2$, one necessarily has $s = n-1$ and $\ell = 0$.

To obtain explicit parameter bounds in the first case, use

$$\sigma_{n-s+j}(x, \widehat{\pi} + \varepsilon\rho) = \varepsilon^j \widehat{\sigma}_{n-s+j}(x, \widehat{\pi}, \rho, \varepsilon), \quad j \geq 1$$

to determine

$$\begin{aligned}
\widetilde{L}_j(\widehat{\pi}, \rho) &:= \inf_{x \in \widetilde{Y} \cap K} \left| \frac{\widehat{\sigma}_{n-s+j}(x, \widehat{\pi}, \rho, 0)}{\widehat{\sigma}_{n-s+j-1}(x, \widehat{\pi}, \rho, 0)\, \sigma_1(x, \widehat{\pi})} \right|, \\
\widetilde{U}_j(\widehat{\pi}, \rho) &:= \sup_{x \in \widetilde{Y} \cap K} \left| \frac{\widehat{\sigma}_{n-s+j}(x, \widehat{\pi}, \rho, 0)}{\widehat{\sigma}_{n-s+j-1}(x, \widehat{\pi}, \rho, 0)\, \sigma_1(x, \widehat{\pi})} \right|,
\end{aligned}$$

and small parameters

$$\delta_{j*} := \varepsilon \cdot \widetilde{L}_j(\widehat{\pi}, \rho, 0), \quad \delta_j^* := \varepsilon \cdot \widetilde{U}_j(\widehat{\pi}, \rho, 0), \quad j \geq 2.$$

Remark 5 In the first case, there is a notable correspondence to eigenvalues (thus to timescales). A variant of the argument in Proposition 6 shows that

$$\frac{\widetilde{\sigma}_{n-s+k}}{\widetilde{\sigma}_1\, \widetilde{\sigma}_{n-s+k-1}} = \varepsilon \frac{\tau_k(\widehat{\lambda}_{n-s+1}, \ldots, \widehat{\lambda}_n)}{(\lambda_1 + \cdots + \lambda_{n-s}) \cdot \tau_{k-1}(\widehat{\lambda}_{n-s+1}, \ldots, \widehat{\lambda}_n)} + \varepsilon^2(\cdots),$$

where τ_ℓ denotes the ℓ^{th} elementary symmetric polynomial in s variables.

5.4 Dimension Three

We specialize the results to dimension three and $s = 2$, assuming nondegeneracy. By (44), $\widetilde{\sigma}_2$ is of order ε, and $\widetilde{\sigma}_3$ is of order ε^2.

In view of Propositions 5 and 6, we consider

$$\frac{\widetilde{\sigma}_2}{\widetilde{\sigma}_1^2} = \varepsilon \frac{\widehat{\lambda}_2 + \widehat{\lambda}_3}{\lambda_1} + \varepsilon^2 \cdots.$$

Informally speaking, this expression governs the ratio of the fastest slow timescale to the fast timescale, which is the pertinent ratio according to Sect. 9.1.2. We obtain

$$U = \sup_{x \in \widetilde{Y} \cap K} \left| \frac{\widehat{\sigma}_2(x, \widehat{\pi}, \rho, 0)}{\sigma_1(x, \widehat{\pi})^2} \right|, \quad \varepsilon^* = \varepsilon \cdot U$$

as well as

$$L = \inf_{x\in\widetilde{Y}\cap K}\left|\frac{\widehat{\sigma}_2(x,\widehat{\pi},\rho,0)}{\sigma_1(x,\widehat{\pi})^2}\right|, \quad \varepsilon_* = \varepsilon\cdot L.$$

Similar to the observations in Remark 4, disparate slow eigenvalues may indicate a scenario with three timescales (informally speaking, fast, slow and very slow). To measure the disparity, we use Proposition 7 and consider

$$\frac{\widetilde{\sigma}_3}{\widetilde{\sigma}_1\widetilde{\sigma}_2} = \varepsilon\frac{\lambda_1\widehat{\lambda}_2\widehat{\lambda}_3}{(\lambda_1+\varepsilon\cdots)(\lambda_1(\widehat{\lambda}_2+\widehat{\lambda}_3)+\varepsilon\cdots)} = \varepsilon\frac{\widehat{\lambda}_2\widehat{\lambda}_3}{\lambda_1(\widehat{\lambda}_2+\widehat{\lambda}_3)}+\varepsilon^2\cdots.$$

Combining parameters shows

$$\frac{\widetilde{\sigma}_1\widetilde{\sigma}_3}{\widetilde{\sigma}_2^2} = \frac{\widehat{\lambda}_2\widehat{\lambda}_3}{(\widehat{\lambda}_2+\widehat{\lambda}_3)^2}+\varepsilon\cdots = \frac{\widehat{\lambda}_3/\widehat{\lambda}_2}{(1+\widehat{\lambda}_3/\widehat{\lambda}_2)^2}+\varepsilon\cdots.$$

Thus, the constants

$$\kappa^* := \sup_{x\in\widetilde{Y}\cap K}\frac{\sigma_1(x,\widehat{\pi})\widehat{\sigma}_3(x,\widehat{\pi},\rho,0)}{\widehat{\sigma}_2(x,\widehat{\pi},\rho,0)^2} \text{ and } \kappa_* := \inf_{x\in\widetilde{Y}\cap K}\frac{\sigma_1(x,\widehat{\pi})\widehat{\sigma}_3(x,\widehat{\pi},\rho,0)}{\widehat{\sigma}_2(x,\widehat{\pi},\rho,0)^2}$$

measure the disparity of $\widehat{\lambda}_2$ and $\widehat{\lambda}_3$. In particular, given that $|\lambda_3|\leq|\lambda_2|$ one has

$$\left|\frac{\lambda_3}{\lambda_2}\right| \geq \kappa_* \text{ throughout } \widetilde{Y}\cap K.$$

6 Case Studies: Reduction from Dimension Three to One

In this section, we discuss two biochemically relevant modifications of the MM reaction mechanism and a non-Michaelis–Menten reaction mechanism, with low enzyme concentration, and their familiar (quasi-steady state) reductions to dimension one. This seems to be the first instance that small parameters in the spirit of Segel and Slemrod—although consistently based on linear timescales—are derived for these reaction mechanisms in a systematic manner. Note that, in the application-oriented literature, the perturbation parameter of choice mostly seems to be $\varepsilon_{BH} = e_0/s_0$, on loan from the MM reaction mechanism.

We will directly consider the asymptotic small parameters ε^*, ε_*, μ^* by application of the results in Sect. 3, and obtain rather satisfactory estimates for these. Considering the steps outlined in the Introduction, we thus complete a substantial part of Step 1. Proceeding beyond this, along the lines of Sect. 9.1, would involve considerable and lengthy work for each system, so we will not go further. However, to test and illustrate the efficacy of the parameters, we include extensive numerical simulations. We also include examples that demonstrate the limitations of the local timescale approach,

and in particular show that the nondegeneracy conditions imposed on the "non-small" parameters are necessary.

6.1 Cooperativity Reaction Mechanism

The (irreversible) cooperative reaction mechanism

$$\begin{aligned} E + S &\underset{k_{-1}}{\overset{k_1}{\rightleftharpoons}} C_1 \overset{k_2}{\rightharpoonup} E + P, \\ S + C_1 &\underset{k_{-3}}{\overset{k_3}{\rightleftharpoons}} C_2 \overset{k_4}{\rightharpoonup} C_1 + P \end{aligned} \tag{49}$$

is a non-Michaelis–Menten reaction mechanism of enzyme action. It is modeled by the mass action equations

$$\begin{aligned} \dot{s} &= -k_1(e_0 - c_1 - c_2)s + k_{-1}c_1 - k_3 s c_1 + k_{-3}c_2, \\ \dot{c}_1 &= k_1(e_0 - c_1 - c_2)s - (k_{-1} + k_2)c_1 - k_3 s c_1 + (k_4 + k_{-3})c_2, \\ \dot{c}_2 &= k_3 s c_1 - (k_4 + k_{-3})c_2, \end{aligned} \tag{50}$$

via stoichiometric conservation laws. Typical initial conditions are $s(0) = s_0$, $e(0) = e_0$, and $c_1(0) = c_2(0) = p(0) = 0$. The conservation laws yield the compact positively invariant set

$$K := \{(s, c_1, c_2) \in \mathbb{R}^3_{\geq 0} : 0 \leq s \leq s_0, 0 \leq c_1 + c_2 \leq e_0^*\}, \tag{51}$$

with some reference value $e_0^* > 0$. The parameter space $\Pi = \mathbb{R}^8_{\geq 0}$ has elements $(e_0, s_0, k_1, k_{-1}, k_2, k_3, k_{-3}, k_4)^{\mathrm{tr}}$, and setting $e_0 = 0$ defines a TFPV,

$$\widehat{\pi} := (0, s_0, k_1, k_{-1}, k_2, k_3, k_{-3}, k_4)^{\mathrm{tr}}$$

for dimension one, subject to certain nondegeneracy conditions on the k_i. The associated critical manifold is

$$\widetilde{Y} := \{(s, c_1, c_2) \in \mathbb{R}^3_{\geq 0} : c_1 = c_2 = 0\}. \tag{52}$$

We now set $\rho = (e_0^*, 0, \ldots, 0)^{\mathrm{tr}}$, and consider the perturbed system with parameter $\pi = \widehat{\pi} + \varepsilon\rho$. The singular perturbation reduction (according to formula (9) in Sect. 2.1) was carried out in Noethen and Walcher (2007, Section 4) and Goeke and Walcher (2013, Examples 8.2 and 8.7). This reduction agrees with the well known classical quasi-steady state reduction for complexes of the cooperativity reaction mechanism (see Keener and Sneyd 2009, Section 1.4.4). We have

$$\dot{s} = -\frac{k_1 e_0 s\,(k_3 k_4 s + k_2(k_{-3} + k_4))}{(k_1 s + k_{-1} + k_2)(k_{-3} + k_4) + k_1 k_3 s^2}, \quad s(0) = s_0. \tag{53}$$

The quasi-steady state variety (see, Keener and Sneyd 2009) is given parametrically by

$$\begin{pmatrix} c_1 \\ c_2 \end{pmatrix} = \frac{k_1 e_0 s}{(k_{-1}+k_2)(k_{-3}+k_4) + k_1(k_{-3}+k_4)s + k_1 k_3 s^2} \cdot \begin{pmatrix} k_{-3}+k_4 \\ k_3 s \end{pmatrix}, \quad 0 \le s \le s_0,$$

and agrees with the first order approximation of the slow manifold. Fenichel theory guarantees that (53) holds for sufficiently small $e_0 = \varepsilon e_0^*$, up to errors of order ε^2. The initial value for the reduced equation is generally chosen as s_0, and we adopt this choice here (refraining from a closer analysis of the approximation error).

6.1.1 Asymptotic Small Parameters

According to the first blanket assumption in Sect. 2.4, we will assume that $(s_0, k_1, k_{-1}, k_2, k_3, k_{-3}, k_4)^{\mathrm{tr}}$ is contained in a compact subset of $\mathbb{R}^7_{>0}$. In particular s_0 and all the k_i are bounded above by some positive constants. We now further specify this compact parameter set. On $\widetilde{Y} \cap K$ with $\pi = \widehat{\pi}$, we have

$$\begin{aligned} \sigma_1 &= (k_1+k_3)s + k_{-1} + k_2 + k_{-3} + k_4; \\ \sigma_2 &= k_1 k_3 s^2 + k_1(k_{-3}+k_4)s + (k_{-1}+k_2)(k_{-3}+k_4); \\ \widehat{\sigma}_3 &= k_1 e_0^* \cdot (k_3 k_4 s + k_2(k_{-3}+k_4)) . \end{aligned}$$

Due to the TFPV requirement, σ_1 and σ_2 must be bounded below on $K \cap \widetilde{Y}$ by positive constants,

$$\begin{aligned} k_{-1} + k_2 + k_{-3} + k_4 &= \min \sigma_1 > 0, \\ (k_{-1}+k_2)(k_{-3}+k_4) &= \min \sigma_2 > 0, \end{aligned}$$

and from this one sees that the TFPV conditions hold if and only if both $k_{-1} + k_2$ and $k_{-3} + k_4$ are bounded below by positive constants. Nontriviality of the reduced equation (53) also imposes conditions on k_1, k_2, k_3, and k_4. Moreover, for instance, in the limit $k_3 \to 0$, with k_4 bounded below by a positive constant, the reduced equation is nontrivial but approaches the Michaelis–Menten equation. We will take a closer look at this situation below.

Generally, the TFPV and nondegeneracy conditions will certainly hold whenever $(s_0, k_1, k_{-1}, k_2, k_3, k_{-3}, k_4)^{\mathrm{tr}}$ is contained in a compact subset of the open positive orthant. Our aim is now to determine a suitable dimensionless parameter that corresponds to the legitimacy of (53). The typical requirement in the literature, that $e_0/s_0 \ll 1$, yields a sufficient asymptotic condition for bounded s_0, since singular perturbation theory guarantees convergence as $e_0 \to 0$, but no quantitative information can be inferred. In contrast, we use the results of Sect. 3 to provide a correspondence to linear timescales.

The explicit calculation of ε^* according to Proposition 2, i.e., determining the maximum of

$$s \mapsto r(s) := \frac{\widehat{\sigma}_3}{\sigma_1 \sigma_2}, \quad 0 \le s \le s_0 \tag{55}$$

involves the computation of the roots of the numerator of the derivative, thus of a parameter-dependent cubic polynomial q in s. The signs of all the coefficients[15] are negative, except possibly the constant coefficient. By the Descartes rule of signs, the polynomial q has at most one positive zero. If there exists no positive zero, then r is strictly decreasing for $0 \leq s < \infty$ and attains its maximum at $s = 0$,[16] and in any case one has

$$\varepsilon^* \geq r(0) = \varepsilon_{MM} \cdot \frac{k_{-1} + k_2}{k_{-1} + k_2 + k_{-3} + k_4}.$$

If a positive zero s^* exists[17], then the maximum of r will be attained there. An exact calculation via Cardano does not provide any palatable information, but an upper bound for ε^* is obtained rather easily from the monotonicity of the σ_j:

$$\begin{aligned} \varepsilon^* &\leq \varepsilon \frac{\sup_{\widetilde{Y}\cap K} \widehat{\sigma}_3}{\inf_{\widetilde{Y}\cap K} \sigma_1 \inf_{\widetilde{Y}\cap K} \sigma_2} \\ &= \frac{k_1 e_0}{k_{-1} + k_2} \cdot \left(\frac{k_3 k_4 s_0 + k_2(k_{-3} + k_4)}{(k_{-1} + k_2 + k_{-3} + k_4)(k_{-3} + k_4)} \right) \\ &= \varepsilon_{MM} \cdot \left(\frac{k_3 k_4 s_0 (k_{-1} + k_2)}{k_2 (k_{-1} + k_2 + k_{-3} + k_4)(k_{-3} + k_4)} + \frac{k_{-1} + k_2}{k_{-1} + k_2 + k_{-3} + k_4} \right) =: \varepsilon_C. \end{aligned} \tag{56}$$

Comparing this to the lower estimate $r(0)$, one finds that the upper estimate by ε_C is acceptable as long as s_0 is not too large, but weakens with increasing s_0. As noted in Sect. 3, ε^*—and by extension ε_C—provides an estimate for the ratio of slowest to fastest timescale. Thus, smallness of ε^* is a necessary condition, but it may not be sufficient when the fast timescales are far apart.

We therefore consider an estimate for the ratio of the slow timescale to the slower of the fast ones via μ^*. It is straightforward to verify that $\sigma_1^2 - 4\sigma_2 \geq 0$, thus all eigenvalues are real, and Proposition 4(b) is applicable. The explicit calculation of μ^* again involves a cubic polynomial in s, for $0 \leq s \leq s_0$. In this case, the Descartes sign rule allows for two or no positive zeros, and there exist at most two local maxima for $0 \leq s < \infty$. One of these is located at $s = 0$, yielding in any case the lower estimate

$$\mu^* \geq \varepsilon_{MM} \cdot \frac{k_{-1} + k_2 + k_{-3} + k_4}{k_{-3} + k_4}, \tag{57}$$

[15] It is unproblematic to determine these explicitly, but the expressions are unwieldy.

[16] Straightforward computation yields a condition on k_3 that ensures the maximum of r being attained at $s = 0$.

[17] This case does occur.

but an explicit computation of the maximum provides little information. Instead, we again resort to an upper bound

$$\begin{aligned}\mu^* &\leq \varepsilon \frac{\sup_{\widetilde{Y}\cap K} \widehat{\sigma}_3 \sup_{\widetilde{Y}\cap K} \sigma_1}{\inf_{\widetilde{Y}\cap K} \sigma_2^2} \\ &= \varepsilon_{MM} \cdot \left(\frac{k_3k_4s_0 + k_2(k_{-3}+k_4)}{k_2(k_{-3}+k_4)} \cdot \frac{(k_1+k_3)s_0 + k_{-1} + k_2 + k_{-3} + k_4}{k_{-3}+k_4} \right) =: \mu_C.\end{aligned} \tag{58}$$

Comparison with (57) shows that the estimate by μ_C is satisfactory as long as s_0 is not too large, but it will become rather weak with increasing s_0.

All estimates involve the distinguished Michaelis–Menten parameter ε_{MM}, multiplied by some positive factor. For both estimates in (57), (58) this factor is > 1.

6.1.2 Numerical Simulations

While we have obtained asymptotic timescale estimates for given reaction parameters, these estimates are unsatisfactory for large substrate concentrations. Moreover, by its nature our approach alone does not provide an upper estimate for the distance of the solution to the slow manifold. So, to obtain a priori gauge of the efficacy of (53), it is natural to resort to numerical simulations. These simulations serve two purposes: a positive and a negative. On the positive side, they illustrate that the small parameters ε^* and μ^* are good indicators for viability of the QSS reduction, in a wide parameter range. On the negative side, numerical examples highlight parameter combinations where consideration of ε^* and μ^* is misleading. Such cases can be traced back to problems with the blanket assumptions from Sect. 2.4, or with assumptions implicit in the proofs of Propositions 2 and 3.

We will consider some specific examples, and instead of relying on ε_C and μ_C we will compute both ε^* and μ^* numerically in the simulations that follow. This is still far less computationally involved than working with eigenvalues of linearizations on $\widetilde{Y}\cap K$. In the figures illustrating all the simulations, to show the behavior of trajectories over the interval $0 \leq t < \infty$, time is mapped to

$$\tau = t/T, \ \ \tau \in [0, 1],$$

where the numerical solution has been computed on the interval $[0, T]$, and T is chosen large enough to ensure the numerical simulations capture the long-time dynamics of the reaction. We start with some examples that document the efficacy of the parameters in "normal" parameter domains:

1. In a first numerical study, we compare the numerical solution to the mass action equations (50) with the numerical solution to (53) in the scenario when all parameters except e_0 are of the same order of magnitude. In the simulations, all parameter values except e_0 are set equal to 1, and e_0 is varied from 10^0–10^{-3}. The simulation results are reported in Fig. 1 , which reinforces the assertion that $\varepsilon^* \ll 1$ and $\mu^* \ll 1$ support the validity of (53). Moreover, we see that smallness of μ^* is the more relevant condition.

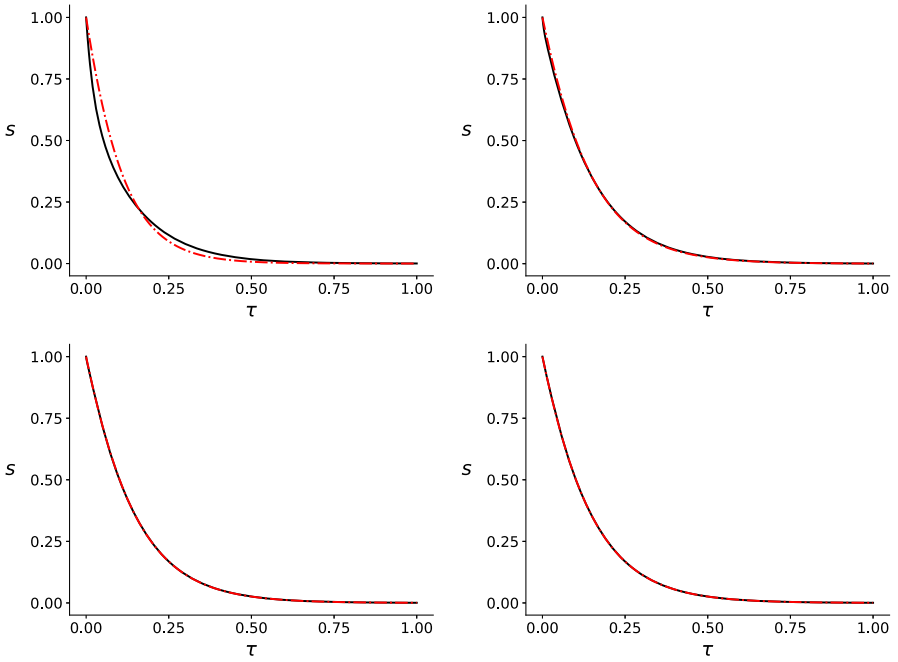

Fig. 1 Cooperativity reaction mechanism: Numerical simulations indicate that the accuracy of (53) improves along the parameter ray direction as both $\varepsilon^* \to 0$ and $\mu^* \to 0$. In both panels, the parameters (in arbitrary units) are: $s_0 = 1.0$, $k_1 = 1.0$, $k_2 = 1.0$, $k_{-1} = 1.0$, $k_3 = 1.0$, $k_{-3} = 1.0$ and $k_4 = 1.0$. Time has been mapped to the τ scale: $\tau = t/T$, $\tau \in [0, 1]$. The solid black curve is the numerical solution to the mass action system (50). The broken red curve is the numerical solution to (53). *Top left panel*: Simulation performed with $e_0 = 1.0$. The numerically computed dimensionless parameters are: $\varepsilon^* = 1.25 \times 10^{-1}$, $\mu^* = 5 \times 10^{-1}$, and there is visible error. *Top Right panel*: Simulation performed with $e_0 = 10^{-1}$. The numerically computed dimensionless parameters are: $\varepsilon^* = 1.25 \times 10^{-2}$, $\mu^* = 5 \times 10^{-2}$. There is visible error, but the approximation (53) appears to improve. *Bottom Left panel*: Simulation performed with $e_0 = 10^{-2}$. The numerically computed dimensionless parameters are: $\varepsilon^* = 1.25 \times 10^{-3}$, $\mu^* = 5 \times 10^{-3}$. The QSS reduction (53) is virtually indistinguishable from (50). *Bottom Right panel*: Simulation performed with $e_0 = 10^{-3}$. The numerically computed dimensionless parameters are: $\varepsilon^* = 1.25 \times 10^{-4}$, $\mu^* = 5 \times 10^{-4}$. The QSS reduction (53) is again virtually indistinguishable from (50) (Color figure online)

2. In a second numerical study, we examine a case with varied parameter values, but all (except e_0) within the same order of magnitude. The results are reported in Fig. 2, and once again support the claim that the accuracy of (53) improves as $\varepsilon^* \to 0$ and $\mu^* \to 0$, with higher relevance for μ^*.
3. As a third numerical example, we consider a combination of parameter values that are somewhat disparate in terms of the magnitudes. Nevertheless, we once again confirm that that the accuracy of (53) improves as $\varepsilon^* \to 0$ and $\mu^* \to 0$, again with higher relevance for μ^* (see, Fig. 3). This simulation also debunks the commonly accepted notion that $e_0/s_0 \ll 1$ is sufficient for the accuracy of (53).

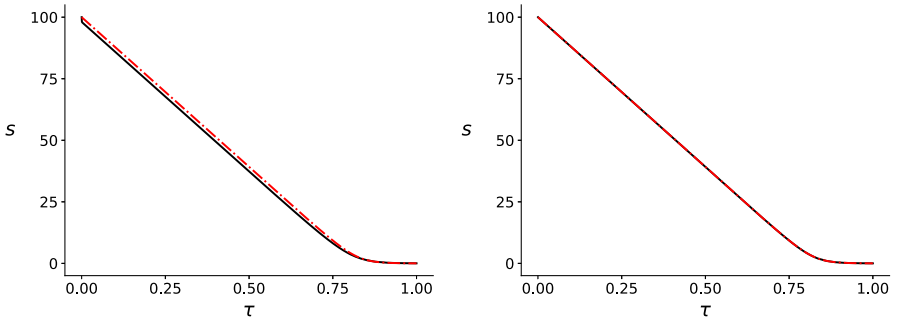

Fig. 2 Cooperativity reaction mechanism: Numerically computed μ^* and ε^* give an a priori indication of the accuracy of (53). In both panels, the parameters (in arbitrary units) are: $s_0 = 10^2$, $k_1 = 20$, $k_2 = 50$, $k_{-1} = 50$, $k_3 = 10$, $k_{-3} = 20$ and $k_4 = 40$. The solid black curve is the numerical solution to the mass action system (50). The broken red curve is the numerical solution to (53). Time has been mapped to the τ scale: $\tau = t/T$, $\tau \in [0, 1]$. *Left panel*: $e_0 = 1.0$ and $\varepsilon^* = 6.25 \times 10^{-2}$ but μ^* is roughly 2.67×10^{-1} and the QSS approximation (53) is inaccurate. *Right panel*: $e_0 = 10^{-2}$, ε^* is numerically estimated to be 6.25×10^{-4} and μ^* is numerically estimated to be roughly 2.67×10^{-3}. In this simulation the validity of (53) clearly improves along the parameter ray $\rho = (e_0^*, 0, \ldots, 0)^{\text{tr}}$ as $\mu^* \to 0$. Thus, e_0 must be small enough so that $0 < \mu^* \ll 1$ (recall that $\mu^* \ll 1$ implies $\varepsilon^* \ll 1$). We see that $\varepsilon^* \ll 1$ provides a too optimistic prediction and that $\mu^* \ll 1$ is a better indicator for the accuracy of the reduction (50) (Color figure online)

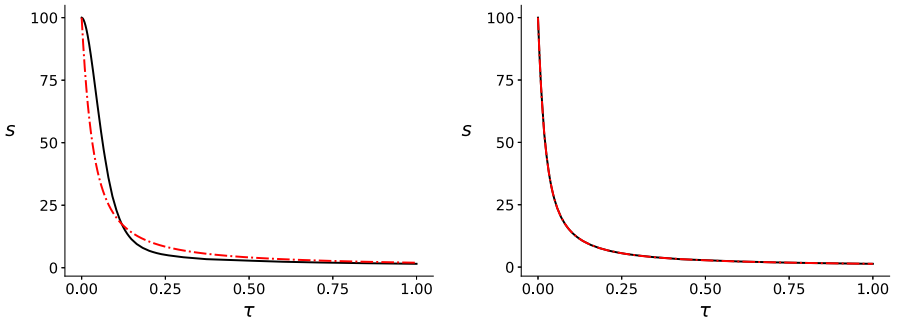

Fig. 3 Cooperativity reaction mechanism: Numerically computed μ^* and ε^* give an a priori indication of the long-time accuracy of (53). In both panels, the parameters (in arbitrary units) are: $s_0 = 100$, $k_1 = 1.0$, $k_2 = k_{-1} = 10^2$, $k_3 = 2 \times 10^3$, $k_{-3} = k_4 = 10^5$. The solid black curve is the numerical solution to the mass action system (50). The broken red curve is the numerical solution to (53). Time has been mapped to the τ scale: $\tau = t/T$, $\tau \in [0, 1]$. *Left panel*: $e_0 = 1.0$ and $\varepsilon^* \approx 6.5 \cdot 10^{-4}$ but μ^* is roughly 1.0. *Right panel*: $e_0 = 10^{-3}$, $\varepsilon^* \approx 6.5 \times 10^{-7}$ and $\mu^* \approx 10^{-3}$; the reduction (53) is an excellent approximation to (50). Note that although $e_0/s_0 \ll 1$ the reduction (53) is inaccurate: The failure in the left panel is immediate (and severe), despite the fact that $e_0/s_0 = 10^{-2}$ (Color figure online)

Throughout these simulations we observe that the magnitude of μ^* is more relevant for the quality of the QSS approximation than the magnitude of ε^*. This is in accordance with the results of Sect. 3.2.

6.1.3 Exceptional Cases: Near-Degeneracy and Near-Invariance

Here, we briefly discuss two special scenarios with $\mu^* \gg 1$, but precede this by a word of caution. Obviously, whenever $\mu^* > 1$, then the implicit assumptions in the proofs

of Propositions 3 and 4 are violated for the given values of e_0, and the propositions are not applicable in this range. To enable applicability, $\varepsilon_{\max}$ would have to be adjusted to a smaller value. However, the consideration of such extreme cases provides insight into the significance of various parameters.

The first case involves a near-degeneracy scenario. The critical variety contains a degenerate point and $1 \ll \mu^*$, while at first sight the QSS reduction (53) *appears* to be highly accurate. In the second case, a two-dimensional nearly invariant subspace emerges within phase space. Here we present a description of the cases:

1. Consider the parameter point

$$\pi^{\ddagger} = (s_0, 0, k_1, 0, 0, k_3, k_{-3}, k_4)^{\mathrm{tr}},$$

thus in addition to $e_0 = 0$ one has $k_{-1} = k_2 = 0$ (which is problematic in view of nondegeneracy conditions). The associated critical variety, Y, consists of two intersecting lines of equilibria (and is therefore not a manifold)[18]

$$Y := \{(s, c_1, c_2) \in \mathbb{R}^3_{\geq 0} : c_1 = c_2 = 0\} \cup \{(s, c_1, c_2) \in \mathbb{R}^3_{\geq 0} : s = c_2 = 0\}.$$

The perturbation form of the mass action equations with $e_0 = \varepsilon e_0^*$, $k_2 = \varepsilon k_2^*$ and $k_{-1} = \varepsilon k_{-1}^*$ is

$$\begin{pmatrix} \dot{s} \\ \dot{c}_1 \\ \dot{c}_2 \end{pmatrix} = \begin{pmatrix} (k_1 - k_3) & k_1 s + k_{-3} \\ -(k_1 + k_3) & -k_1 s + k_4 + k_{-3} \\ k_3 & -(k_{-3} + k_4) \end{pmatrix} \begin{pmatrix} s c_1 \\ c_2 \end{pmatrix} + \varepsilon \begin{pmatrix} k_1 e_0^* s + k_{-1}^* c_1 \\ k_1 e_0^* s - (k_{-1}^* + k_2^*) c_1 \\ 0 \end{pmatrix}. \tag{59}$$

In this case, the rank of the Jacobian is not constant

$$\begin{aligned} &\text{rank} \;\; D_1 h(s, c_1, c_2, \pi^{\ddagger}) = 1, \quad \text{if} \;\; (s_1, c_1, c_2) = (0, 0, 0); \\ &\text{rank} \;\; D_1 h(s, c_1, c_2, \pi^{\ddagger}) = 2, \quad \text{otherwise.} \end{aligned}$$

While the rank condition from Sect. 2.1 fails[19] on Y, it is straightforward to verify that the compact submanifolds defined by

$$\begin{aligned} \widetilde{Y}_1 &:= \{(s, c_1, c_2) \in K : c_1 = c_2 = 0 \;\text{ and }\; s \geq \theta_1\}, \quad 0 < \theta_1 < s_0, \\ \widetilde{Y}_2 &:= \{(s, c_1, c_2) \in K : s = c_2 = 0 \;\text{ and }\; c_1 \geq \theta_2\}, \quad 0 < \theta_2 < e_0^*, \end{aligned}$$

are normally hyperbolic and attracting. Thus, for π sufficiently close to $\pi^{\ddagger}$, and for $s_0 > 0$, trajectories will rapidly approach the attracting branch $\widetilde{Y}_1$. Projection

[18] Recall a similar scenario for Michaelis–Menten in Sect. 4.4.

[19] A dynamic transcritical bifurcation occurs at the point where the rank of $D_1 h(x, \pi^{\ddagger})$ is 1. See Krupa and Szmolyan (2001) for a general discussion of such scenarios.

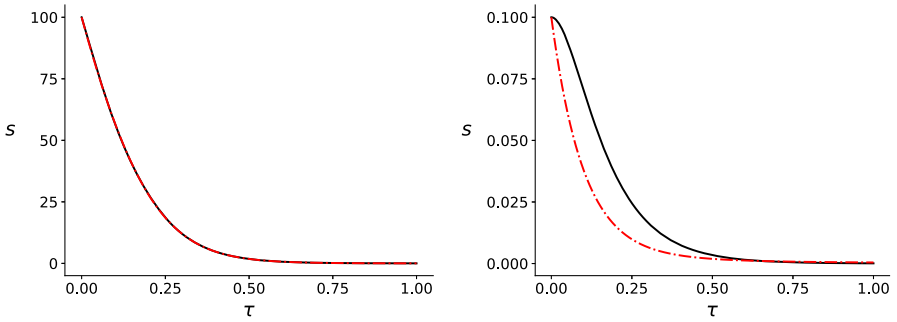

Fig. 4 Cooperativity reaction mechanism: Numerically computed μ^* and ε^* give an a priori indication of the long-time accuracy of (53). In both panels, the parameters (in arbitrary units) are: $e_0 = 10^{-5}, k_1 = 1.0$, $k_2 = k_{-1} = 10^{-3}, k_3 = 10^4, k_{-3} = 10^2$ and $k_4 = 10^6$. The solid black curve is the numerical solution to the mass action system (50). The broken red curve is the numerical solution to (53). Time has been mapped to the τ scale: $\tau = t/T,\ \tau \in [0, 1]$. *Left panel*: $s_0 = 100$ and $\varepsilon^* \approx 10^{-8}$ but numerically computed μ^* is roughly 10^1. Nevertheless, the QSS reduction (53) appears to be very good. However, the reduction fails near the origin, which is not captured in the *Left panel* due to limited resolution. *Right panel*: $s_0 = 10^{-1}$, and the reduction (53) clearly fails to approximate the timecourse of s. This example illustrates that $\mu^* \ll 1$ is necessary for the long-time validity of (53) (Color figure online)

of the perturbation onto the tangent space of $\widetilde{Y}_1$, according to (9), yields

$$\begin{pmatrix} \dot{s} \\ \dot{c}_1 \\ \dot{c}_2 \end{pmatrix} = \varepsilon \begin{pmatrix} 1 & \frac{k_1(k_3 s + k_4 + k_{-3}) - k_3 k_4}{k_1(k_3 s + k_4 + k_{-3})} & \frac{(2k_3 s + k_4 + 2k_{-3})k_1 - k_3 k_4}{k_1(k_3 s + k_4 + k_{-3})} \\ 0 & 0 & 0 \\ 0 & 0 & 0 \end{pmatrix} \begin{pmatrix} -k_1 e_0^* s \\ k_1 e_0^* s \\ 0 \end{pmatrix}$$

and the corresponding reduction on $\widetilde{Y}_1$ is

$$\dot{s} = -\frac{e_0 k_4 k_3 s}{k_{-3} + k_4 + k_3 s}. \tag{62}$$

Remarkably, one can recover (62) by setting $k_{-1} = k_2 = 0$ in (53). Thus, equation (62) can be viewed as a special case of (53) in the limit of small k_2 and k_{-1}. Moreover, numerical simulations seem to indicate that the reduction (53) is valid over the full time course, even when μ^* is quite large (see, Fig. 4, *Left panel*. But, this is illusory. Both (53) and (62) fail to approximate the depletion of s near the origin, as the *Right panel* shows. Thus, near-degeneracy scenarios can generate conditions in which (53) may appear to yield an excellent approximation. But recall that small ε^* combined with large μ^* indicates that two eigenvalues are small, and this necessarily prohibits the reduction from being valid over the complete time course.

There are other degenerate scenarios for this reaction (for instance, $k_{-3} = k_4 = 0$ or $k_{-3} = k_4 = k_2 = k_{-1} = 0$ with all other parameters bounded below by a positive constant). We will not further investigate these.

2. In the final numerical example of this case study, we exhibit a scenario for which (53) provides a valid approximation even though $1 \ll \mu^*$. This can happen, for

instance, in the limit of small e_0 and small k_3. For $k_3 = 0$, the two-dimensional subspace $V := \{(s, c_1, c_2) \in \mathbb{R}^3 : c_2 = 0\}$ is invariant. One approach to such a scenario is to consider a singular perturbation reduction with both $e_0 = \varepsilon e_0^\star$, $k_3 = \varepsilon k_3^\star$ of order ε. The perturbation form of the mass action system is

$$\begin{pmatrix} \dot{s} \\ \dot{c}_1 \\ \dot{c}_2 \end{pmatrix} = \begin{pmatrix} k_1 s + k_{-1} & k_1 s + k_{-3} \\ -k_1 s - (k_{-1} + k_2) & k_1 s + (k_{-3} + k_4) \\ 0 & -(k_{-3} + k_4) \end{pmatrix} \begin{pmatrix} c_1 \\ c_2 \end{pmatrix} + \varepsilon \begin{pmatrix} -k_1 e_0^* s - k_3^* c_1 s \\ k_1 e_0^* s - k_3^* c_1 s \\ k_3^* c_1 s \end{pmatrix}, \tag{63}$$

with the critical manifold given by $c_1 = c_2 = 0$. Projection onto the critical manifold according to (9) yields

$$\begin{pmatrix} \dot{s} \\ \dot{c}_1 \\ \dot{c}_2 \end{pmatrix} = \varepsilon \begin{pmatrix} 1 & \dfrac{k_1 s + k_{-1}}{k_1 s + k_{-1} + k_2} & \dfrac{k_1 s(k_2 + k_4) + k_4 k_{-1} - k_2 k_{-3}}{(k_1 s + k_{-1} + k_2)(k_{-3} + k_4)} \\ 0 & 0 & 0 \\ 0 & 0 & 0 \end{pmatrix} \begin{pmatrix} -k_1 e_0^* s \\ k_1 e_0^* s \\ 0 \end{pmatrix},$$

and thus the QSS reduction

$$\dot{s} = -\frac{k_1 k_2 e_0 s}{k_1 s + k_{-1} + k_2},$$

which corresponds to the sQSSA of the MM reaction mechanism.
One may regard this also from a different perspective: For fixed k_3, one obtains the reduction (53). Then, letting $k_3 \to 0$ yields the Michaelis–Menten equation. Notably, the lower estimate (57) for μ^* is independent of k_3, and thus large μ^* will remain large as $k_3 \to 0$. On the other hand, the upper estimate for ε^* decreases as $k_3 \to 0$. We recover the Michaelis–Menten equation, because a slight perturbation to $k_3 = 0$ results in V being *nearly* invariant (see, e.g., Goeke et al. 2017 for the notion). Biochemically, near invariance of V is equivalent to gradually "turning off" the cooperative mechanism, since the secondary complex C_2 is being produced at a very small rate. Mathematically, the near invariance of V implies for the given initial values, thus $c_2(0) = 0$, that the relevant dynamics are essentially two-dimensional even prior to reduction, and further reduction to a one-dimensional manifold depends only on a single eigenvalue ratio. In the simulation example, the fast eigenvalue with smaller absolute value—which generally is responsible for the slow-fast separation—has negligible influence, since the dynamics evolves on an invariant manifold very near $c_2 = 0$. Consequently ε^* (or indeed ε_{MM}) is the relevant quantity rather than μ^*; see Fig. 5.

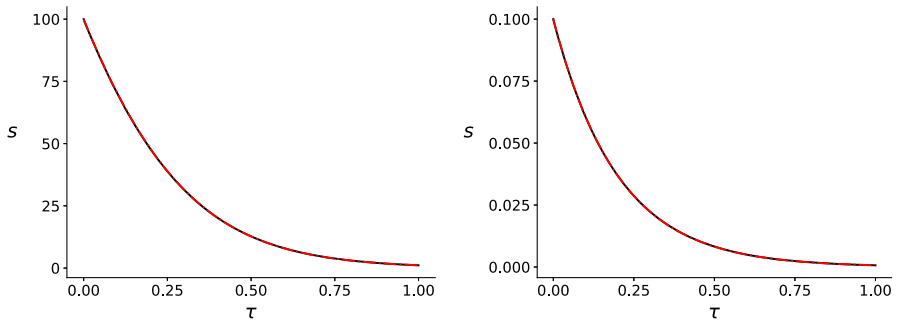

Fig. 5 Cooperative reaction mechanism with nearly invariant subspace: When the three-dimensional dynamics is nearly two-dimensional, ε^* provides a good a priori measure for the accuracy of (53). In both panels the solid black curve is the numerical solution to the mass action equations (50). The broken red curve is the numerical solution to the QSS reduction (53). Time has been mapped to the τ scale: $\tau = t/T,\ \tau \in [0, 1]$, and the parameters (in arbitrary units) are: $e_0 = 1.0, k_1 = 1.0, k_2 = k_{-1} = 10^2, k_3 = 10^{-5}, k_{-3} = 10^{-1}$ and $k_4 = 10^{-1}$. *Left panel*: $s_0 = 100$ and $\varepsilon^* \approx 2.5 \times 10^{-3}$ but the numerically computed μ^* is roughly 2.5. Nevertheless, the QSS reduction (53) is very accurate. By near-invariance of V, (53) effectively reduces to the Michaelis–Menten equation, and the pertinent dynamics unfold in the two-dimensional subspace V. *Right panel*: $s_0 = 10^{-1}$, and we have confirmation that the long-time accuracy of the reduction (53) holds, even though $\mu^* \approx 2.5$ remains of order unity (Color figure online)

6.2 Uncompetitive Inhibition Reaction Mechanism

The irreversible MM reaction mechanism in the presence of an uncompetitive inhibitor

$$\begin{aligned} E + S &\underset{k_{-1}}{\overset{k_1}{\rightleftharpoons}} C_1 \overset{k_2}{\rightarrow} E + P, \\ C_1 + I &\underset{k_{-3}}{\overset{k_3}{\rightleftharpoons}} C_2, \end{aligned} \tag{64}$$

is modeled deterministically by the system

$$\begin{aligned} \dot{s} &= -k_1(e_0 - c_1 - c_2)s + k_{-1}c_1, \\ \dot{c}_1 &= k_1(e_0 - c_1 - c_2)s - (k_{-1} + k_2)c_1 - k_3(i_0 - c_2)c_1 + k_{-3}c_2, \\ \dot{c}_2 &= k_3(i_0 - c_2)c_1 - k_{-3}c_2, \end{aligned} \tag{65}$$

via stoichiometric conservation laws. The standard initial conditions are $(s, c_1, c_2)(0) = (s_0, 0, 0)$. We fix a reference value e_0^* and obtain from the conservation laws the compact positively invariant set

$$K := \{(s, c_1, c_2) \in \mathbb{R}^3_{\geq 0} : 0 \leq s \leq s_0,\ \ c_1 + c_2 \leq e_0^*,\ \ c_2 \leq \min\{e_0^*, i_0\}\}.$$

The parameter space $\Pi = \mathbb{R}^8_{\geq 0}$ has elements $\pi = (e_0, s_0, k_1, k_{-1}, k_2, k_3, k_{-3}, i_0)^{\mathrm{tr}}$. Given suitable nondegeneracy conditions on the parameters (to be specified below), setting $e_0 = 0$ defines a TFPV for dimension one:

$$\widehat{\pi} := (0, s_0, k_1, k_{-1}, k_2, k_3, k_{-3}, i_0)^{\mathrm{tr}},$$

with associated critical manifold

$$\widetilde{Y} := \{(s, c_1, c_2) \in \mathbb{R}^3_{\geq 0} : c_1 = c_2 = 0\}.$$

We set $\rho = (e_0^*, 0, \ldots, 0)^{\mathrm{tr}}$ and consider the ray $\varepsilon \mapsto \widehat{\pi} + \varepsilon\rho$ in parameter space. Then, the perturbed system has the form

$$\begin{pmatrix} \dot{s} \\ \dot{c}_1 \\ \dot{c}_2 \end{pmatrix} = \begin{pmatrix} k_1 s + k_{-1} & k_1 s \\ -k_1 s - (k_{-1} + k_2) - k_3(i_0 - c_2) & -k_1 s + k_{-3} \\ k_3(i_0 - c_2) & -k_{-3} \end{pmatrix} \begin{pmatrix} c_1 \\ c_2 \end{pmatrix} + \varepsilon \begin{pmatrix} -k_1 e_0^* s \\ k_1 e_0^* s \\ 0 \end{pmatrix}. \tag{66}$$

According to (9), the singular perturbation reduction of (66) is given by

$$\begin{pmatrix} \dot{s} \\ \dot{c}_1 \\ \dot{c}_2 \end{pmatrix} = \varepsilon \begin{pmatrix} 1 & \frac{(k_1 s + k_{-1})k_{-3} + i_0 k_1 k_3 s}{(k_1 s + k_2 + k_{-1})k_{-3} + i_0 k_1 k_3 s} & \frac{(k_1 s + k_{-1})k_{-3} + (i_0 k_3 + k_2)k_1 s}{(k_1 s + k_2 + k_{-1})k_{-3} + i_0 k_1 k_3 s} \\ 0 & 0 & 0 \\ 0 & 0 & 0 \end{pmatrix} \begin{pmatrix} -k_1 e_0^* s \\ k_1 e_0^* s \\ 0 \end{pmatrix}, \tag{67}$$

thus $\dot{c}_1 = \dot{c}_2 = 0$ and

$$\dot{s} = -\frac{k_1 e_0 k_2 k_{-3}\, s}{(k_1 s + k_2 + k_{-1})k_{-3} + i_0 k_1 k_3 s}, \quad s(0) = s_0, \tag{68}$$

in the limiting case of small $e_0 = \varepsilon e_0^*$, up to errors of order ε^2.

The reduced equation (77) has been previously reported in the literature (see, e.g., Schnell and Mendoza 2001). It is different from the classical QSS reduction, which is obtained by substituting exact equations for the c_1—and c_2—nullclines into (65). But, in accordance with (Goeke et al. 2017, Proposition 5), the difference between the classical reduction and (68) will be of order ε^2. Typically, in numerical simulations there will only be noticeable differences between the classical reduction and the Fenichel reduction at very large substrate concentrations.

6.2.1 Asymptotic Small Parameters

On $\widetilde{Y} \cap K$, we have at $\pi = \widehat{\pi}$

$$\begin{aligned} \sigma_1 &= k_1 s + k_{-1} + k_2 + k_3 i_0 + k_{-3}, \\ \sigma_2 &= k_1 s(k_3 i_0 + k_{-3}) + (k_{-1} + k_2)k_{-3}, \\ \widehat{\sigma}_3 &= k_2 k_1 e_0^* k_{-3}. \end{aligned}$$

As always, we assume that all the parameters are contained in a suitable compact subset of parameter space, in particular they are bounded above by positive constants.

The TFPV property requires, in addition, that σ_1 and σ_2 are bounded below on $K \cap \widetilde{Y}$ by positive constants, thus

$$\begin{aligned} k_3 i_0 + k_{-3} + k_{-1} + k_2 &= \min \sigma_1 > 0, \\ (k_{-1} + k_2) k_{-3} &= \min \sigma_2 > 0, \end{aligned}$$

and therefore the TFPV conditions hold if and only if both $k_{-1}+k_2$ and k_{-3} are bounded below by positive constants. Moreover, the reduction (68) should be significantly different from a trivial equation, and hence one also requires k_2 to be bounded below by some positive constant. No lower bound for $k_3 i_0$ is imposed by the TFPV conditions, but note that (68) approaches the Michaelis–Menten equation as $i_0 \to 0$ or $k_3 \to 0$. We will discuss this scenario below.

As before, we will obtain usable estimates for the timescale ratio from Propositions 2, 3 and 4. For uncompetitive inhibition, the maxima can be determined explicitly.

The distinguished small parameter ε^*, with σ_1, σ_2 and $\widehat{\sigma}_3$ evaluated at $\pi = \widehat{\pi}$, may be determined from

$$\begin{aligned} \varepsilon^* &= \varepsilon \max_{0 \le s \le s_0} \frac{\widehat{\sigma}_3(s, \widehat{\pi}, \rho, 0)}{\sigma_1(s, \widehat{\pi}) \sigma_2(s, \widehat{\pi})} \\ &= \varepsilon \frac{\widehat{\sigma}_3(0, \widehat{\pi}, \rho, 0)}{\sigma_1(0, \widehat{\pi}) \sigma_2(0, \widehat{\pi})} \\ &= \frac{k_2 k_1 e_0}{(k_{-1} + k_2)^2} \cdot \frac{k_{-1} + k_2}{k_3 i_0 + k_{-3} + k_{-1} + k_2} \\ &= \varepsilon_{MM} \cdot \frac{k_{-1} + k_2}{k_3 i_0 + k_{-3} + k_{-1} + k_2} =: \varepsilon_U, \end{aligned} \tag{69}$$

with the distinguished parameter ε_{MM} from the MM reaction mechanism. Note that to see why the first equality sign in (69) holds, you can determine the derivative and verify that it is negative for $s \ge 0$.

It is straightforward to verify that all eigenvalues are real, since $\sigma_1^2 - 4\sigma_2 \ge 0$. Thus, from σ_1, σ_2 and $\widehat{\sigma}_3$ evaluated at $\widehat{\pi}$, the parameter μ^* is obtained from

$$\begin{aligned} \mu^* &= \varepsilon \max_{0 \le s \le s_0} \frac{\widehat{\sigma}_3(s, \widehat{\pi}, \rho, 0) \sigma_1(s, \widehat{\pi})}{\sigma_2(s, \widehat{\pi})^2} \\ &= \frac{k_2 k_1 e_0}{(k_{-1} + k_2)^2} \cdot \left(\frac{k_3 i_0 + k_2 + k_{-1} + k_{-3}}{k_{-3}} \right) \\ &= \varepsilon_{MM} \cdot \left(\frac{k_3 i_0 + k_2 + k_{-1} + k_{-3}}{k_{-3}} \right) =: \mu_U. \end{aligned} \tag{70}$$

Note that the first equality holds, because the derivative of

$$s \mapsto \frac{\widehat{\sigma}_3(s, \widehat{\pi}, \rho, 0) \sigma_1(s, \widehat{\pi})}{\sigma_2(s, \widehat{\pi})^2}$$

is negative for all $s \ge 0$.

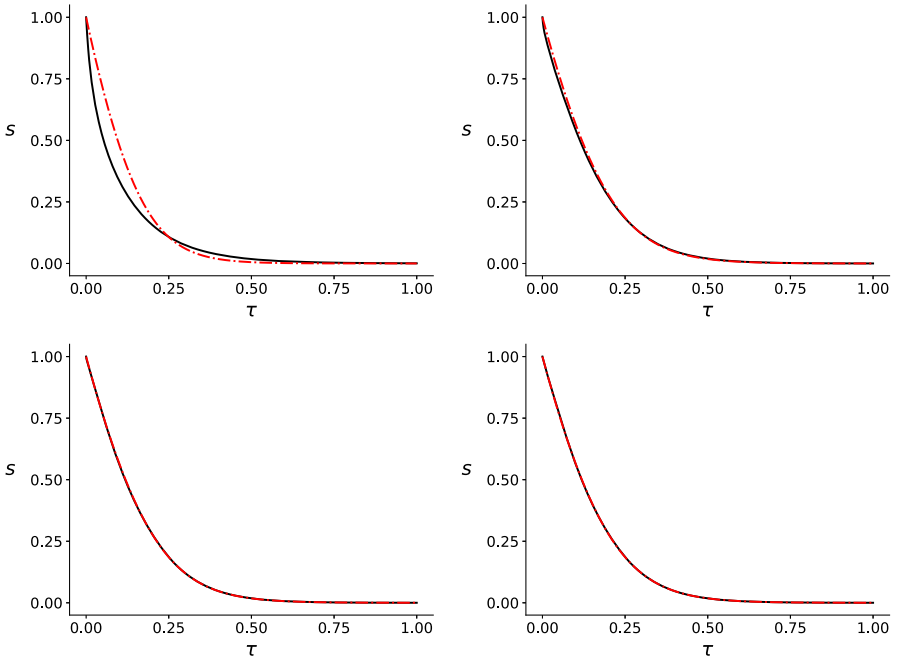

Fig. 6 Uncompetitive inhibition reaction mechanism: Numerical simulations indicate that the accuracy of (68) improves as both $\varepsilon_U \to 0$ and $\mu_U \to 0$ along the parameter ray direction. In both panels, the parameters (in arbitrary units) are: $s_0 = 1.0$, $k_1 = 1.0$, $k_2 = 1.0$, $k_{-1} = 1.0$, $k_3 = 1.0$, $k_{-3} = 1.0$ and $i_0 = 1.0$. The solid black curve is the numerical solution for s to the mass action system (65). The broken red curve is the numerical solution to (68). Time has been mapped to the τ scale: $\tau = t/T$, $\tau \in [0, 1]$. *Top Left panel*: Simulation performed with $e_0 = 1.0$. There is visible error with $\varepsilon_U = 1.25 \times 10^{-1}$ and $\mu_U = 1.0$. *Top Right panel*: Simulation performed with $e_0 = 10^{-1}$. Although there is visible error with $\mu_U = 10^{-1}$ and $\varepsilon_U = 1.25 \times 10^{-2}$, the approximation (68) does appear to be improving along the parameter ray direction. *Bottom Left panel*: Simulation performed with $e_0 = 10^{-2}$ and thus $\mu_U = 10^{-2}$ and $\varepsilon_U = 1.25 \times 10^{-3}$. The QSS reduction (68) is nearly indistinguishable from (65). *Bottom Right panel*: Simulation performed with $e_0 = 10^{-3}$ with $\mu_U = 10^{-3}$ and $\varepsilon_U = 1.25 \times 10^{-4}$. The QSS reduction (68) is again practically indistinguishable from (65). Note that $\mu_U \ll 1$ is still a better indicator of accuracy than $\varepsilon_U \ll 1$ (Color figure online)

6.2.2 Numerical Simulations

We now turn to numerical simulations, with the same dual motivation as in Sect. 6.1. Parallel to our analysis of (56) and (58), we discuss the reliability of the qualifiers $\varepsilon_U \ll 1$ and $\mu_U \ll 1$ in gauging the validity of (68):

1. We begin with the special case $\pi = (e_0, 1, 1, 1, 1, 1, 1, 1)$, representing a scenario where all parameters except e_0 are of the same order 1, and vary e_0 from 1 to 10^{-3}. The results are reported in Fig. 6, and collectively support the statement that (68) holds when μ_U is sufficiently less than 1. With all "non-small" parameters having the same order, one also sees that sufficiently small ε_U suffices.
2. Parallel to our analysis of the cooperative reaction, we next consider parameters with widely disparate magnitude. In this simulation, the accuracy of (68) improves

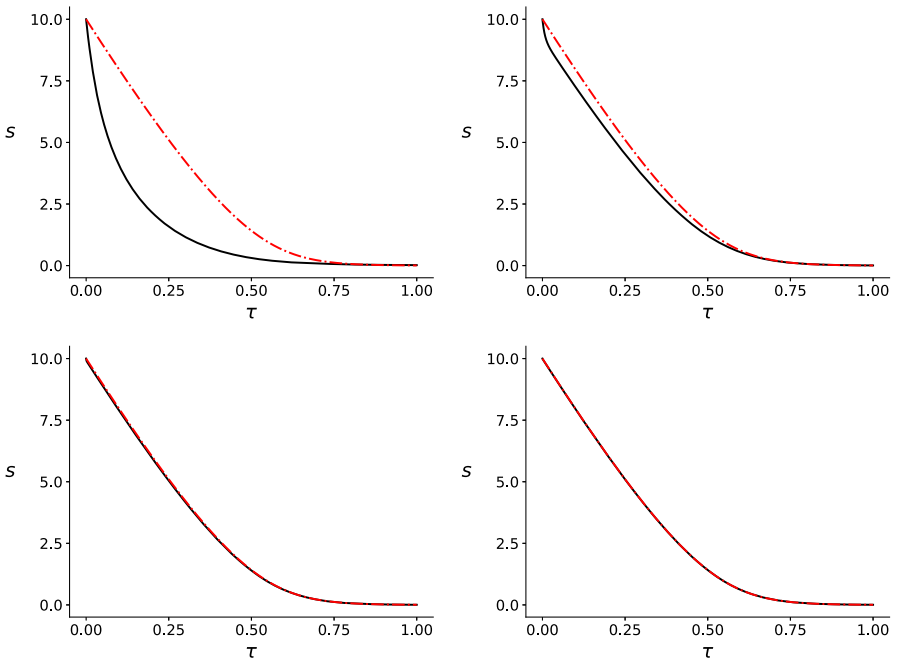

Fig. 7 Uncompetitive inhibition reaction mechanism: The accuracy of (68) is reflected in the magnitude of the dimensionless parameter μ_U. The solid black curve is the numerical solution for s to (65). The broken red curve is the numerical solution to (68). Time has been mapped to the τ scale: $\tau = t/T,\ \tau \in [0, 1]$. The parameters (in arbitrary units) are: $s_0 = 10^1, k_{-3} = 10^{-1}, k_3 = 10^1, i_0 = 10^1, k_1 = 1.0, k_2 = k_{-1} = 10^3$. *Top Left panel*: $e_0 = 1.0$ and $\varepsilon_U \approx 2.38 \times 10^{-4},\ \ \mu_U \approx 5.25$. *Top Right panel*: $e_0 = 10^{-1}$ and $\varepsilon_U \approx 2.38 \times 10^{-5},\ \ \mu_U \approx 5.25 \times 10^{-1}$. *Bottom Left panel*: $e_0 = 10^{-2}$ and $\varepsilon_U \approx 2.38 \times 10^{-6},\ \ \mu_U \approx 5.25 \times 10^{-2}$. *Bottom Right panel*: $e_0 = 10^{-3}$ and $\varepsilon_U = 2.38 \times 10^{-7},\ \ \mu_U \approx 5.25 \times 10^{-3}$. Note that the solutions to (65) and (68) are virtually indistinguishable in the last panel (Color figure online)

only as $\mu_U \to 0$, and this illustrates the relevance of μ_U as the dimensionless parameter that indicates the accuracy of (68); see Fig. 7.

6.2.3 Near-Invariance

As in the case of the cooperative reaction mechanism, near-invariance scenarios also exist for uncompetitive inhibition. Setting $e_0 = i_0 = 0$ (also) yields a TFPV for dimension one, viz.

$$\widehat{\widetilde{\pi}} := (0, s_0, k_1, k_{-1}, k_2, k_3, k_{-3}, 0)^{\mathrm{tr}},$$

with the same associated critical manifold $\widetilde{Y}$, defined by $c_1 = c_2 = 0$. We fix a further reference value i_0^* and consider the ray direction $\rho^\dagger = (e_0^*, 0, \ldots, 0, i_0^*)^{\mathrm{tr}}$. Then, the perturbed system with $\pi = \widehat{\widetilde{\pi}} + \varepsilon\rho^\dagger$ has the form

$$\begin{pmatrix} \dot{s} \\ \dot{c}_1 \\ \dot{c}_2 \end{pmatrix} = \begin{pmatrix} k_1 s + k_{-1} & k_1 s \\ -k_1 s - (k_{-1} + k_2) + k_3 c_2 & -k_1 s + k_{-3} \\ -k_3 c_2 & k_{-3} \end{pmatrix} \begin{pmatrix} c_1 \\ c_2 \end{pmatrix} + \varepsilon \begin{pmatrix} -k_1 e_0^* s \\ k_1 e_0^* s - k_3 i_0^* c_1 \\ k_3 i_0^* c_1 \end{pmatrix} \tag{71}$$

Applying the reduction according to (9) yields

$$\begin{pmatrix} \dot{s} \\ \dot{c}_1 \\ \dot{c}_2 \end{pmatrix} = \varepsilon \begin{pmatrix} 1 & \dfrac{k_1 s + k_{-1}}{k_1 s + k_{-1} + k_2} & \dfrac{(k_1 s + k_{-1}) k_{-3} + k_1 k_2 s}{k_{-3}(k_1 s + k_{-1} + k_2)} \\ 0 & 0 & 0 \\ 0 & 0 & 0 \end{pmatrix} \begin{pmatrix} -k_1 e_0^* s \\ k_1 e_0^* s \\ 0 \end{pmatrix}$$

and thus, with $\dot{c}_1 = \dot{c}_2 = 0$,

$$\dot{s} = -\frac{k_1 e_0 k_2 s}{k_1 s + k_2 + k_{-1}}, \quad s(0) = s_0, \tag{72}$$

which is valid asymptotically as $\varepsilon \to 0$. Here, we recover the familiar Michaelis–Menten equation in the limit when the concentrations of both enzyme and inhibitor approach zero of order ε. (The same reduction is obtained for $k_3 = \varepsilon k_3^*$ and $e_0 = \varepsilon e_0^*$.)

From a different perspective, when the term $k_3 i_0$ vanishes, the subspace $W := \{(s, c_1, c_2) \in \mathbb{R}^3 : c_2 = 0\}$ is invariant, and a slight perturbation (not necessarily of order ε) results in the near-invariance of W. Considering the expressions (69) and (70) for ε^* and μ^*, respectively, one sees that $k_3 i_0 \to 0$ has no strong effect on these parameters and that ε_{MM} is a good upper estimate for ε_U. One may rewrite (68) as

$$\dot{s} = -\frac{k_1 e_0 k_2 s}{k_1 s (1 + k_3 i_0 / k_{-3}) + k_{-1} + k_2}, \tag{73}$$

thus, when $k_3 i_0 / k_{-3} \ll 1$, then the standard Michaelis–Menten reduction is approximately valid. In this case, the dynamics are effectively two-dimensional. Hence (for the given initial values) the magnitude of μ_U is irrelevant, and (68) will hold even if $1 < k_1 e_0 / k_{-3}$ and $1 < \mu_U$ [20] since $\varepsilon_{MM} \ll 1$ automatically ensures the validity of (68) when W is nearly invariant (see, Fig. 8).

6.3 Competitive Inhibition Reaction Mechanism

The irreversible competitive inhibition reaction mechanism

$$\begin{aligned} E + S &\underset{k_{-1}}{\overset{k_1}{\rightleftharpoons}} C_1 \overset{k_2}{\rightharpoonup} E + P, \\ E + I &\underset{k_{-3}}{\overset{k_3}{\rightleftharpoons}} C_2 \end{aligned} \tag{74}$$

[20] The implicit assumptions in the proof of Proposition 3 are then not satisfied.

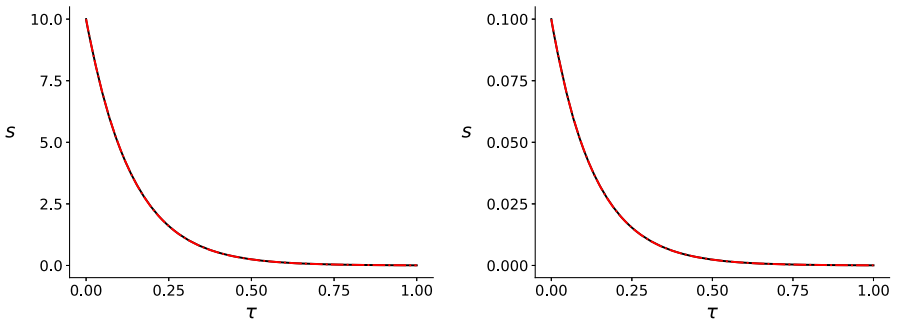

Fig. 8 Uncompetitive inhibition reaction mechanism: Near-invariance may lead to scenarios in which the reduction 68) is accurate even when $1 < \mu_U$. The solid black curve is the numerical solution to (65). The broken red curve is the numerical solution to (68). Time has been mapped to the τ scale: $\tau = t/T$, $\tau \in [0, 1]$. The parameters (in arbitrary units) are: $k_1 = 1.0$, $e_0 = 1.0$, $k_{-3} = 10^{-1}$, $k_3 = 10^{-2}$, $i_0 = 10^{-3}$, $k_2 = k_{-1} = 10^2$ with $\varepsilon_U \approx 2.5 \times 10^{-3}$ and $\mu_U \approx 5.0$. *Left panel*: $s_0 = 10.0$. *Right panel*: The long-time validity is verified with $s_0 = 10^{-1}$. Note that $k_1 e_0/k_{-3}$ is large, thus μ_U is of order one. However, since $k_3 i_0/k_{-3} = 10^{-2}$ and $c_1(0) = c_2(0) = 0$, the dynamics prior to reduction are essentially two-dimensional. Consequently, (68) holds since $\varepsilon_{MM} \ll 1$ (Color figure online)

corresponds (with mass action kinetics and stoichiometric conservation laws) to the ODE system

$$\begin{aligned} \dot{s} &= -k_1(e_0 - c_1 - c_2)s + k_{-1}c_1, \\ \dot{c}_1 &= k_1(e_0 - c_1 - c_2)s - (k_{-1} + k_2)c_1, \\ \dot{c}_2 &= k_3(e_0 - c_1 - c_2)(i_0 - c_2) - k_{-3}c_2. \end{aligned} \tag{75}$$

The usual initial conditions are $s(0) = s_0$, $e(0) = e_0$, $i(0) = i_0$ and $c_1(0) = c_2(0) = p(0) = 0$. We fix a reference value e_0^*, and then from the conservation laws we obtain the compact positively invariant set

$$K := \{(s, c_1, c_2) \in \mathbb{R}^3_{\geq 0} : 0 \leq s \leq s_0, \quad 0 \leq c_1 \leq e_0^*, \quad 0 \leq c_2 \leq \min\{e_0^*, i_0\}\}.$$

The parameter space $\Pi = \mathbb{R}^8_{\geq 0}$ has elements

$$(e_0, s_0, i_0, k_1, k_{-1}, k_2, k_3, k_{-3})^{\text{tr}},$$

and it is known that $e_0 = 0$, with all other parameters positive, defines a TFPV,

$$\widehat{\pi} := (0, s_0, i_0, k_1, k_{-1}, k_2, k_3, k_{-3})^{\text{tr}} \tag{76}$$

with corresponding critical manifold

$$\widetilde{Y} := \{(s, c_1, c_2) \in \mathbb{R}^3_{\geq 0} : c_1 = c_2 = 0\}.$$

(see, below for nondegeneracy conditions on the remaining parameters.) We choose the parameter ray direction $\rho = (e_0^*, 0, \ldots, 0)^{\text{tr}}$, with $e_0 = \varepsilon e_0^*$. The singular perturbation

reduction (see, Goeke and Walcher 2014, Section 3.2) yields the equation

$$\dot{s} = -\frac{k_1 k_{-3} k_2 e_0 s}{(k_1 s + k_{-1} + k_2)k_{-3} + k_3 i_0 (k_{-1} + k_2)}. \tag{77}$$

The reduced equation (68) has been previously reported in the literature (see, e.g., Schnell and Mendoza 2001). Note that the reduction (77) again differs from the classical QSS reduction (see, e.g., Keener and Sneyd 2009, Section 1.4.3). However, (77) and the classical reduction agree up to a term of order ε^2 and are therefore asymptotically equivalent.

6.3.1 Asymptotic Small Parameters

The coefficients of the characteristic polynomial on the critical manifold are

$$\begin{aligned}
\sigma_1 &= k_1 s + k_{-1} + k_2 + k_3 i_0 + k_{-3};\\
\sigma_2 &= k_{-3} k_1 s + (k_3 i_0 + k_{-3})(k_{-1} + k_2);\\
\widehat{\sigma}_3 &= k_2 k_1 e_0^* \cdot (k_3 i_0 + k_{-3})\,.
\end{aligned}$$

We generally assume that all parameters are contained in a compact subset of the positive orthant, hence are bounded above by certain positive constants. Moreover $\sigma_1(\widehat{\pi}, s)$ and $\sigma_2(\widehat{\pi}, s)$ satisfy the TFPV property

$$\begin{aligned}
k_3 i_0 + k_{-3} + k_{-1} + k_2 &= \min \sigma_1 > 0,\\
(k_{-1} + k_2)(k_3 i_0 + k_{-3}) &= \min \sigma_2 > 0
\end{aligned}$$

if and only if $k_{-1} + k_2$ and $k_3 i_0 + k_{-3}$ are bounded below by certain positive constants. More restrictively, we will assume that i_0 is bounded below by some positive constant. Finally k_2 and k_{-3} should be bounded below by positive constants, lest the reduced equation (77) is too close to trivial.

With σ_1, σ_2 and $\widehat{\sigma}_3$ evaluated at $\widehat{\pi}$, we obtain the distinguished small parameter

$$\begin{aligned}
\varepsilon^* &= \varepsilon \sup_{\widehat{Y} \cap K} \frac{\widehat{\sigma}_3(s, \widehat{\pi}, \rho, 0)}{\sigma_1(s, \widehat{\pi})\sigma_2(s, \widehat{\pi})}\\
&= \frac{k_2 k_1 e_0}{(k_{-1} + k_2)^2} \cdot \frac{k_{-1} + k_2}{k_{-1} + k_2 + k_3 i_0 + k_{-3}}\\
&= \varepsilon_{MM} \cdot \frac{k_{-1} + k_2}{k_{-1} + k_2 + k_3 i_0 + k_{-3}} := \varepsilon_I
\end{aligned} \tag{78}$$

To verify the equalities, note that $\widehat{\sigma}_3$ is constant while $\sigma_1,\ \sigma_2$ are increasing with s.

It is straightforward to check that $\sigma_1^2 - 4\sigma_2 \geq 0$, thus all eigenvalues are real, and Proposition 3 is applicable. Determining the parameter μ^* requires a distinction of cases. The derivative of

$$s \mapsto q(s) := \frac{\widehat{\sigma}_3(s, \widehat{\pi}, \rho, 0)\sigma_1(s, \widehat{\pi})}{\sigma_2(s, \widehat{\pi})^2}$$

is a rational function in s with numerator of degree one. Both coefficients are negative if and only if

$$2k_{-3}(k_3 i_0 + k_{-3}) + k_{-3}(k_{-1} + k_2) \geq (k_{-1} + k_2) i_0 k_3, \tag{79}$$

otherwise they have opposite signs. Note that (79) is satisfied whenever $(k_3 i_0)/(k_{-3}) \leq 1$. This inequality admits a direct interpretation in terms of the reaction mechanism. On the one hand, it places a lower bound on the allowable size of k_{-3}. More importantly, it holds whenever the inhibitor concentration is not too high, thus it is controllable by experimental design.

When (79) holds then $s \mapsto q(s)$ is strictly decreasing for $s \geq 0$, and

$$\mu^* = \mu_I^{(1)} := \varepsilon \frac{\widehat{\sigma}_3(0, \widehat{\pi}, \rho, 0)\sigma_1(0, \widehat{\pi})}{\sigma_2(0, \widehat{\pi})^2} = \varepsilon_{MM} \cdot \frac{k_{-1} + k_2 + k_3 i_0 + k_{-3}}{k_3 i_0 + k_{-3}}. \tag{80}$$

Whenever (79) does not hold then a straightforward calculation shows that the maximum of $s \mapsto q(s)$ for $0 \leq s < \infty$ is given by

$$\begin{aligned} \mu^* = \mu_I^{(2)} &= \frac{k_2 k_1 e_0 \cdot (k_3 i_0 + k_{-3})}{4k_{-3} \cdot \Big(k_3 i_0 (k_{-1} + k_2) - k_{-3}(k_3 i_0 + k_{-3}) \Big)} \\ &= \varepsilon_{MM} \cdot \frac{(k_{-1} + k_2)^2 \cdot (k_3 i_0 + k_{-3})}{4k_{-3} \cdot \Big(k_3 i_0 (k_{-1} + k_2) - k_{-3}(k_3 i_0 + k_{-3}) \Big)}. \end{aligned} \tag{81}$$

This expression is somewhat unwieldy. But $\mu_I^{(2)}$ admits an obvious lower bound, obtained by discarding the negative term in the denominator:

$$\mu_I^{(2)} \geq \frac{1}{4} \cdot \frac{k_1 k_2 e_0}{k_{-3}(k_{-1} + k_2)} \cdot \left(1 + \frac{k_{-3}}{k_3 i_0} \right).$$

Moreover, the negation of (79) provides an estimate for the denominator which yields an upper bound

$$\mu_I^{(2)} \leq \frac{1}{4} \cdot \frac{k_2 k_1 e_0 (k_3 i_0 + k_{-3})}{k_{-3}^2 (k_3 i_0 + k_{-3} + k_{-1} + k_2)}.$$

The lower bound shows that it is necessary to require $k_1 e_0 \ll \min\{k_{-3}, k_3 i_0\}$ whenever k_{-1} and k_2 are of the same order.

Finally, whenever s_0 is not too large one may also consider the estimate

$$\begin{aligned}\mu^* &\leq \varepsilon \frac{\widehat{\sigma}_3(s_0, \widehat{\pi}, \rho, 0)\sigma_1(s_0, \widehat{\pi})}{\sigma_2(0, \widehat{\pi})^2} \\ &= \frac{k_2 k_1 e_0}{(k_{-1}+k_2)^2} \cdot \frac{k_1 s_0 + k_{-1} + k_2 + k_3 i_0 + k_{-3}}{k_3 i_0 + k_{-3}} \\ &= \varepsilon_{MM} \cdot \frac{k_1 s_0 + k_{-1} + k_2 + k_3 i_0 + k_{-3}}{k_3 i_0 + k_{-3}} =: \widetilde{\mu}_I,\end{aligned} \tag{82}$$

which is a direct consequence of monotonicity properties of the σ_j. This inequality is exact whenever (79) does not hold and s_0 is smaller than the argument of $\max q$.

6.3.2 Numerical Simulations

Generally, by Fenichel theory the accuracy of the reduction (77) improves along the parameter ray as $\varepsilon_I \to 0$ and $\mu_I^{(i)} \to 0$, for $i = 1, 2$, respectively. Continuing the procedure employed in the previous case studies, we illustrate the efficacy of the qualifiers $\varepsilon_I \ll 1, \mu_I^{(i)} \ll 1$ (with appropriate index i) with several numerical simulations:

1. For our first example, we once again consider the case in which all parameters except e_0 are equal, which is a representative of parameters of the same magnitude. Numerical simulations confirm that the accuracy of (77) improves as $\varepsilon_I \to 0$ and $\mu_I^{(1)} \to 0$ (see, Fig. 9).
2. In our second example, we demonstrate the effectiveness of ε_I and $\mu_I^{(i)}$ with parameters that have disparate magnitudes. We observe that $\mu_I^{(1)}$ is the definitive indicator of the accuracy of (77) when (79) holds, while $\mu_I^{(2)}$ is the indicator of the accuracy of (77) whenever (79) fails, reflecting the fact that one eigenvalue must have much smaller absolute value than the other two (see, Figs. 10, 11).

6.3.3 Near-Invariance

As in the previous sections, we now discuss special instances of near-invariance. The inhibitory mechanism can be turned off by requiring $k_3 i_0 = 0$, which implies that, for sufficiently small k_3 or i_0, the subspace $U := \{(s, c_1, c_2) \in \mathbb{R}^3 : c_2 = 0\}$ will be nearly invariant. One perspective is to define the parameter ray by $k_3 = \varepsilon k_3^*$ and $e_0 = \varepsilon e_0^*$. Then, the perturbation form of the mass action equations is

$$\begin{pmatrix}\dot{s}\\ \dot{c}_1\\ \dot{c}_2\end{pmatrix} = \begin{pmatrix}k_1 s + k_{-1} & k_1 s\\ -k_1 s - (k_{-1}+k_2) & -k_1 s\\ 0 & -k_{-3}\end{pmatrix}\begin{pmatrix}c_1\\ c_2\end{pmatrix} + \varepsilon \begin{pmatrix}-k_1 e_0^* s\\ k_1 e_0^* s\\ -k_3^*(c_1+c_2)(i_0 - c_2)\end{pmatrix} + \mathcal{O}(\varepsilon^2).$$

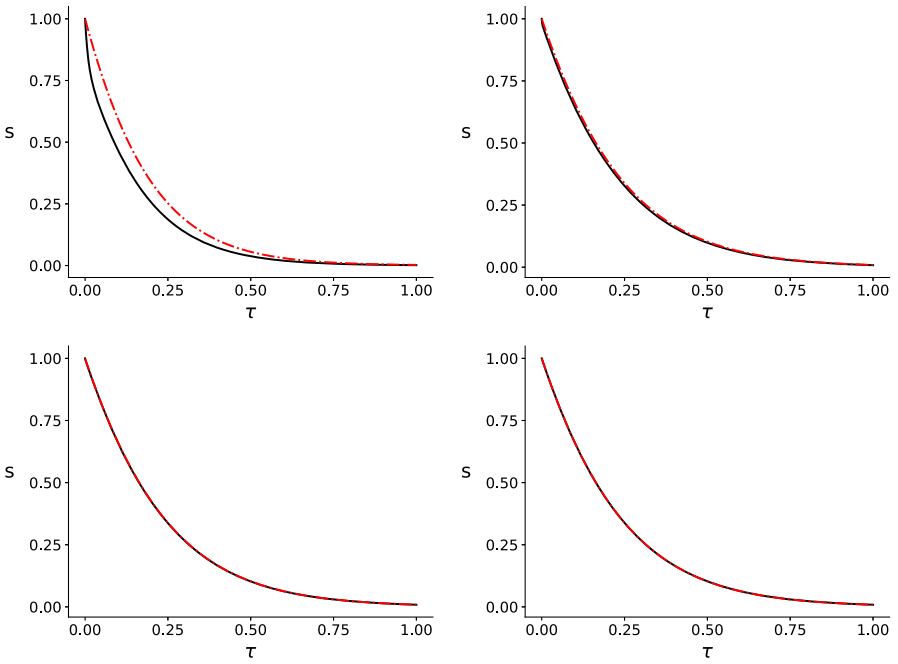

Fig. 9 Competitive inhibition reaction mechanism: With parameters of unit magnitude, and (79) valid, numerical simulations indicate that the accuracy of (77) improves along the parameter ray as both $\varepsilon_I \to 0$ and $\mu_I^{(1)} \to 0$. In all panels, the parameters (in arbitrary units) are: $s_0 = 1.0$, $k_1 = 1.0$, $k_2 = 1.0$, $k_{-1} = 1.0$, $k_3 = 1.0$, $k_{-3} = 1.0$ and $i_0 = 1.0$. The solid black curve is the numerical solution to the mass action system (75). The broken red curve is the numerical solution to (77). Time has been mapped to the τ scale: $\tau = t/T$, $\tau \in [0, 1]$ *Top Left panel*: $e_0 = 1.0$ with $\varepsilon_I = 1.25 \times 10^{-1}$ and $\mu_I^{(1)} = 5 \times 10^{-1}$. *Top Right panel*: $e_0 = 10^{-1}$ with $\varepsilon_I = 1.25 \times 10^{-2}$ and $\mu_I^{(1)} = 5 \times 10^{-2}$. *Bottom Left panel*: $e_0 = 10^{-2}$ with $\varepsilon_I = 1.25 \times 10^{-3}$ and $\mu_I^{(1)} = 5 \times 10^{-3}$. The reduction (77) is nearly indistinguishable from (75). *Bottom Right panel*: $e_0 = 10^{-4}$ with $\varepsilon_I = 1.25 \times 10^{-4}$ and $\mu_I^{(1)} = 5 \times 10^{-4}$. The QSS reduction (77) is again practically indistinguishable from (75) (Color figure online)

The QSS reduction is obtained by projecting the leading order perturbation onto the critical manifold, thus

$$\begin{pmatrix} \dot{s} \\ \dot{c}_1 \\ \dot{c}_2 \end{pmatrix} = \varepsilon \begin{pmatrix} 1 & \dfrac{k_1 s + k_{-1}}{k_1 s + k_{-1} + k_2} & \dfrac{k_1 k_2 s}{(k_1 s + k_{-1} + k_2) k_{-3}} \\ 0 & 0 & 0 \\ 0 & 0 & 0 \end{pmatrix} \begin{pmatrix} -k_1 e_0^* s \\ k_1 e_0^* s \\ 0 \end{pmatrix},$$

from which we recover

$$\dot{s} = -\frac{k_1 k_2 e_0 s}{k_1 s + k_{-1} + k_2},$$

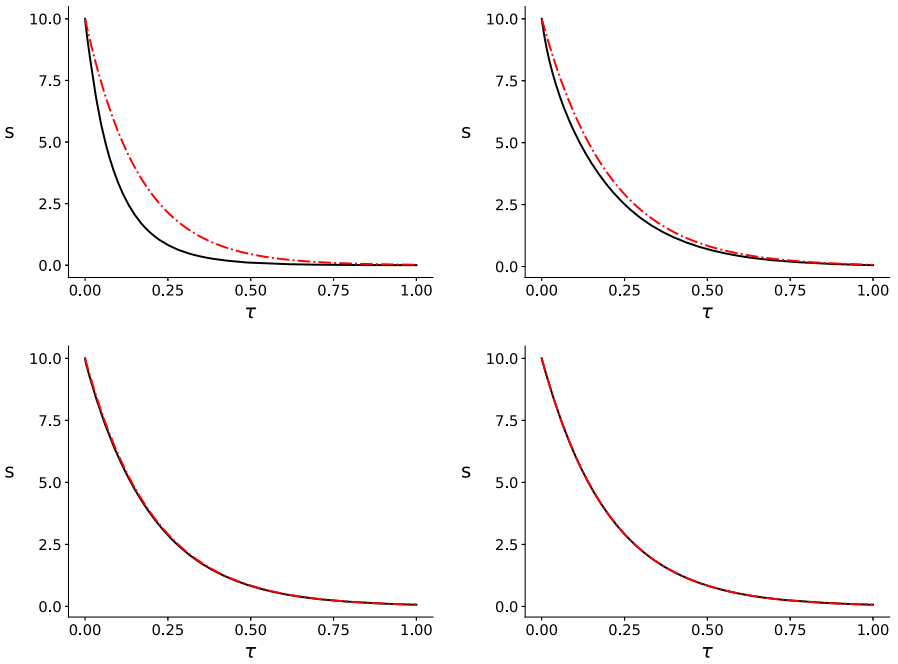

Fig. 10 Competitive inhibition reaction mechanism: When parameter values are disparate in magnitude, numerical simulations indicate that the accuracy of (77) improves along the parameter ray as $\mu_I^{(1)} \to 0$ when (79) holds. In all panels, the parameters (in arbitrary units) are: $s_0 = 10.0, k_1 = 1.0, k_2 = k_{-1} = 10^2$, $k_3 = k_{-3} = 10^{-1}$ and $i_0 = 1.0$. The solid black curve is the numerical solution for s to the mass action system (75). The broken red curve is the numerical solution to (77). Time has been mapped to the τ scale: $\tau = t/T,\ \ \tau \in [0, 1]$. *Top Left panel*: $e_0 = 1.0$, $\varepsilon_I \approx 2.5 \times 10^{-3}$, and $\mu_I^{(1)} \approx 2.5$. *Top Right panel*: $e_0 = 10^{-1}$, $\varepsilon_I \approx 2.5 \times 10^{-4}$, and $\mu_I^{(1)} \approx 2.5 \times 10^{-1}$. *Bottom Left panel*: $e_0 = 10^{-2}$, $\varepsilon_I \approx 2.5 \times 10^{-5}$, and $\mu_I^{(1)} \approx 2.5 \times 10^{-2}$. *Bottom Right panel*: $e_0 = 10^{-3}$, $\varepsilon_I \approx 2.5 \times 10^{-6}$, $\mu_I^{(1)} \approx 2.5 \times 10^{-3}$ and the QSS reduction (77) is nearly indistinguishable from (75). Collectively, these simulations indicate that $\mu_I^{(1)} \ll 1$ is the qualifier that ensures the validity of (77) when (79) holds (Color figure online)

i.e., the sQSSA of the MM reaction mechanism. This is not surprising. With initial conditions $s(0) = s_0, c_1(0) = c_2(0) = 0$, the dynamics are approximately two-dimensional. From a different perspective (taking independent limits), we can write (77) as

$$\dot{s} = -\frac{k_1 k_2 e_0 s}{k_1 s + (k_{-1} + k_2)\left(1 + \dfrac{k_3 i_0}{k_{-3}}\right)},$$

from which it is clear by inspection that the sQSSA is recoverable from (77) whenever $k_3 i_0 / k_{-3} \ll 1$. Consequently, whenever $k_3 i_0 / k_{-3} \ll 1$ we need only consider the magnitude of ε_I to ascertain the accuracy of (77) (see, Fig. 12).

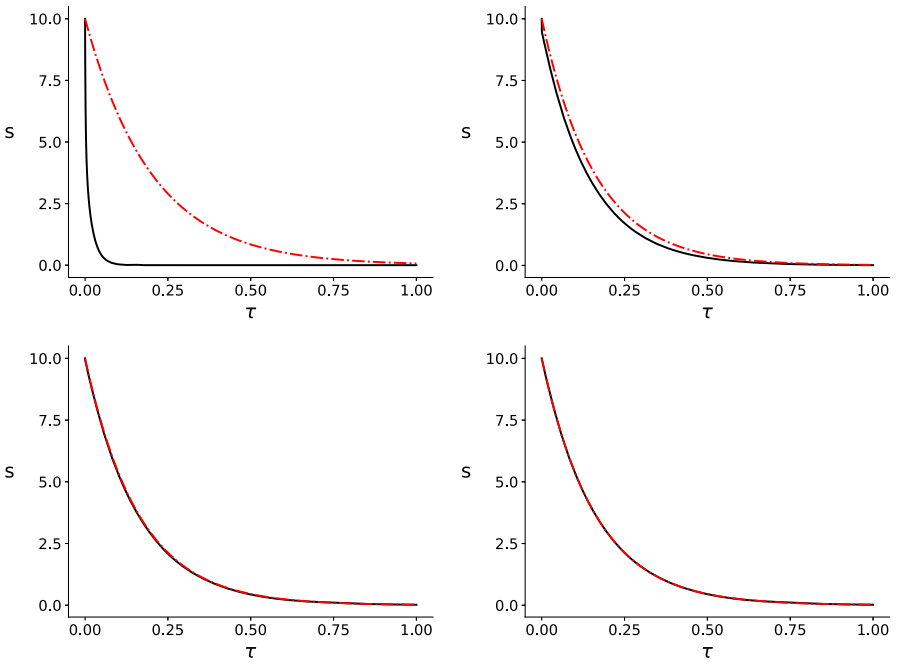

Fig. 11 Competitive inhibition reaction mechanism: When parameter values are disparate in magnitude, numerical simulations indicate that the accuracy of (77) improves along the search direction as $\mu_I^{(2)} \to 0$ when (79) fails. In all panels, the parameters (in arbitrary units) are: $s_0 = 10.0, k_1 = 1.0, k_2 = k_{-1} = 10^2$, $k_{-3} = 10^{-2}$ and $k_3 = i_0 = 1.0$. The solid black curve is the numerical solution for s to the mass action system (75). The broken red curve is the numerical solution to (77). Time has been mapped to the τ scale: $\tau = t/T, \ \tau \in [0, 1]$. *Top Left panel*: $e_0 = 1.0$, $\varepsilon_I \approx 2.5 \times 10^{-3}$, and $\mu_I^{(2)} \approx 12.6$. *Top Right panel*: $e_0 = 10^{-1}$, $\varepsilon_I \approx 2.5 \times 10^{-4}$, and $\mu_I^{(2)} \approx 12.6 \times 10^{-1}$. *Bottom Left panel*: $e_0 = 10^{-2}$, $\varepsilon_I \approx 2.5 \times 10^{-5}$, and $\mu_I^{(2)} \approx 12.6 \times 10^{-2}$. *Bottom Right panel*: $e_0 = 10^{-3}$, $\varepsilon_I \approx 2.5 \times 10^{-6}$, and $\mu_I^{(2)} \approx 12.6 \times 10^{-3}$. Observe the QSS reduction (77) is nearly indistinguishable from (75), which indicates that $\mu_I^{(2)} \ll 1$ is the qualifier that ensures the validity of (77) when (79) fails (Color figure online)

7 Case Studies: Reduction from Dimension Three to Two

In this section, we further discuss the uncompetitive and competitive inhibition reaction mechanisms, but now we consider exemplary cases of reduction to dimension two. These scenarios are of less practical relevance than those in the previous section, but we present them for illustrative purposes. We will provide less detailed discussions, and will be content to show the feasibility of the method. The results from Sect. 5, in particular Proposition 5 and Sect. 5.4, will be employed. The determination of distinguished parameters now amounts to finding (or estimating) the maximum and minimum of rational functions in two variables on some compact set.

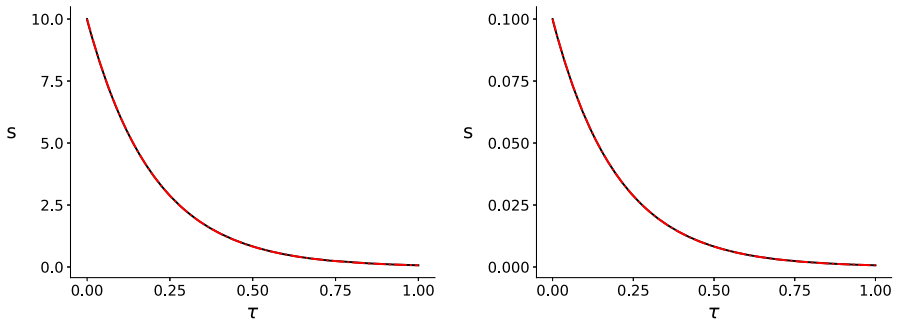

Fig. 12 Competitive inhibition reaction mechanism: If $k_3 i_0/k_{-3} \ll 1$, the subspace U is nearly invariant, and (77) will be accurate provided $\varepsilon_{RS} \ll 1$. In both panels, the parameters (in arbitrary units) are: $e_0 = 10.0$, $k_1 = 1.0$, $k_2 = k_{-1} = 10^3$, $k_3 = 10^{-7}$, $k_{-3} = 10^{-1}$ and $i_0 = 10^0$. It is straightforward to verify that (79) is satisfied, and that $\varepsilon_{MM} = 2.5 \times 10^{-3}$, and $\mu_I^{(1)} \approx 50$. The solid black curve is the numerical solution for s to the mass action system (75). The broken red curve is the numerical solution to (77). Time has been mapped to the τ scale: $\tau = t/T$, $\tau \in [0, 1]$. *Left panel*: $s_0 = 10.0$ and the reduction (77) is very accurate. *Right panel*: Here $s_0 = 10^{-1}$ and the reduction (77) is still accurate; this confirms the long-time validity of (77) is regulated by the magnitude of ε_{MM} whenever $k_3 i_0/k_{-3} \ll 1$ (Color figure online)

7.1 Uncompetitive Inhibition Reaction Mechanism

For the uncompetitive inhibition reaction mechanism, (64) and (65), one sees that $k_1 = k_{-3} = 0$, with all other parameters contained in some compact subset of the open positive orthant, defines a TFPV $\widehat{\pi}$, with a two-dimensional critical manifold $\widetilde{Y}$ given by $c_1 = 0$. The TFPV conditions mean that both elementary reactions responsible for the formation of C_1 are slow.

We consider system (65) with initial values $s(0) = s_0$, $c_1(0) = c_2(0) = 0$ on the compact positively invariant set

$$K := \{(s, c_1, c_2) \in \mathbb{R}^3_{\geq 0} : 0 \leq s \leq s_0, \quad c_1 + c_2 \leq e_0, \quad c_2 \leq \min\{e_0, i_0\}\},$$

and take the ray direction

$$\rho = (0, 0, k_1^*, 0, 0, 0, k_{-3}^*)^{\mathrm{tr}}$$

in parameter space, with $k_i = \varepsilon k_i^*$, $k_i^* > 0$, for $i \in \{1, -3\}$. Straightforward computations yield the reduced system

$$\begin{pmatrix} \dot{s} \\ \dot{c}_2 \end{pmatrix} = \frac{1}{k_{-1} + k_2 + k_3(i_0 - c_2)} \begin{pmatrix} -k_1(e_0 - c_2)(k_2 + k_3(i_0 - c_2))s + k_{-3}k_{-1}c_2 \\ k_1 k_3 (e_0 - c_2)(i_0 - c_2)s - k_{-3}(k_{-1} + k_2)c_2 \end{pmatrix}, \tag{83}$$

with initial conditions $s(0) = s_0$, $c_2(0) = 0$. A straightforward phase plane analysis of system (83) (respectively, of the orbitally equivalent system with the common denominator discarded) shows that every solution in the positive quadrant converges to the stationary point 0.

7.1.1 Asymptotic Small Parameters

We now determine dimensionless parameters that gauge the accuracy of (83). For the sake of brevity, we will restrict attention to the case $e_0 > i_0$. The coefficients of the characteristic polynomial on $\widetilde{Y}$ are given by

$$\begin{aligned}
\widetilde{\sigma}_1 &= k_{-1} + k_2 + k_3(i_0 - c_2) + \varepsilon\,(\cdots)\\
\widetilde{\sigma}_2 &= k_1\,(k_3(i_0 - c_2)(e_0 - c_2 + s) + k_2(e_0 - c_2)) + k_{-3}(k_{-1} + k_2) + \varepsilon^2\,(\cdots)\\
\widetilde{\sigma}_3 &= k_1 k_{-3} k_2 (e_0 - c_2).
\end{aligned}$$

Thus,

$$\begin{aligned}
\sigma_1 &= k_{-1} + k_2 + k_3(i_0 - c_2)\\
\widehat{\sigma}_2 &= k_1^*\,(k_3(i_0 - c_2)(e_0 - c_2 + s) + k_2(e_0 - c_2)) + k_{-3}^*(k_{-1} + k_2)\\
\widehat{\sigma}_3 &= k_1^* k_{-3}^* k_2 (e_0 - c_2),
\end{aligned}$$

and the first nondegeneracy condition from Lemma 7 is satisfied since $e_0 > i_0$.

According to Propositions 5 and 6 and their proofs, for timescale comparisons we consider the rational function

$$q(s, c_2) = \frac{\widehat{\sigma}_2(s, c_2.\widehat{\pi}, \rho, 0)}{\sigma_1(s, c_2, \widehat{\pi})^2}, \quad 0 \le s \le s_0, \quad 0 \le c_2 \le i_0.$$

Since $\widehat{\sigma}_2$ decreases with c_2 and increases with s, while σ_1 decreases with c_2, we obtain an upper estimate from

$$\varepsilon^* \le \varepsilon \frac{\max \widehat{\sigma}_2}{(\min \sigma_1)^2} = \frac{k_1(k_3 i_0(e_0 + s_0) + k_2 e_0) + k_{-3}(k_{-1} + k_2)}{(k_{-1} + k_2)^2} =: \delta^*.$$

Moreover from $\varepsilon^* \ge q(s_0, 0)$, we find that

$$\frac{k_1(k_3 i_0(e_0 + s_0) + k_2 e_0) + k_{-3}(k_{-1} + k_2)}{(k_{-1} + k_2 + k_3 i_0)^2} \le \varepsilon^*.$$

Likewise, we obtain lower timescale estimates from

$$\varepsilon_* \ge \varepsilon \frac{\min \widehat{\sigma}_2}{(\max \sigma_1)^2} = \frac{k_1 k_2 (e_0 - i_0) + k_{-3}(k_{-1} + k_2)}{(k_{-1} + k_2 + k_3 i_0)^2} =: \delta_*.$$

Thus, for i_0 not too large, the estimates by δ^* and δ_* are quite acceptable.

To estimate the disparity of the slow eigenvalues, according to Sect. 5.4, we consider

$$\kappa^* = \max \frac{\sigma_1 \widehat{\sigma}_3}{\widehat{\sigma}_2^2} \le \frac{(k_{-1} + k_2 + k_3 i_0) k_1^* k_{-3}^* k_2 e_0}{(k_1^* k_2 e_0 + k_{-3}^*(k_{-1} + k_2))^2} =: \nu^*$$

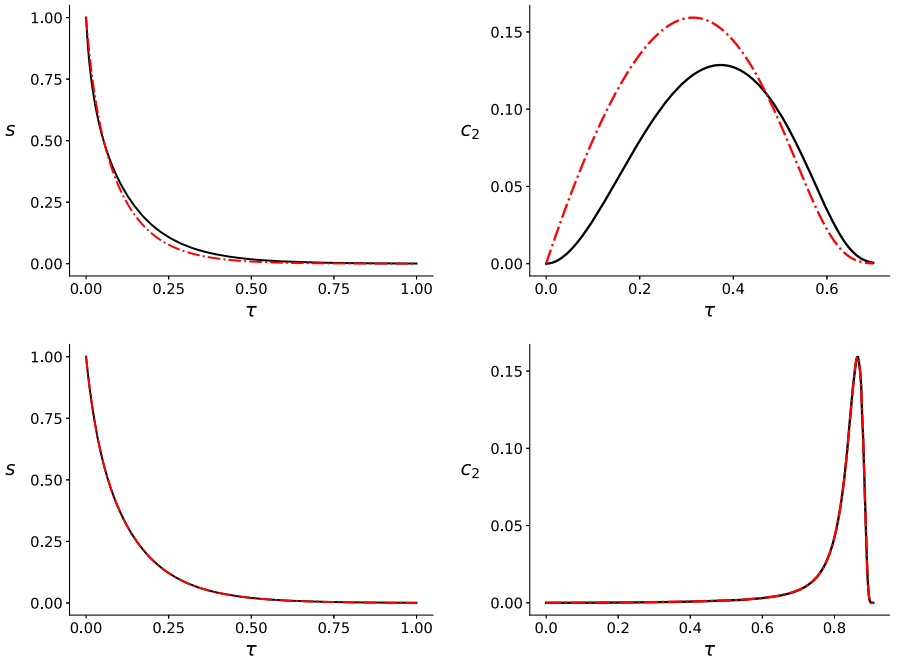

Fig. 13 Uncompetitive inhibition reaction mechanism with reduction to dimension two. In all panels, the parameters (in arbitrary units) are: $e_0 = 2.0$, $s_0 = 1.0$, $k_2 = k_{-1} = 1.0$, $k_3 = 1.0$, and $i_0 = 1.0$. The solid black curve is the numerical solution to the mass action system (65). The dashed/dotted red curve is the numerical solution to (83). Time has been mapped to the τ scale: $\tau = t/T$, $\tau \in [0, 1]$. *Top panels*: $k_1 = k_{-3} = 10^{-1}$ with $\delta^* = 1.75 \times 10^{-1}$ and $\delta_* = 3.33 \times 10^{-2}$. *Bottom panels*: $k_1 = k_{-3} = 10^{-3}$ with $\delta^* = 1.75 \times 10^{-3}$ and $\delta_* = 3.33 \times 10^{-4}$. As expected, the accuracy of (83) improves as the perturbation decreases along the parameter ray (Color figure online)

as well as

$$\kappa_* = \min \frac{\sigma_1 \widehat{\sigma}_3}{\widehat{\sigma}_2^2} \geq \frac{(k_{-1} + k_2) k_1^* k_{-3}^* k_2 (e_0 - i_0)}{(k_1^* (k_3 i_0 (e_0 + s_0) + k_2 e_0) + k_{-3}^* (k_{-1} + k_2))^2} =: \nu_*.$$

Whenever i_0 is not too large, these two parameters are close, and so are the slow eigenvalues.

7.1.2 Numerical Simulations

From Fenichel theory, it is known that the accuracy of the reduction (83) improves along the perturbation direction as $\varepsilon \to 0$. We include some numerical simulations to gauge the efficacy of the parameter δ^*:

1. Following the outline established in Sect. 6, we first consider a case when all parameters are of unit order. Numerical simulations confirm that the accuracy of (83) improves as $\delta^* \to 0$ along the parameter ray direction (see, Fig. 13). We include the values of δ_* to indicate the variation of timescale ratios.

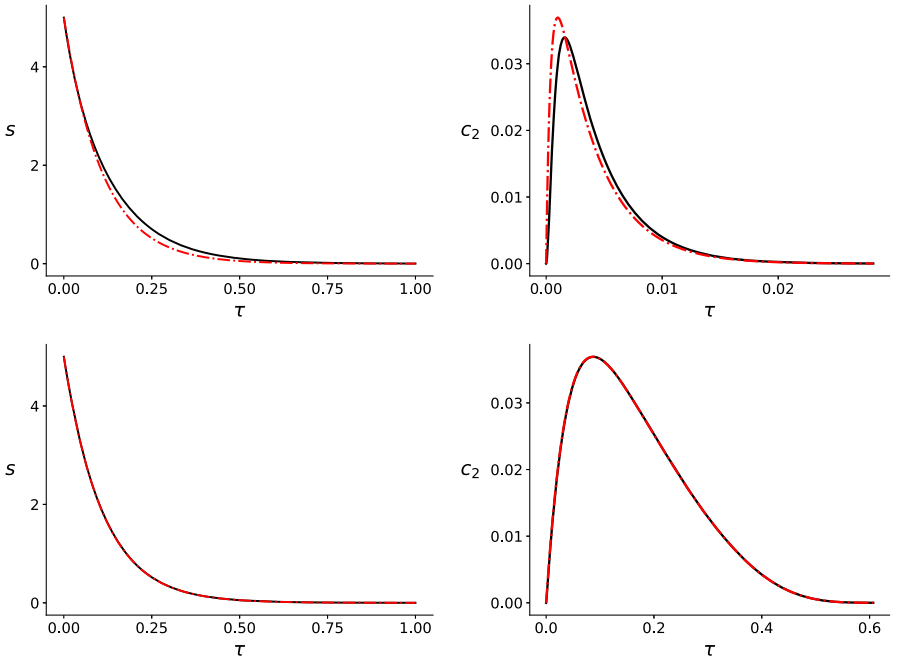

Fig. 14 Uncompetitive inhibition reaction mechanism with reduction to dimension two and disparate parameter values. In all panels, the parameters (in arbitrary units) are: $e_0 = 10.0$, $s_0 = 5.0$, $k_2 = 10^3$, $k_{-1} = 10^2$, $k_3 = 10.0$, and $i_0 = 1.0$. The solid black curve is the numerical solution to the mass action system (65). The broken red curve is the numerical solution to (83). Time has been mapped to the τ scale: $\tau = t/T$, $\tau \in [0, 1]$. *Top panels*: $k_1 = k_{-3} = 10^2$ with $\delta^* \approx 9.3 \times 10^{-1}$ and $\delta_* \approx 8.2 \times 10^{-1}$. *Bottom panels*: $k_1 = k_{-3} = 1.0$ with $\delta^* \approx 9.3 \times 10^{-3}$ and $\delta_* \approx 8.3 \times 10^{-3}$. Again, it is clear that the accuracy of (83) improves as the perturbation decreases along the parameter ray. Notably, the approximation in the second case is very good although $k_1 = k_{-3} = 1$. (As always, the expression "$\ll 1$" should not be taken too literally.) As for measuring the discrepancy of the "slow" eigenvalues, one finds $\kappa_* \geq \nu_* \approx 7.8 \cdot 10^{-2}$ and $\kappa^* \leq \nu^* \approx 9.0 \cdot 10^{-2}$. This indicates a ratio of about 10^{-1} (Color figure online)

2. In a second set of simulations, we consider the case of parameter values that are disparate in magnitude. Numerical simulations confirm once again that the accuracy of (83) improves along the parameter ray direction as $\delta^* \to 0$ (see, Fig. 14).

7.2 Competitive Inhibition Reaction Mechanism

For the competitive inhibition reaction mechanism, (74) and (75), we consider the case that formation of complex C_1, and both formation and degradation of complex C_2, are slow. Setting $k_1 = k_3 = k_{-3} = 0$, with all the other parameters contained in a compact subset of the positive orthant, defines a TFPV $\widehat{\pi}$ for dimension $s = 2$, the critical manifold $\widetilde{Y}$ being given by $c_1 = 0$ (see, Kruff and Walcher 2019). We consider

the system on the compact positively invariant set K defined by

$$K := \{(s, c_1, c_2) \in \mathbb{R}^3_{\geq 0} : 0 \leq s \leq s_0, \quad 0 \leq c_1 \leq e_0, \quad 0 \leq c_2 \leq \min\{e_0, i_0\}\},$$

choosing the ray direction

$$\rho = (0, 0, k_1^*, 0, 0, k_3^*, k_{-3}^*)^{\text{tr}}$$

in parameter space, and $k_i = \varepsilon k_i^*$ with $k_i^* > 0$ for $i \in \{1, 3, -3\}$. Standard computations yield the reduced system

$$\begin{aligned} \dot{s} &= -\frac{k_1 k_2}{k_{-1} + k_2}(e_0 - c_2)s \\ \dot{c}_2 &= k_3(e_0 - c_2)(i_0 - c_2) - k_{-3}c_2 \end{aligned} \tag{84}$$

with initial conditions $s(0) = s_0$, $c_2(0) = 0$. The qualitative behavior of this system is easily determined. All solutions in the positive quadrant converge to a stationary point $(0, c_2^*)$, with $0 < c_2^* < \min\{e_0, i_0\}$.[21]

7.2.1 Asymptotic Small Parameters

For the sake of brevity, we will consider only the case $e_0 > i_0$. The coefficients of the characteristic polynomial on $\widetilde{Y}$ are

$$\begin{aligned} \widetilde{\sigma}_1 &= k_{-1} + k_2 + \varepsilon\,(\cdots) \\ \widetilde{\sigma}_2 &= k_1 k_2(e_0 - c_2) + k_3(e_0 + i_0 - 2c_2)(k_{-1} + k_2) + k_{-3}(k_{-1} + k_2) + \varepsilon^2\,(\cdots) \\ \widetilde{\sigma}_3 &= k_1 k_3 \cdot (k_2 e_0(e_0 + i_0 - 2c_2) + k_2 c_2(2c_2 - e_0 - i_0)) + k_1 k_{-3} \cdot k_2(e_0 - c_2), \end{aligned}$$

and we obtain

$$\begin{aligned} \sigma_1 &= k_{-1} + k_2 \\ \widehat{\sigma}_2 &= k_1^* k_2(e_0 - c_2) + k_3^*(e_0 + i_0 - 2c_2)(k_{-1} + k_2) + k_{-3}^*(k_{-1} + k_2) \\ \widehat{\sigma}_3 &= k_1^* k_2(e_0 - c_2)\left(k_3^*(e_0 + i_0 - 2c_2) + k_{-3}^*\right). \end{aligned}$$

The nondegeneracy conditions are satisfied (also at $c_2 = i_0$), due to $e_0 > i_0$. As for timescales, we need to analyze the rational function

$$q(s, c_2) = \frac{\widehat{\sigma}_2(s, c_2, \widehat{\pi}, \rho, 0)}{\sigma_1(s, c_2, \widehat{\pi})^2}, \quad 0 \leq s \leq s_0, \quad 0 \leq c_1 \leq e_0, \quad 0 \leq c_2 \leq i_0.$$

Since σ_1 is constant and $\widehat{\sigma}_2$ is decreasing with c_2, attaining its maximum at $c_2 = 0$, and its minimum at $c_2 = i_0$, we find the distinguished parameters

$$\varepsilon^* = \frac{k_1 k_2 e_0 + (k_3(e_0 + i_0) + k_{-3})(k_{-1} + k_2)}{(k_{-1} + k_2)^2}$$

[21] Incidentally, it is possible to compute the solutions to (84) via quadratures. The second equation is separable, and upon substitution the first equation is non-autonomous linear.

and

$$\varepsilon_* = \frac{k_1 k_2 (e_0 - i_0) + (k_3 (e_0 - i_0) + k_{-3})(k_{-1} + k_2)}{(k_{-1} + k_2)^2}.$$

Furthermore, according to Sect. 5.4, we consider

$$\kappa^* = \max \frac{\sigma_1 \widehat{\sigma}_3}{\widehat{\sigma}_2^2} \leq \frac{k_1^* k_2 e_0 (k_3^* (e_0 + i_0) + k_{-3}^*)(k_{-1} + k_2)}{\left(k_1^* k_2 (e_0 - i_0) + (k_3^* (e_0 - i_0) + k_{-3}^*)(k_{-1} + k_2)\right)^2} =: \nu^* \tag{85}$$

and

$$\kappa_* = \min \frac{\sigma_1 \widehat{\sigma}_3}{\widehat{\sigma}_2^2} \geq \frac{k_1^* k_2 (e_0 - i_0)(k_3^* (e_0 - i_0) + k_{-3}^*)(k_{-1} + k_2)}{\left(k_1^* k_2 e_0 + (k_3^* (e_0 + i_0) + k_{-3}^*)(k_{-1} + k_2)\right)^2} =: \nu_* \tag{86}$$

to measure the disparity between the eigenvalues λ_2 and λ_3.

7.2.2 Numerical Simulations

We present numerical examples to gauge the accuracy of the reduction (84) with decreasing ε^*:

1. For our first example, we consider the case with $\pi := \varepsilon(k_1^*, 1.0, 1.0, 1.0, 1.0., k_3^*, k_{-3}^*, 1.0)^{\text{tr.}}$ (see, Fig. 15). We include the values of ε^*, ε_* to indicate the variation of timescale ratios.
2. For our second example, we again consider a case when parameters are of differing magnitudes. Once more, numerical simulations confirm that the QSS reduction (84) improves as $\varepsilon^* \to 0$ along the parameter ray (see, Fig. 16).

7.2.3 The Case of Very Small k_1: Three Timescales

Finally, we discuss a scenario mentioned in Sect. 5.4. From equations (85) and (86), below one sees that both κ^* and κ_* approach zero as $k_1^* \to 0$. This may indicate three timescales. Moreover, from equation (75), one sees that the plane defined by $c_1 = 0$ is invariant when $k_1 = 0$, thus nearly invariant when k_1 is small. A coordinate-independent approach to a three-timescale scenario was presented in Kruff and Walcher (2019), based on work of Cardin and Texeira (2017). We introduce two small parameters ε_1, ε_2 and

$$k_3 = \varepsilon_1 k_3^\dagger,\ k_{-3} = \varepsilon_1 k_{-3}^\dagger,\ k_1 = \varepsilon_1 \varepsilon_2 k_1^\dagger,$$

and rewrite system (75) with three timescales. As detailed in Kruff and Walcher (2019), the system admits a sequence of two reductions, with nested invariant manifolds:

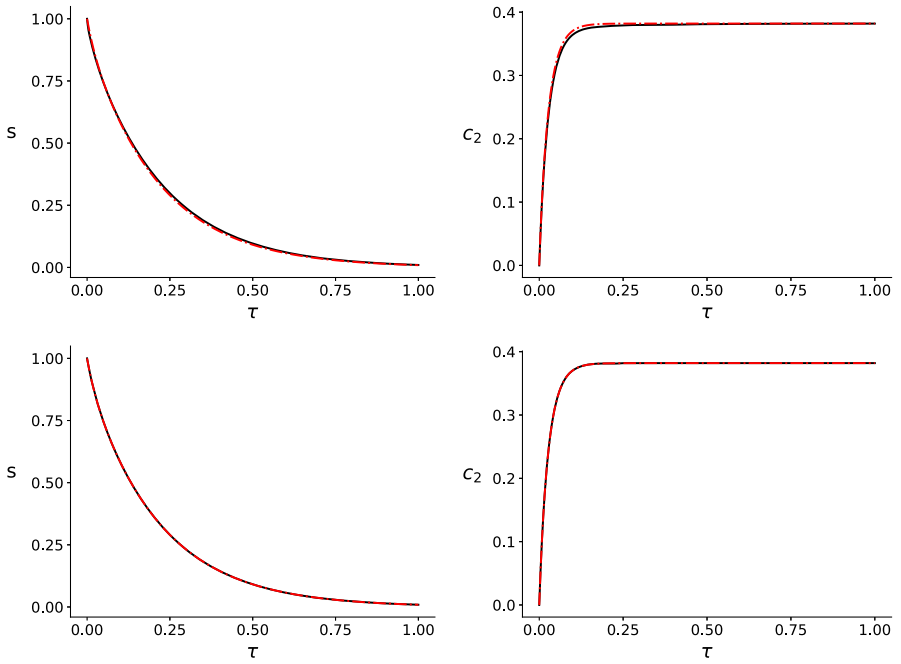

Fig. 15 Competitive inhibition reaction mechanism with reduction to dimension two. The accuracy of (84) improves along the parameter ray. In all panels, the parameters (in arbitrary units) are: $e_0 = 1.0$, $s_0 = 1.0$, $k_2 = 1.0$, $k_{-1} = 1.0$, and $i_0 = 1.0$. The solid black curve is the numerical solution to the mass action system (75). The broken red curve is the numerical solution to (84). Time has been mapped to the τ scale: $\tau = t/T, \quad \tau \in [0, 1]$. *Top panels*: Simulation performed with $k_1 = k_{-3} = k_3 = 10^{-1}$ and $\varepsilon^* = 1.75 \times 10^{-1}$, $\varepsilon_* = 5.0 \times 10^{-2}$. *Bottom panels*: Simulation performed with $k_1 = k_{-3} = k_3 = 10^{-3}$ and $\varepsilon^* = 1.75 \times 10^{-3}$, $\varepsilon_* = 5.0 \times 10^{-4}$. The singular perturbation reduction (84) is practically indistinguishable from (75) (Color figure online)

A reduction to slow dynamics on a two-dimensional invariant manifold close to $c_1 = 0$, with reduced system

$$\begin{pmatrix} \dfrac{\mathrm{d}s}{\mathrm{d}\tau_1} \\ \dfrac{\mathrm{d}c_2}{\mathrm{d}\tau_1} \end{pmatrix} = \begin{pmatrix} 0 \\ k_3^{\dagger}(e_0 - c_2)(i_0 - c_2) - k_{-3}^{\dagger} c_2 \end{pmatrix} \tag{87}$$

with $\tau_1 = \varepsilon_1 t$.

A subsequent reduction to "very slow" dynamics on a one-dimensional invariant manifold close to $c_1 = 0$, $c_2 = \widetilde{c}_2$, with

$$\widetilde{c}_2 = \frac{k_3(e_0 + i_0) + k_{-3} - \sqrt{(k_3(e_0 + i_0) + k_{-3})^2 - 4e_0 i_0 k_3^2}}{2k_3}.$$

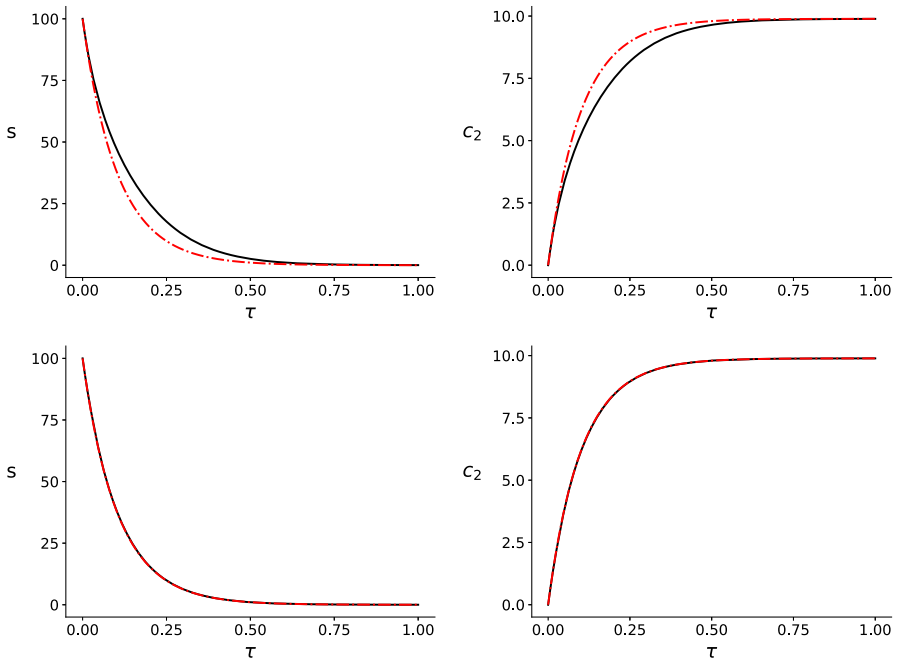

Fig. 16 Competitive inhibition reaction mechanism with reduction to dimension two and disparate parameters. In all panels, the "non-small" parameters (in arbitrary units) are: $e_0 = 10^2$, $s_0 = 10^2$, $k_2 = 10^2$, $k_{-1} = 1.0$, and $i_0 = 10.0$. The solid black curve is the numerical solution to the mass action system (75). The broken red curve is the numerical solution to (84). Time has been mapped to the τ scale: $\tau = t/T$, $\tau \in [0, 1]$. *Top panels*: Simulation performed with $k_1 = k_{-3} = k_3 = 1.0$ and $\varepsilon^* \approx 2.08$, $\varepsilon_* \approx 1.78$. This scenario is outside the range of applicability for Proposition 6. *Bottom panels*: Simulation performed with $k_1 = k_{-3} = k_3 = 10^{-2}$ and $\varepsilon^* \approx 2.08 \times 10^{-2}$, $\varepsilon_* \approx 1.78 \times 10^{-2}$. The singular perturbation reduction (84) here is very close to (75) (Color figure online)

The fully reduced one-dimensional equation is then

$$\frac{\mathrm{d}s}{\mathrm{d}\tau_2} = -\frac{k_2 \cdot k_1^{\dagger}(e_0 - \widetilde{c}_2)}{k_{-2} + k_{-1}} s$$

with $\tau_2 = \varepsilon_1 \varepsilon_2 t$, or, restated in fast time,

$$\dot{s} = -\frac{k_2 \cdot k_1(e_0 - \widetilde{c}_2)}{k_{-2} + k_{-1}} s. \tag{88}$$

Figure 17 illustrates the "slow–very slow" dynamics for a numerical example.

8 Discussion

While the underlying theory and the qualitative analysis concerning the reduction of biochemical and chemical reaction networks is well understood and rests on solid

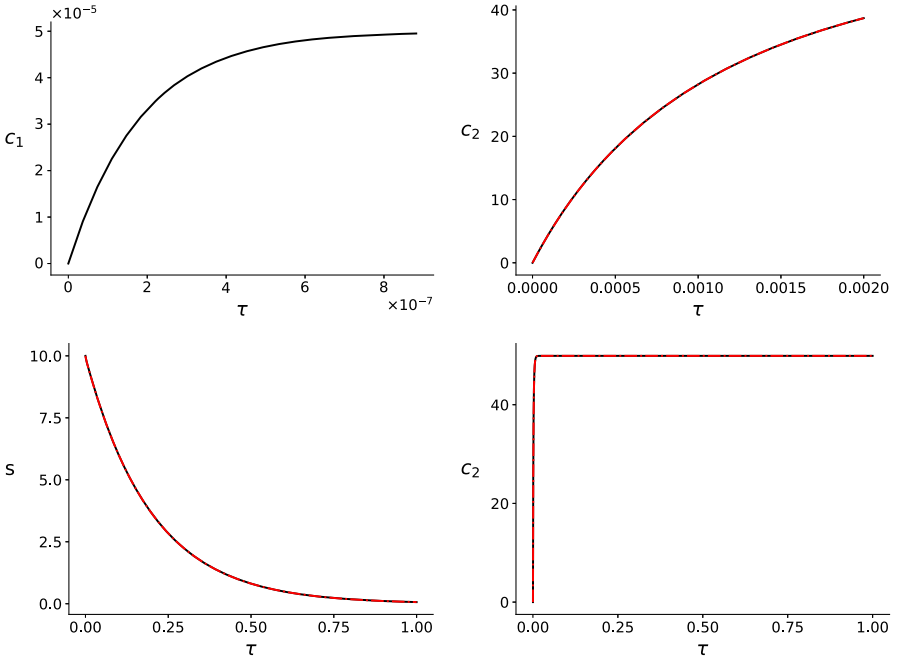

Fig. 17 Competitive inhibition reaction mechanism with a three timescale scenario. In both panels, the parameters (in arbitrary units) are: $s_0 = 10.0$, $e_0 = 10^2$, $k_1 = 1 \times 10^{-4}$, $k_2 = 2 \times 10^3$, $k_{-1} = 1.0$,$k_3 = 10^{-1}$, $k_{-3} = 10^{-3}$ and $i_0 = 50.0$. The solid black curve is the numerical solution to the mass action system (75). The dashed/dotted red curves are the numerical solutions to (87) and (88). Time has been mapped to the τ scale: $\tau = t/T$. For the chosen parameter values, $\varepsilon^* \approx 7.5 \times 10^{-3}$ and $\varepsilon_* \approx 2.5 \times 10^{-3}$. Moreover, the two slow eigenvalues are disparate since $\nu^* \approx 6 \times 10^{-3}$, this is consistent with a three timescale scenario. *Top Left panel*: The initial accumulation of c_1 occurs on the fast timescale; the concentrations of c_2 and s are approximately constant on the fast timescale. *Top Right panel*: The reduction (87) is accurate on the slow timescale as c_2 approaches its threshold value, $\widetilde{c}_2$. *Bottom Left panel*: The reduction (88) is accurate on the very slow timescale, τ_2, on which the depletion of s is significant. *Bottom Right panel*: On the very slow timescale, c_2 is effectively constant: $c_2 \approx \widetilde{c}_2$ (Color figure online)

ground, there is a sizable gap between available theory and applications to parameter identification problems in laboratory settings, where heuristics and ad hoc approaches are (perforce) still prevalent. Closing the gap requires further, more precise theoretical results. The present paper contributes toward this goal, by introducing a general consistent method to obtain perturbation parameters, based on local linear timescales. Note that by its nature, our approach is focused on and limited to the local behavior.

We briefly recall the context and reviewing the results of the present paper:

1. We start from a singular perturbation reduction with a well-defined critical manifold. This is crucial to ensure appropriateness of linearizability. Considering the three steps (as outlined in Introduction) that are necessary for a global quantitative estimate of the approximation error, our results amount to an essential part of Step 1. In absence of results concerning Steps 2 and 3, direct applications are limited. But, our results permit consistency checks, which show that certain common perturbation parameters are not feasible.

2. Using classical results from algebra to approximate eigenvalue ratios in the asymptotic limit, we obtained parameters that are computable, palatable, and admit a biochemical interpretation.
3. We first applied our methods to the Michaelis–Menten reaction mechanism. As it turns out, even for such a familiar system our approach provides new and elucidating perturbation parameters. Moreover, we included a partial discussion of Step 3 for the irreversible system with small product formation rate.
4. For two relevant extensions of the Michaelis–Menten reaction mechanism (like the uncompetitive inhibition and competitive inhibition), and a non-Michaelis–Menten reaction mechanism (like the cooperative system with two complexes), we derived perturbation parameters in the spirit of Segel and Slemrod (1989), but without resorting to nonlinear timescales. This stands in contrast to the practice of using ε_{BH} or ε_{SSl}, or ad hoc modifications of these. We augmented these results by an extensive discussion of numerical examples to illustrate the efficacy of these parameters, but also to highlight the importance of the compactness requirements we impose throughout. We also discussed one case that leads to a system with three timescales.
5. Finally, we discussed exemplary cases of reduction from dimension three to dimension two for both reaction inhibition scenarios, to verify the feasibility of our approach. Numerical simulations illustrate the quality and accuracy of the approximations.

The remaining items (Step 2 and Step 3) as stated in the Introduction need to be handled on a case-by-case basis. We will provide a complete analysis of the irreversible Michaelis–Menten reaction mechanism with low enzyme in forthcoming work.

9 Appendix

In this section, we collect some technical matters and proofs, as well as recalling some known results for which a concise presentation seems appropriate and useful.

9.1 Lyapunov Function Arguments

Lyapunov functions can be used to estimate the approach to the slow manifold in a singularly perturbed system, as was mentioned in Introduction. This estimate gives rise to a small parameter ε_L which controls the distance of the solution to the slow manifold. We give an account of the relevant facts here.

We first state an auxiliary result that goes back to Lyapunov.

Lemma 5 *Let Q be a real $n \times n$-matrix, with eigenvalues $\mu_1, \ldots, \mu_n$, and let $\delta > 0$. Then there exists a scalar product $\langle \cdot, \cdot \rangle$ on $\mathbb{R}^n$ such that for all x one has*

$$\left(\min_{1 \le i \le n} \operatorname{Re} \mu_i - \delta \right) \langle x,\ x \rangle \le \langle x,\ Qx \rangle \le \left(\max_{1 \le i \le n} \operatorname{Re} \mu_i + \delta \right) \langle x,\ x \rangle ,$$

and

$$\left(\min_{1\le i\le n} |\mu_i|^2 - \delta\right) \langle x,\ x\rangle \le \langle Qx,\ Qx\rangle \le \left(\max_{1\le i\le n} |\mu_i|^2 + \delta\right) \langle x,\ x\rangle\,.$$

This can be proven as in Walter (1998, Chapter VII, §30) [see, also Arnold (1992, Chapter 22)]. For matrices that are diagonalizable over $\mathbb{C}$ build a real basis from real and imaginary parts of a complex eigenbasis. For the non-diagonalizable case, by suitable choice of basis elements the nilpotent part can be chosen to have norm $< \delta$.

9.1.1 Estimates

This presentation follows (Berglund and Gentz 2006, Section 2.1 ff.), but for illustrative purposes, we are satisfied with a local version. Consider a smooth system

$$\begin{aligned} \dot{x} &= \varepsilon \widetilde{f_1}(x, y, \varepsilon) \\ \dot{y} &= f_2(x, y, \varepsilon) \end{aligned}, \quad \text{briefly } \begin{pmatrix} \dot{x} \\ \dot{y} \end{pmatrix} = F\left(\begin{pmatrix} x \\ y \end{pmatrix}\right) \tag{89}$$

with $\begin{pmatrix} x \\ y \end{pmatrix}$ in some open subset of $\mathbb{R}^n$, $x \in \mathbb{R}^m$, and a nonnegative parameter ε. Moreover let $\begin{pmatrix} x_0 \\ y_0 \end{pmatrix}$ be such that $f_2(x_0, y_0, 0) = 0$, and M a suitable compact neighborhood of this point. (More conditions on M will be implicitly imposed below, by further assumptions.)

- Assume furthermore that

$$f_2(x, y, \varepsilon) = 0 \Longleftrightarrow y = g(x, \varepsilon)$$

for $\begin{pmatrix} x \\ y \end{pmatrix} \in M$ and $\varepsilon \le \varepsilon_{\max}$, with some positive $\varepsilon_{\max}$ and a smooth function g. The zero set Y_ε of $f_2(\cdot, \cdot, \varepsilon)$ in M will be called the slow manifold, or QSS manifold,[22] for ε. By Hadamard's lemma, after possibly shrinking M there exists a smooth matrix valued function A such that

$$f_2(x, y, \varepsilon) = A(x, y, \varepsilon) \cdot (y - g(x, \varepsilon)).$$

Thus, we may rewrite system (89) as

$$\begin{aligned} \dot{x} &= \varepsilon \widetilde{f_1}(x, y, \varepsilon) \\ \dot{y} &= A(x, y, \varepsilon) \cdot (y - g(x, \varepsilon)). \end{aligned} \tag{90}$$

With

$$D_y f_2(x, y, \varepsilon) = A(x, y, \varepsilon) + \big(D_y A(x, y, \varepsilon)\big)\,(y - g(x, \varepsilon)),$$

[22] This is an order ε approximation of the slow manifold in a singular perturbation setting.

one finds in particular

$$D_y f_2(x, y, \varepsilon) = A(x, y, \varepsilon) \text{ on } Y_\varepsilon.$$

- Now assume that all eigenvalues of $A(x_0, y_0, 0)$ have negative real parts. By continuity and suitable choice of M and $\varepsilon_{\max}$, all eigenvalues of $A(x, y, \varepsilon)$ have negative real part for $\begin{pmatrix} x \\ y \end{pmatrix} \in M$ and $0 \le \varepsilon \le \varepsilon_{\max}$. Due to Lemma 5, there exists a scalar product $\langle \cdot, \cdot \rangle$ on $\mathbb{R}^{n-m}$ and some $\gamma > 0$ such that

$$\langle z, A(x_0, y_0, 0)z \rangle \le -2\gamma \langle z, z \rangle, \quad \text{all } z \in \mathbb{R}^{n-m}.$$

(Recall the correspondence between 2γ and eigenvalues.) Thus, we may assume that

$$\langle z, A(x, y, \varepsilon)z \rangle \le -\gamma \langle z, z \rangle, \quad \text{all } z \in \mathbb{R}^{n-m}, \tag{91}$$

on M, with $0 \le \varepsilon \le \varepsilon_{\max}$. Denote by $\| \cdot \|$ the norm associated with this scalar product.

The following line of arguments is a slight variant of classical reasoning [which uses Gronwall's lemma, see, e.g., Evans (2014, Appendix B) for the latter]. For solutions of (89) we find

$$\begin{aligned} \frac{\mathrm{d}}{\mathrm{d}t} \langle y - g(x, \varepsilon), y - g(x, \varepsilon) \rangle &= 2 \langle y - g(x, \varepsilon), \dot{y} - D_x g(x, \varepsilon) f_1(x, y, \varepsilon) \rangle \\ &= 2 \langle y - g(x, \varepsilon), A(x, y, \varepsilon) (y - g(x, \varepsilon)) \rangle \\ &\quad -2 \langle y - g(x, \varepsilon), D_x g(x, \varepsilon) f_1(x, y, \varepsilon) \rangle . \end{aligned}$$

The first term on the right-hand side can be estimated by $-\gamma \cdot \langle y - g(x, \varepsilon), y - g(x, \varepsilon) \rangle$. As for the second term, by Cauchy-Schwarz one has

$$\begin{aligned} 2 \, |\langle y - g(x, \varepsilon), D_x g(x, \varepsilon) f_1(x, y, \varepsilon) \rangle| &\le 2 \| y - g(x, \varepsilon) \|_2 \cdot \| D_x g(x, \varepsilon) f_1(x, y, \varepsilon) \|_2 \\ &\le 2 \| y - g(x, \varepsilon) \|_2 \cdot (\| D_x g(x, \varepsilon) \| \cdot \| f_1(x, y, \varepsilon) \|) \end{aligned}$$

with suitable norms in the second and third factor.

Now, there exists a positive constant $\kappa = \varepsilon \widetilde{\kappa}$ such that

$$\| D_x g(x, \varepsilon) \| \cdot \| f_1(x, y, \varepsilon) \| \le \kappa.$$

So, for $V := \| y - g(x, \varepsilon) \|^2$ one obtains the differential inequality

$$\frac{\mathrm{d}V}{\mathrm{d}t} \le -2\gamma V + 2\kappa \sqrt{V}.$$

Comparison with the solution of the corresponding Bernoulli equation yields

$$V \leq V(0)\exp(-\gamma t) + \left(\frac{\kappa}{\gamma}\right)^2 \cdot (1 - \exp(-\gamma t)), \tag{92}$$

thus $\|y - g(x,\varepsilon)\| = \sqrt{V(t)}$ can be estimated, e.g., by $\sqrt{2}\frac{\kappa}{\gamma}$ as $t \to \infty$.[23] Therefore, after a transient phase the proximity of the solution to the slow manifold is controlled by

$$\varepsilon_L := \sqrt{2}\frac{\kappa}{\gamma} = \sqrt{2}\varepsilon\frac{\widetilde{\kappa}}{\gamma}. \tag{93}$$

More precisely, once $V(0)\exp(-\gamma t) \leq \left(\frac{\kappa}{\gamma}\right)^2$, the stated estimate holds. The inequality is satisfied whenever

$$t \geq \frac{1}{\gamma}\log\left(\frac{\gamma^2 V(0)}{\kappa^2}\right) \sim \log\frac{1}{\varepsilon_L},$$

and this indicates that the time span for the approach to the QSS manifold is of order $|\log\varepsilon_L|$ in the fast timescale, and of order $\varepsilon_L|\log\varepsilon_L|$ in the slow timescale $\varepsilon_L t$. (A more detailed analysis will provide a lower estimate by a variant of (91), and confirm that the asymptotic estimate cannot be improved.) In particular time spans of order 1 will not suffice for the transient.

In reaction network settings, ε_L is a dimensional parameter (with dimension concentration); a suitable normalization needs to be chosen.

9.1.2 A Correspondence to Eigenvalues

We sketch the relation of the small parameter ε_L to eigenvalues of the Jacobian. For the sake of simplicity, we only consider the linearization here, disregarding higher-order terms. Given the system

$$\begin{aligned}\dot{x} &= -\varepsilon\widetilde{U}x + \varepsilon\widetilde{V}y \\ \dot{y} &= \quad Wx \quad - \quad Zy \quad = -Z\left(y - Z^{-1}W\right)x\end{aligned} \quad , \text{ briefly } \begin{pmatrix}\dot{x}\\ \dot{y}\end{pmatrix} = F(x,y,\varepsilon),$$

and keeping the notation from above, we have $A = -Z$, $g(x) = Z^{-1}Wx$, $D_x g = Z^{-1}W$. The slow manifold Y_ε is given by $Wx - Zy = 0$, up to higher-order terms. Moreover

$$\widetilde{f}_1 = -\widetilde{U}x + \widetilde{V}y = \left(-\widetilde{U} + \widetilde{V}Z^{-1}W\right)x \quad \text{on } Y_\varepsilon.$$

[23] One may replace $\sqrt{2}$ by any smaller constant which is > 1.

Now consider the eigenvalues of the matrix $DF = \begin{pmatrix} -\varepsilon\widetilde{U} & \varepsilon\widetilde{V} \\ W & -Z \end{pmatrix}$; see also Lemma 7. Thus, let $\alpha_0+\varepsilon\alpha_1+\cdots$ be an eigenvalue with eigenvector $\begin{pmatrix} x_0+\varepsilon x_1+\cdots \\ y_0+\varepsilon y_1+\cdots \end{pmatrix}$; $\begin{pmatrix} x_0 \\ y_0 \end{pmatrix} \neq 0$. For $\alpha_0 \neq 0$, comparing lowest order terms in the eigenvalue condition yields

$$x_0 = 0 \text{ and } Wx_0 - Zy_0 = \alpha_0 y_0,$$

thus $-\alpha_0$ is an eigenvalue of Z. By Lemma 5, we see that 2γ can be chosen near the nonzero eigenvalue of $DF(x, y, 0)$ with smallest absolute real part.

For $\alpha_0 = 0$, thus the eigenvalue has order ε, comparing lowest orders in the eigenvalue condition yields

$$-\widetilde{U}x_0 + \widetilde{V}y_0 = \alpha_1 x_0 \text{ and } Wx_0 - Zy_0 = 0,$$

hence α_1 is an eigenvalue for $-\widetilde{U} + \widetilde{V}Z^{-1}W = \widetilde{f_1}$. An upper estimate for $\varepsilon\|\widetilde{f_1}\|$ can be obtained from Lemma 5: Choose the order ε eigenvalue with greatest absolute value, multiplied by some factor accounting for a coordinate change. Thus, we see that κ is composed of the factor $\|Z^{-1}W\|$ (which reflects the geometry of the slow manifold), the absolutely largest eigenvalue of order ε and some multiplicative constants from coordinate transformations. In our local setting, all the multiplicative constants mentioned above are of order one.

To summarize, the small parameter $\varepsilon_L = \kappa/\gamma$ is determined by the ratio of the largest absolute eigenvalue of order ε to the smallest absolute real part of eigenvalues of order one. From this perspective, for slow manifolds of dimension one in particular, the relevance of the parameters ε^* and μ^* is obvious. Their advantage lies in their (relative) computational accessibility. Likewise, ε^* is a both relevant and computationally accessible parameter for three-dimensional systems with two-dimensional slow manifolds.

9.1.3 Remarks on Steps 2 and 3

Lyapunov function arguments provide a small parameter ε_L which characterizes closeness of a solution of (89) to the slow manifold. This takes care of Step 1 described in Introduction, and clarifies the role of eigenvalues up to (ε-independent) factors due to coordinate changes.

For the ultimate goal of obtaining quantitative estimates for the discrepancy between the true solution and the singular perturbation approximation, one needs to go further. In Step 2, an appropriate critical time for the onset of the slow dynamics, as well as an appropriate initial value for the reduced system, must be determined. As for Step 3, by a continuity and compactness argument, the right-hand sides of the full and the reduced equation differ by ε_L times some constant. With this, and an error estimate for the initial value for the reduced system, continuous dependence provides an estimate of the approximation error on compact time intervals. Further work may be required, since one is mostly interested in unbounded time intervals, so one cannot rely only on standard continuous dependence theorems.

In the present manuscript, we generally did not address the determination of ε_L in examples and case studies. The only exception is irreversible Michaelis–Menten with slow product formation (see, Sect. 4.1), which also contains partial results for Step 3. For the (more familiar and more relevant) irreversible Michaelis–Menten system with small enzyme concentration all three steps can dealt with completely (even if some complications arise), as will be shown in a forthcoming paper. For any system of dimension > 2, even completing Step 1 seems quite demanding.

9.2 A Proof of Lemma 2

Proof Part (a) is a special case of Lemma 7 below. To prove part (b), abbreviate $\sigma_i^*(x) := \sigma_i(x, \widehat{\pi})$ for $x \in \widetilde{Y} \cap K$, $1 \le i \le n-1$. Then the nonzero roots of the characteristic polynomial χ are the roots of

$$\zeta(x, \tau) := \tau^{n-1} + \sigma_1^*(x)\tau^{n-2} + \cdots + \sigma_{n-1}^*(x).$$

By the blanket assumptions, the σ_i^* are bounded above and below by positive constants, hence the absolute values of all zeros of the $\zeta(x, \cdot)$ are bounded above by some constant. Since $\widehat{\pi}$ is a TFPV, all zeros have negative real parts. Now assume that for every positive constant δ, some $\zeta(x, \tau)$ has a zero with real part $\ge -\delta$. Then there exist sequences (x_k) in $\widetilde{Y} \cap K$ and (μ_k) in $\mathbb{C}$ such that $\zeta(x_k, \mu_k) = 0$ and $\operatorname{Re} \mu_k \to 0$. Due to boundedness of the sequence (μ_k) and compactness of $\widetilde{Y} \cap K$ we may assume that the μ_k converge to μ^*, $\operatorname{Re} \mu^* = 0$, and the x_k converge to $x^* \in \widetilde{Y} \cap K$. By continuity $\zeta(x^*, \mu^*) = 0$; a contradiction. Part (c) follows by continuity and compactness arguments.

9.3 Parameter Dependence of Eigenvalues

Recall from (39) the definition

$$\widetilde{\sigma}_i(x, \varepsilon) := \sigma_i(x, \widehat{\pi} + \varepsilon\rho), \quad 1 \le i \le n, \quad \widetilde{\sigma}_0 := 1.$$

We first prove (44), concerning the orders of the $\widetilde{\sigma}_i$ whenever $s > 1$.

Lemma 6 *Let $\widehat{\pi}$ be a TFPV for dimension s, with critical manifold $\widetilde{Y}$. Then for all $x \in \widetilde{Y} \cap K$ one has*

$$\widetilde{\sigma}_i(x, \varepsilon) = \varepsilon^{i-n+s}\widehat{\sigma}_i(x, \varepsilon) \text{ for all } x \in \widetilde{Y} \cap K, \quad n - s \le i \le n,$$

with polynomial $\widehat{\sigma}_i$.

Proof The arguments we will use are similar to those in the proof of Goeke et al. (2015, Proposition 3). We set

$$\widetilde{h}(x, \varepsilon) := h(x, \widehat{\pi} + \varepsilon\rho) \text{ for } x \in \widetilde{Y} \cap K.$$

There exists a local transformation of $\widetilde{h}$ into Tikhonov standard form. Thus, there exists a local analytic diffeomorphism Φ and a vector field $\widetilde{q}$ such that

$$D\Phi(x)\widetilde{h}(x,\varepsilon) = \widetilde{q}(\Phi(x),\varepsilon)$$

and consequently

$$D\Phi(x)D\widetilde{h}(x,\varepsilon) = D\widetilde{q}(\Phi(x),\varepsilon)D\Phi(x), \quad x \in \widetilde{Y} \cap K.$$

Therefore the Jacobian of $\widetilde{h}$ at x and the Jacobian of $\widetilde{q}$ at $\Phi(x)$ are conjugate; in particular they have the same characteristic polynomial. Denoting by $\widetilde{\nu}_i(y)$ the coefficients of the characteristic polynomial of $D\widetilde{q}(y)$, this means

$$\widetilde{\sigma}_i(x,\varepsilon) = \widetilde{\nu}_i(\Phi(x),\varepsilon) \text{ for all } x \in \widetilde{Y} \cap K.$$

Since $\widetilde{q}$ is in Tikhonov standard form, we have

$$\widetilde{q}(y,\varepsilon) = \begin{pmatrix} \varepsilon\widetilde{q}_1(y,\varepsilon) \\ \widetilde{q}_2(y,\varepsilon) \end{pmatrix},$$

with q_1 having s entries, and

$$D\widetilde{q}(y,\varepsilon) = \begin{pmatrix} \varepsilon D\widetilde{q}_1(y,\varepsilon) \\ D\widetilde{q}_2(y,\varepsilon) \end{pmatrix}.$$

Thus, every entry of the first s rows of the Jacobian is a multiple of ε, and with the Laplace expansion of the determinant this implies

$$\widetilde{\nu}_i(x,\varepsilon) = \varepsilon^{i-n+s}\,\widehat{\nu}_i(x,\varepsilon), \quad n-s < i \le n,$$

and finally (44).

Now we turn to determining the orders of the eigenvalues.

Lemma 7 *With objects and notation as in Lemma 6, let (44) hold, and furthermore consider the nondegeneracy conditions:*

(i) $\widehat{\sigma}_{n-s}(x,0) \neq 0$ *and* $\widehat{\sigma}_n(x,0) \neq 0$ *on* $\widetilde{Y} \cap K$.
(ii) *The polynomials*

$$\widehat{\sigma}_{n-s}(x,0)\tau^s + \widehat{\sigma}_{n-s+1}(x,0)\tau^{s-1} + \cdots + \widehat{\sigma}_n(x,0) \tag{94}$$

admit only simple zeros, for all $x \in \widetilde{Y} \cap K$.

(a) *Whenever (i) holds, the zeros* $\lambda_i(x,\varepsilon)$ *of the characteristic polynomial can be labeled such that*

$$\lambda_1(x,0) \neq 0, \ldots, \lambda_{n-s}(x,0) \neq 0 \quad \text{on } \widetilde{Y} \cap K,$$

and

$$\lambda_i(x,\varepsilon) = \varepsilon\widehat{\lambda}_i(x,\varepsilon), \quad x \in \widetilde{Y} \cap K, \quad i > n-s,$$

with continuous $\widehat{\lambda}_i$ *such that* $\widehat{\lambda}_i(x,0) \neq 0$ *on* $\widetilde{Y} \cap K$, $n-s+1 \leq i \leq n$.[24]

(b) *Whenever (ii) holds in addition to (i) then all* $\widehat{\lambda}_i$, $n-s+1 \leq i \leq n$, *are analytic in* (x,ε).

Proof The proof rests on the Newton–Puiseux theorem and on Hensel's lemma; we refer specifically to Abhyankar (1990, Lectures 12 and 13). According to Newton–Puiseux, the equation $\lambda^n + \sum \widetilde{\sigma}_i \lambda^{n-i} = 0$ admits series solutions

$$\lambda = \alpha\varepsilon^{\gamma} + \cdots$$

in rational exponents of ε, with a positive rational number γ and $\alpha \neq 0$. For such an expansion to hold with some γ and $\alpha \neq 0$, cancellation of lowest order terms in (10) is necessary. The lowest orders of the terms in the monomials are

$$(n-i)\gamma \text{ for } 0 \leq i \leq s, \quad \text{and} \quad (n-j)\gamma + j - n + s \text{ for } s+1 \leq j \leq n,$$

and for cancellation one must have equality between two of these orders. Clearly two orders in the first block cannot be equal. Assuming that an order from the first block equals an order in the second block, we get

$$(n-i)\gamma = (n-j)\gamma + j - n + s \Rightarrow \gamma = \frac{j-(n-s)}{j-i} < 1 \text{ unless } i = n-s.$$

But in case $\gamma < 1$ the lowest order equals $s\gamma$, with no cancellation; so only $\gamma = 1$ remains. Finally, if two orders in the second block are equal then one directly sees $\gamma = 1$. This shows part (a).

Continuing the argument, $\gamma = 1$ implies that precisely the monomials of degree $\leq n-s$ contribute to the lowest order, and the ansatz yields

$$\widehat{\sigma}_{n-s}(x,0)\alpha^s + \widehat{\sigma}_{n-s+1}(x,0)\alpha^{s-1} + \cdots + \widehat{\sigma}_n(x,0) = 0,$$

thus s distinct choices for α by condition (ii), and $\alpha \neq 0$. By Hensel's lemma, each choice for α yields a series $\lambda = \alpha\varepsilon + \cdots$, in positive integer powers of ε. This shows part (b).

Remark 6 In case $s = 1$ the second condition is automatic. Therefore Lemma 2 (a) is also proven.

[24] The $\widehat{\lambda}_i$ can be represented as convergent power series in $(x, \varepsilon^{1/m})$ for some positive integer m.

References

Abhyankar SS (1990) Algebraic geometry for scientists and engineers. American Mathematical Society, Providence

Arnold VI (1992) Ordinary differential equations. Springer, Berlin

Berglund N, Gentz B (2006) Noise-induced phenomena in slow-fast dynamical systems. A sample-paths approach. Springer, London

Briggs GE, Haldane JBS (1925) A note on the kinetics of enzyme action. Biochem J 19:338–339

Cardin PT, Texeira MA (2017) Fenichel theory for multiple time scale singular perturbation problems. SIAM J Appl Dyn Syst 16:1452–1452

Choi B, Rempala GA, Kim JK (2017) Beyond the Michaelis-Menten equation: accurate and efficient estimation of enzyme kinetic parameters. Sci Rep 7:17018

Eilertsen J, Schnell S (2018) A kinetic analysis of coupled (or auxiliary) enzyme reactions. Bull Math Biol 80:3154–3183

Eilertsen J, Schnell S (2020) The quasi-steady-state approximations revisited: timescales, small parameters, singularities, and normal forms in enzyme kinetics. Math Biosci 325:108339

Eilertsen J, Stroberg W, Schnell S (2018) Phase-plane geometries in coupled enzyme assays. Math Biosci 306:126–135

Eilertsen J, Tyczynska MA, Schnell S (2021) Hunting ϵ: the origin and validity of quasi-steady-state reductions in enzyme kinetics. SIAM J Appl Dyn Syst 20:2450–2481

Eilertsen J, Roussel MR, Schnell S, Walcher S (2021) On the quasi-steady state approximation in an open Michaelis-Menten reaction mechanism. AIMS Math 6:6781–6814

Eilertsen J, Schnell S, Walcher S (2022) On the anti-quasi-steady-state conditions of enzyme kinetics. Math Biosci 350:108870

Evans LC (2014) Partial differential equations, 2nd edn. American Mathematical Society

Eyers PA, Murphy JM (2016) The evolving world of pseudoenzymes: proteins, prejudice and zombies. BMC Biol 14:98

Fenichel N (1979) Geometric singular perturbation theory for ordinary differential equations. J Differ Equ 31:53–98

Gantmacher FR (2005) Applications of the theory of matrices. Dover, Mineola

Goeke A, Walcher S (2013) Quasi-steady state: searching for and utilizing small parameters. In: Johann A, Kruse H-P, Rupp F, Schmitz S (eds) Recent trends in dynamical systems. Springer, New York, pp 153–178

Goeke A, Walcher S (2014) A constructive approach to quasi-steady state reduction. J Math Chem 52:2596–2626

Goeke A, Walcher S, Zerz E (2015) Determining "small parameters" for quasi-steady state. J Differ Equ 259:1149–1180

Goeke A, Walcher S, Zerz E (2017) Classical quasi-steady state reduction—a mathematical characterization. Physica D 345:11–26

Heineken FG, Tsuchiya HM, Aris R (1967) On the mathematical status of the pseudo-steady hypothesis of biochemical kinetics. Math Biosci 1:95–113

Keener J, Sneyd J (2009) Mathematical physiology I: cellular physiology, 2nd edn. Springer, New York

Kruff N, Walcher S (2019) Coordinate-independent singular perturbation reduction for systems with three time scales. Math Biosci Eng 16:5062–5091

Krupa M, Szmolyan P (2001) Extending slow manifolds near transcritical and pitchfork singularities. Nonlinearity 14:1473–1491

Lam SH, Goussis DA (1994) The CSP method for simplifying kinetics. Int J Chem Kinet 26:461–486

Michaelis L, Menten ML (1913) Die Kinetik der Invertinwirkung. Biochem Z 49:333–369

Miller WG, Alberty RA (1958) Kinetics of the reversible Michaelis-Menten mechanism and the applicability of the steady-state approximation. J Am Chem Soc 80:5146–5151

Murphy JM, Farhan H, Eyers PA (2017) Bio-Zombie: The rise of pseudoenzymes in biology. Biochem Soc Trans 45:537–544

Noethen L, Walcher S (2007) Quasi-steady state in the Michaelis–Menten system. Nonlinear Anal Real World Appl 8:1512–1535

Noethen L, Walcher S (2011) Tikhonov's theorem and quasi-steady state. Discrete Contin Dyn Syst Ser B 16(3):945–961

Palsson BO, Lightfoot EN (1984) Mathematical modelling of dynamics and control in metabolic networks. I. On Michaelis–Menten kinetics. J Theor Biol 111:273–302
Patsatzis DG, Goussis DA (2019) A new Michaelis-Menten equation valid everywhere multi-scale dynamics prevails. Math Biosci 315:108220
Reich JG, Selkov EE (1974) Mathematical analysis of metabolic networks. FEBS Lett 40(Suppl. 1):S119–S127
Schnell S (2014) Validity of the Michaelis-Menten equation-steady-state, or reactant stationary assumption: that is the question. FEBS J 281:464–472
Schnell S, Maini PK (2000) Enzyme kinetics at high enzyme concentration. Bull Math Biol 62:483–499
Schnell S, Mendoza C (2001) A fast method to estimate kinetic constants for enzyme inhibitors. Acta Biotheor 49:109–113
Segel LA (1988) On the validity of the steady state assumption of enzyme kinetics. Bull Math Biol 50:579–593
Segel LA, Slemrod M (1989) The quasi-steady-state assumption: a case study in perturbation. SIAM Rev 31:446–477
Seshadri M, Fritzsch G (1980) Analytical solutions of a simple enzyme kinetic problem by a perturbative procedure. Biophys Struct Mech 6:111–123
Stroberg W, Schnell S (2016) On the estimation errors of K_M and V from time-course experiments using the Michaelis–Menten equation. Biophys Chem 219:17–27
Tikhonov AN (1952) Systems of differential equations containing a small parameter multiplying the derivative (in Russian). Math Sb 31:575–586
Tzafriri AR (2003) Michaelis-Menten kinetics at high enzyme concentrations. Bull Math Biol 65:1111–1129
Walter W (1998) Ordinary differential equations. Springer, New York
Wan FYM (2018) Mathematical models and their analysis. SIAM, Philadelphia
Zagaris A, Kaper HG, Kaper TJ (2004) Analysis of the computational singular perturbation reduction method for chemical kinetics. J Nonlinear Sci 14:59–91

Publisher's Note Springer Nature remains neutral with regard to jurisdictional claims in published maps and institutional affiliations.

Springer Nature or its licensor (e.g. a society or other partner) holds exclusive rights to this article under a publishing agreement with the author(s) or other rightsholder(s); author self-archiving of the accepted manuscript version of this article is solely governed by the terms of such publishing agreement and applicable law.